UNIVERSITÀ DEGLI STUDI DI MILANO

Scuola di Dottorato in Scienze Biologiche e Molecolari

XXVII Ciclo

DECIPHERING THE AGGREGATION MECHANISMS IN HUMAN β2-MICROGLOBULIN

LEVON CHANT HALABELIAN

PhD Thesis

Scientific tutor: Dr. Stefano Ricagno

Co-tutor: Prof. Martino Bolognesi

Academic year: 2013-2014

SSD: Bio/10

Thesis performed at Department of Biosciences, University of Milan.

Table of Contents

MANUSCRIPT IN PREPARATION I:

HALABELIAN L., BARBIROLI A., RELINI A., BOLOGNESI M., RICAGNO S. (2014). "A COVALENT HOMODIMER TO PROBE EARLY OLIGOMERS ALONG AMYLOID AGGREGATION".

SIDE RESEARCHES NOT INCLUDED IN THE MAIN FRAME OF THE THESIS:

NATALELLO A., RELINI A., PENCO A., **HALABELIAN L.,** BOLOGNESI M., DOGLIA SM., AND RICAGNO S. (2014). "WILD TYPE BETA-2 MICROGLOBULIN AND DE LOOP MUTANTS DISPLAY A COMMON FIBRILLAR ARCHITECTURE". UNDER REVIEW IN PLOS ONE.

SUMMARY

Beta2-microglobulin (β2m) is a 99-residue globular protein that represents the light chain of the major histocompatibility complex class I (MHCI). β2m is responsible for two types of human amyloid diseases: dialysis-related amyloidosis (DRA) caused by wt β2m, and hereditary systemic amyloidosis due to the D76N β2m mutant. Two independent projects were carried out during my PhD studies addressing both types of β_2m-related amyloidosis:

(i) The human cells adopt a sophisticated unfolded protein response (UPR) system for targeting misfolded/aggregated polypeptides. However, the D76N variant, which is unstable and aggregation prone, bypasses the UPR system and reaches the extracellular space forming amyloids. To understand the mechanism(s) that allow the D76N variant to escape the UPR system and to characterize its effect on MHCI, we performed a complete structural and biophysical study on a MHCI bearing the D76N variant. Our results show that MHCI acts as a chaperone that stabilize and hide the amyloidogenic variant from the UPR system, and transfers it to cell membrane, where during its normal turnover, the D76N β2m variant dissociates into blood serum and aggregates causing human pathologies.

(ii) The early oligomeric species are responsible for cellular cytotoxicity in amyloidosis. Previous data showed a favourable association interface (between two facing D β-strands) that may involve in β2m oligomerization. To further elucidate its role in aggregation, we created a S-S linked dimer of β2m (DimC33) that interacts via the DD interface. Our data show that DimC33 is highly amyloidogenic compared to wt β2m, suggesting that dimerization through DD interface is instrumental for enhancing its aggregation propensity. Furthermore, DimC33 was co-crystallized in complex with Thioflavin-T (ThT), a well-known amyloid-specific dye, showing unique ThT binding site that may indicate a second key interface involved in β2m oligomerization.

PART I

1. STATE OF THE ART

1.1 Amyloidosis

Amyloidosis is a serious pathological concern resulting from aggregation of precursor proteins or peptides into highly structured fibrillar aggregates called Amyloid fibrils. They are associated with various human amyloid diseases that can be broadly classified into three groups, according to the affected organ or tissue: Neurodegenerative diseases, such as Alzheimer's and Parkinson's disease; Non-neuropathic Localized Amyloidosis, such as Type II diabetes; and Non-neuropathic Systemic Amyloidosis such as Dialysis-related amyloidosis and light chain AL amyloidosis (*1*). Amyloidosis can result from unfolding of a natively folded protein, an amyloidogenic mutant variant of a protein, a cleavage of a protein into amyloidogenic fragments, a dramatic increase of a protein concentration, or over-production of an intrinsically disordered protein (*2*).

However, non-pathogenic and functional amyloids are also known to be part of various normal cellular life, performing useful functional roles. Notable examples include Curli fibrils expressed by *E.coli* that are involved in the colonization process (*3*), Spidroin in certain types of spiders for formation of silk fibers of the web (*4*), and intralumenal fibrous striations in melanosomes upon formation of melanine molecules in mammalian system (*5*).

One of the most important characteristics of amyloid fibrils is the common cross-β arrangement of polypeptide chains along the fibril axis which is observable by X-ray powder diffraction pattern at 4.8Å and 10-11Å spacings (*6*) **(see Fig. 1A&B),** and by FTIR spectroscopy techniques. Amyloid fibrils have distinct fibrillar morphologies, which can be detected by Transmission electron microscopy (TEM) and Atomic-force microscopy (AFM).

The most common methods for detection and diagnosis of amyloid fibrils are achieved by amyloid binding dyes, such as Congo Red staining and Thioflavin-T (ThT) fluorescence. ThT is considered the gold standard for effective and reliable *in vitro* and *in vivo* analysis of amyloid fibrils (*7, 8*); upon binding to amyloid fibrils, ThT exhibits a dramatic shift in its fluorescence excitation and emission maxima, from 385 nm to 450 nm, and from 445 nm to 482 nm, respectively.

1.2 Dialysis-related amyloidosis

In 1980, Assenat *et al.* discovered, for the first time, amyloid fibril deposits in a tissue removed from patients undergoing long-term dialysis during carpal tunnel syndrome surgery (*9*), in which, β2m was the major component of such amyloid deposits (*10-12*).

The onset of dialysis-related amyloidosis (DRA) originates from gradual increase of freely circulating serum concentrations of monomeric β2m, up to 60-fold (*13*), in patients undergoing hemodialysis due to kidney failure—where dialysis membranes were insufficient to degrade and eliminate β2m outside of human body. A simple schematic view characterizing the onset of dialysis-related amyloidosis is shown in **Fig. 1C**. The impairment of β2m system clearance results in an accumulation of the latter as amyloid fibrils in osteoarticular tissues, in cartilage, capsule and synovium, showing clinical symptoms of carpal tunnel syndrome accompanied by amyloid arthropathies in the spine and peripheral joints leading to bone fractures (*14*).

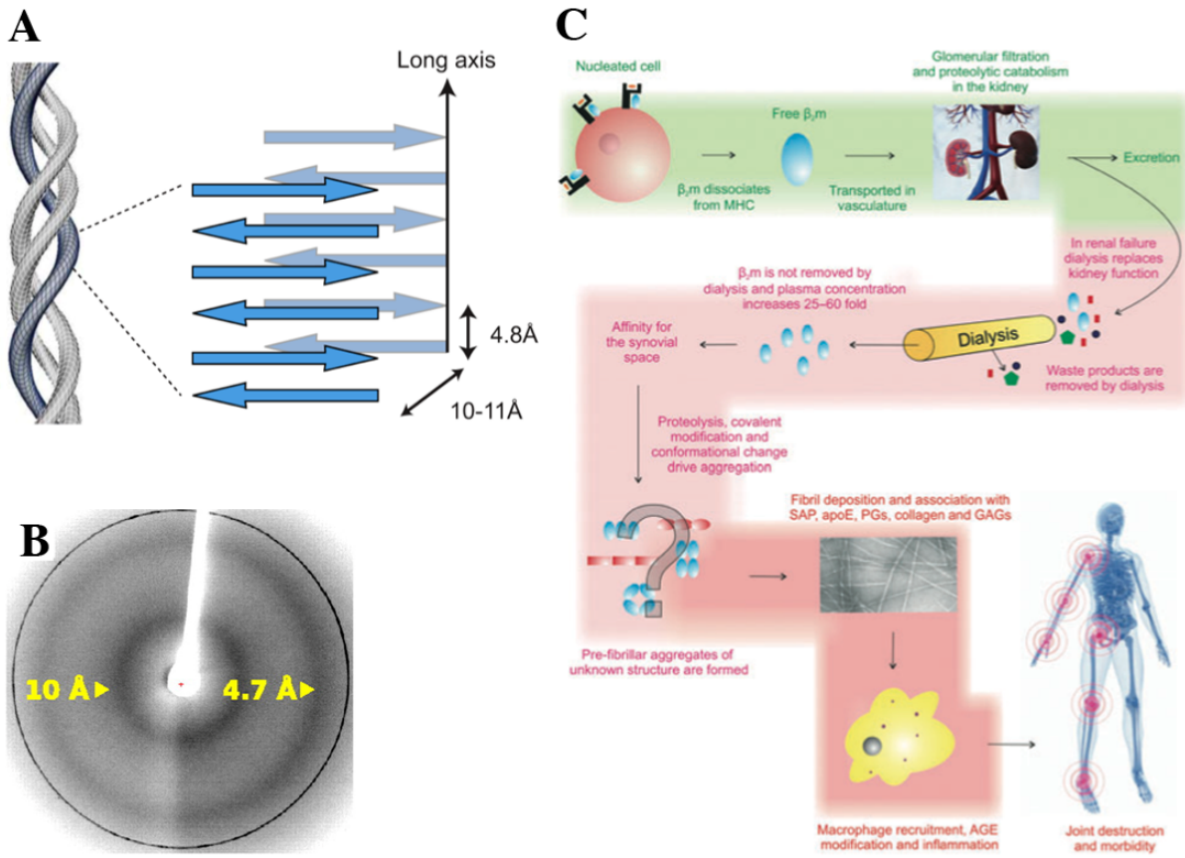

Figure 1. (A) Common cross-β structure of amyloid fibrils (figure acquired from Biancalana M, *et al. Biochem. Boiphys. Acta,* 2010) (*15*)**. (B)** The characteristic cross-β X-ray powder diffraction pattern of amyloid fibrils (figure is modified from Stroud et al. *PNAS,* 2012) (*16*). **(C)** Schematic representation of main steps in the pathogenesis of dialysis-related amyloidosis (figure acquired from Hodkinson JP, *et al. Book chapter:Common Cytotoxins Underlying Degenerative Diseases* 2012) (*17*).

The mechanism of DRA is complex and yet to be elucidated at molecular level; several *in vitro* analyses showed that β2m is very stable and soluble under long term incubations under physiological conditions (37°C, pH 7,4), even at 20-folds higher than *in vivo* concentrations that occur during DRA, suggesting that β2m serum concentration increase on its own is insufficient to self-initiate amyloidosis (*18*). Other factors have been shown to trigger full length β_2m amyloidosis, such as: post translational modifications of β2m (*19*), binding to divalent metal ions (*20*), glycosaminoglycans (*21*), heparins (*22*), collagen (*23*) *etc*.

1.3 Structure and Function of β2m

In higher organisms, β2m is a component of major histocompatibility complex class I (MHCI) molecules (*24*), as well as MHC-related molecules called haemochromatosis protein (HFE) that have a role in regulating iron homeostasis (*25*). MHC class I molecules are expressed abundantly on the surface of nearly all nucleated cells that play a key role in cell-mediated immune system by presenting antigens to CD8-positive T cells. Mature MHC class I molecules consist of one membrane-linked heavy chain, a non-covalently linked β2m, and a 8-10 amino-acids long antigen that is generated from cytosolic proteins by cellular proteasomes (*26*) (**see Fig. 2A)**. Assembly of MHC class I molecules occur in the endoplasmic reticulum (ER), followed by transit through the Golgi apparatus to the cell surface. During their normal turnover, the class I MHC molecules dissociate, releasing β2m and antigen extracellularly, whereas the membrane-associated heavy chain internalize for recycling or degradation (*24*). In healthy individuals, the catabolic degradation of β2m occurs in the proximal tubular cells, in the kidneys (*27, 28*).

β2m is a 99-residue small globular protein with a typical immunoglobulin-like fold composed of seven β-strands (named alphabetically from A-G) arranged in two β-sheets; four β-strands (ABDE) form one β-sheet and the remaining three β-strands (CFG) form the facing β-sheet; the two β-sheets are internally cross-linked by one disulfide bond *via* Cys25 and Cys80 (*29*) (pdb code: 2YXF) (**Fig .2B)**. The disulfide bond is well protected from reduction in the native state as well as in amyloid fibrils of β2m (*30, 31*), and is shown to be necessary for proper formation of mature amyloid fibrils (*32*). The NMR (*33*) and X-ray crystal structures (*34*) of natively folded β2m showed a *cis* conformation for the His31-Pro32 peptidyl-prolyl bond.

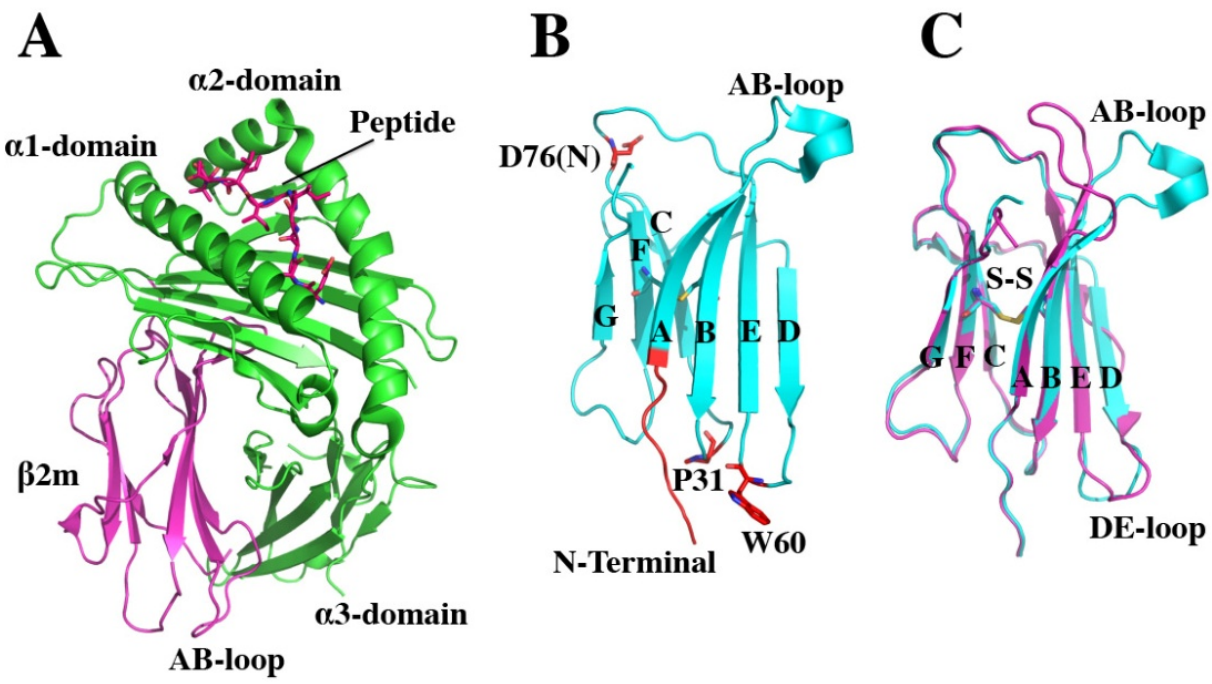

Figure 2. X-ray crystal structures of MHC class I and β2m.
(A) 3D model representation of MHC class I (pdb code: 1JF1) showing the heavy chain with three α domains (α1, α2, α3) in green, the light chain (β2m) in magenta and the peptide bound in a groove between two helices of heavy chain is shown as sticks model in red. **(B)** 3D model of monomeric β_2m is shown in Cyan: the most important residues are shown as sticks model and N-terminal six residues are shown in red (pdb code:2YXF). **(C)** The superposed models of MHC bound conformation of β2m (pdb code: 1JF1) with free-form of wt β2m (pdb code:2YXF), where the two variable conformations of AB-loop is seen on the upper side of the molecule.

The main β2m regions that interact with the heavy chain of MHCI include β-strands A and D, AB-loop, BC-loop and DE-loop (*35*) (pdb code: 1JF1), (**Fig. 2A).** Those regions exhibit dynamic flexibility in the free-form of β2m compared to bound conformation with the heavy chain of MHCI, (**see Fig 2C)** (*36, 37*), and were hypothesized to be directly involved in amyloid fibril formation, (*38-40*). The Trp60 in DE-loop region plays a key role in complex formation with the heavy chain of MHCI as well as in amyloid fibrils (*41*) **(Fig. 2A, B)**. Indeed, the Trp60 substitution to Gly, diminished its assembly within MHCI molecules, abolished its amyloidogenic propensity, and increased its solubility and stability compared to wt β2m (*42*). Whereas, Asp59 substitution to Pro decreased its stability and increased its fibril formation capacity, suggesting that conformational strain in the DE-loop may be crucial for β2m stability and aggregation (*38, 39*).

1.4 β2m folding and amyloidosis

Chiti and co-workers characterized the folding process of β2m by a three sequential phases model with two intermediates: the burst phase, with the formation of partially folded conformers showing partially exposed hydrophobic core (I_1); the fast phase, with the

conversion into more compact and highly structured species (I_2); and the slow phase, with the formation of the final native state (N) **see Fig 3.**

Figure 3. Schematic representation of β_2m four state model (figure obtained from Chiti *et al.* J Mol Biol. 2001) (*43*)**.**

It's worth mentioning, that partially folded intermediate species (I_2) closely resemble the amyloidogenic species of β2m that are generated under mildly acidic pH conditions (*43*). Under some physiologically relevant conditions, a 14 ± 8% amount of (I_2) species was shown to populate at equilibrium with (N) species, displaying a 5-fold higher aggregation rate compared to the native (N) ones, in the presence of *ex vivo* amyloid seeds (*44*).

Chiti and his colleagues proposed that the slow phase of β2m folding refers to the presence of substantial energetic barriers, and is unrelated with *trans* to *cis* isomerisation of His31-Pro32 peptidyl-prolyl bond, since it lacks any sensitivity to peptidyl prolyl isomerase during the slow phase of β2m folding (*43*). Later on, NMR and CD studies on β2m mutants, allowed to conclude that *trans* to *cis* isomerisation of His31-Pro32 peptidyl-prolyl bond was in fact responsible for the slow phase of β2m folding, and for the accumulation of I_2 species. The Pro32 substitution to Val/Gly completely abolished the slow folding phase of β2m by allowing it to maintain a *trans* isomeric conformation at the His31-Val32 peptide bond (*45, 46*). However, the Pro32 to Val β2m variant was unable to elongate the *ex vivo* amyloid fibrils, suggesting that the *trans* peptide form at position Pro32 is insufficient on its own to trigger self-oligomerisation and fibril formation (*46*).

In order to better study the conformational effects of Pro32 in β2m folding and aggregation, Torbeev *et al.* deployed fluorinated derivatives of Proline amino acid in order to modify the equilibrium rates in the *cis* to *trans* isomerization at the His31-Pro32 peptide bond; the results showed a direct influence of Pro32 isomerization rates on stability, folding a aggregation properties of β2m (*47*).

In a pioneering work, Rennella *et al.* characterized the oligomeric species that populate during acid denatured β2m folding by means of hybrid techniques, including real-time 2D NMR, small-angle X-ray scattering (SAXS) and ThT fluorescence (*48*). They identified the presence of oligomeric species (mainly dimers) along the folding process of β2m, with the

long-lived intermediate (I) species having 6 to 7-fold higher rates of self-assembly into dimers compared to the native ones (N). The dimeric species had elongated shapes as a result of head to head interaction at the apical side of β2m where Pro32 is located **(see Fig. 4B, C)**, suggesting that *cis-trans* isomerization of Pro32 could play a key role in oligomerization and fibril formation (*48*). In accordance with their findings, they proposed a five-state model of β2m folding that better describes the formation of dimeric species (**see Fig. 4A)**.

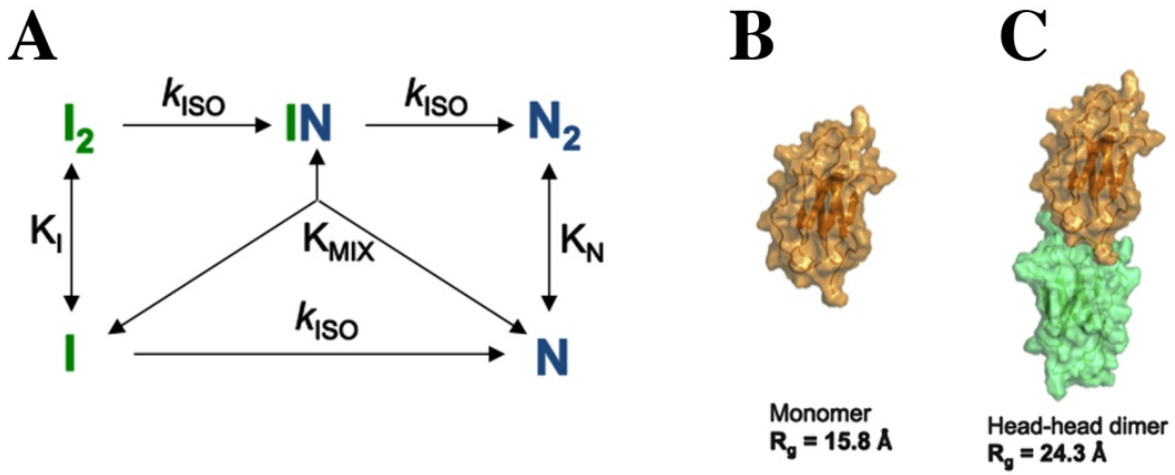

Figure 4. kinetic folding model of **β2m oligomers.**
(A) Five-state kinetic folding model of β2m, where the three dimeric species that accumulate along the folding process of β2m are included: I_2-intermediate homodimer, N_2-native homodimer, IN-intermediate-native heterodimer. **(B, C)** Surface representations of monomeric and head to head dimeric models of β2m observed by SAXS analysis. (figures were modified from Renella *et al.* J Mol Biol. 2013)(*48*).

A similar head to head dimerization interface of two β2m was also reported by NMR studies of Pro32 to Gly β2m variant (*45*), in three crystal structures of DimC20, DimC50 engineered β2m (*49*), the hexameric structure of H13F β2m variant (*50*), as well as by molecular dynamics simulation studies of β2m aggregation (*51*).

Clinical studies performed on patients being treated with long-term dialysis due to kidney failure, revealed a clear link between Cu^{+2} coated dialysis membranes and DRA (*52, 53*). It has been shown, that Cu^{+2} binds to the natively folded β2m through His31 (dissociation constant ~2.7 μM) with a binding specificity for Cu_2^+ over Zn_2^+ and Ni_2^+ (*54*). In the early stages of Cu^{+2}-induced β2m fibrillogenesis, Cu^{+2} is shown to convert the native-state β2m into an active native-like conformation by inducing *cis* to *trans* isomerisation of His31-Pro32 peptide bond that triggers the formation of dimeric species, and later on assembles into higher order species of tetramers and hexamers, eventually forming amyloid fibrils (*55*). Cu^{+2} can also bind to the unfolded-states of β2m mediated by His13, His51, His84 residues excluding His31 (*20*), causing destabilization of human β2m and leading to oligomerization

to dimers and tetramers along the amyloid fibril formation (*56, 57*).

1.5 The role of ΔN6-β2m in dialysis-related amyloidosis

The analysis of ex vivo β2m amyloid fibrils extracted from a patient suffering DRA revealed the presence of over 20% of N-terminally truncated species of β_2m **(Fig. 2B)**, mainly at positions Arg6 (called ΔN6-β2m), and less commonly at Tyr10 (*30*). The ΔN6-β2m variant is shown to have affinity for collagen (*58*), which may indicate its essential role in DRA by triggering amyloidosis at collagen rich regions in the human body.

The ΔN6-β2m truncated species were less stable and highly susceptible for proteolytic degradation in comparison with wt β2m; they readily formed amyloid fibrils at physiological pH (7.4) and temperature (37°C) conditions, without addition of any pre-formed amyloid fibrillar seeds or additives (*19, 59*). The real-time NMR studies of the ΔN6-β2m variant showed a *trans*-isomer at position Pro32, accompanied by global conformational perturbations of β-strands A, C and partially B, although the tertiary structure was intact due to the preserved disulfide bond at Cys25 and Cys80 (*19*); the non-native conformation of ΔN6-β2m resembled, to a great extent, the slow-phase intermediate (I_2) species of β_2m (*40*). Molecular dynamics simulations of the ΔN6-β2m variant suggested that the D-strand is directly involved in early oligomerization interfaces leading to amyloid fibril formation (*19*).

The ΔN6-β2m variant possesses a prion-like catalytic activity promoting the transformation of human wt β2m into non-native amyloidogenic intermediates able to form amyloid fibrils (*40*). In a recent study, Karamanos and co-workers showed that the interaction between amyloidogenic ΔN6-β2m and human β2m (Hβ_2m) results in promotion of amyloidosis, whereas the interaction between ΔN6-β2m and mouse β_2m (Mβ2m) results in inhibition of amyloidosis; in both cases, the same head to head interaction site at apical region of β2m (BC and DE loops) was shown to be involved in inhibition or activation processes of amyloidosis (*60*).

1.6 β2m amyloid Fibrils

β2m-related amyloidosis results from an accumulation of specific amyloidogenic precursors alongside the destabilization of natively folded β2m; the relative population of different amyloidogenic precursors is responsible for *in vitro* amyloid polymorphism (*61*). Indeed, in an acidic pH environment, the stability of β2m decreases causing it to adopt a partially unfolded conformation favoring aggregation (*62*). The pH and ionic strength of the

solution can dramatically influence the fibrillogenesis of native β2m; for instance, under acidic conditions (pH 3.6 – 4.0) and high ionic strength (400mM NaCl), β2m spontaneously forms amyloid fibrils, without any observable nucleation phase, displaying short (50-200 nm) and curvilinear worm-like fibril morphology (*62*). However, at slightly higher pH (> 3.0) and low ionic strength conditions (>30mM NaCl), β2m assemble in a nucleation-dependent manner, forming longer amyloid fibrils that are much similar to *ex vivo* fibrils (*62, 63*). The studies on early stage assembly mechanisms revealed that worm-like fibrils were assembled by constant addition of monomeric species, whereas the long-straight fibrils were formed by a population of oligomeric species (monomers, dimers, trimers and tetramers), which was then accumulated in the nucleation phase forming amyloid fibrils (*64*).

Since natively folded wt β2m species are unable to form amyloid fibrils for long time periods at neutral pH (7.4) *in vitro*, the addition of preformed amyloid seeds and denaturants such as 2,2,2,-trifluoroethanol (TFE) or Urea (*21*) were proposed, in order to trigger and accelerate wt β2m amyloidosis, allowing its characterization and analysis under *in vitro* conditions. By using a combination of biophysical techniques, Santambrogio *et al.* studied the conformational intermediates that generate under neutral pH in the presence of 20% TFE, and under low-acidic pH conditions: in both cases, partially folded species were populated at room temperature, showing a predominant beta type intermediate under low-pH condition compared to helical type under TFE-induced condition (*65*).

The addition of physiologically relevant factors to the fibrillogenesis solution, such as heparin, serum amyloid P component (SAP), apolipoprotein E (apoE), uremic serum, or synovial fluid, was shown to dramatically increase the rates of amyloid fibril formation due to its stabilizing effect on pre-fibrillar seeds (*18*). A crucial role for collagen in β2m-related amyloidosis under physiological conditions was also presented, due to collagen's immobilized charged surface that can act as seed to concentrate β2m molecules and prompt them to interact with each other more efficiently (*66*).

1.7 β2m oligomeric species in amyloidosis

Understanding the chain of events responsible for amyloid fibril formation is essential for identification of new targets for drug design against amyloidosis. A growing evidence suggest the role of oligomeric species in cellular cytotoxicity (*67*). During the early phase of β2m amyloidosis, intermediate oligomeric species are generated that eventually self-aggregate into mature amyloid fibrils (*68*). However, the molecular mechanism(s) responsible

to convert the monomeric species of native β2m into amyloidogenic precursors favoring oligomerisation is yet to be elucidated. Moreover, the oligomeric species are non-homogeneous and transient species, which makes their characterization at molecular level a challenging task. The cryo-electron microscopy analysis of full-length wt β2m amyloid fibrils revealed a globular dimer of dimers arrangement of fibrillar structure, with at least three different subunit interfaces involved (*69*). The IMS-MS characterization of β2m oligomers formed at acidic pH (3.6) conditions revealed the presence of a dynamic fast interchanging pool of oligomeric species, ranging from dimers to hexamers, together with the monomers (*70*).

In order to further characterize the oligomeric species of β2m at a molecular level, Miranker and co-workers engineered two separate β2m mutants, P32A β2m and H13F β2m, which were able to form oligomeric species when incubated in the presence of Cu^{+2}. The P32A β2m variant was crystallized as a dimeric species, showing a dimerization interface mediated by continuous anti-parallel D-strands (**Fig. 5C**). The characteristic β-bulge located at Asp53 of the edge-strand D (which was previously suggested to serve as natural inhibitor of aggregation) was absent, due to the conformational rearrangements required to accommodate a *trans* conformation of peptide bond at P32A mutation site (*71*).

The H13F β2m variant was crystallized as hexamers that also had a *trans*-conformation of the His31-Pro32 peptide bond. Two distinct interfaces were identified in the hexameric structure of H13F β2m: the first interface was formed by a head-to-head arrangement of two β2m molecules showing an anti-parallel DD strands interface **(see Fig 6A);** the second interface was mediated by two adjacent ABDE sheets interacting with each other through stacking of the aromatic residues Tyr 10, Tyr26 and Tyr63 (**see Fig 6D)** (*50*)**.** Later on, the same authors showed that the same ABDE sheets interface in the hexameric structure of H13F β2m can bind Thioflavin-T via stacking interactions with Tyr10 and Tyr26 residues (*72*) (**see Fig 6E)**. However, the oligomeric species generated by P32A and H13F β2m variants failed to form any amyloid fibrils in solution, raising concerns on their relations with on pathway intermediate species preceding β2m aggregation (*73*).

Selective covalent labeling combined with mass spectrometry technique was performed to study the residues involved in interfaces of the oligomeric species that accumulate during the early stages of Cu^{+2}-induced β2m fibrillogenesis (*74*). The results

proposed an anti-parallel ABDE sheets interaction of two monomeric β2m for formation of the dimeric interfaces (*75*), and D strands interaction of one dimer with G strands of the adjacent dimer, for formation of the tetrameric interfaces (*76*).

In a different study, nanobodies were implemented to block and characterize the amyloidogenic intermediate of ΔN6-β2m at atomic resolution (*77*). The crystal structure of nanobody-trapped ΔN6-β2m revealed a domain-swapped dimer as a result of G strands exchange between two ΔN6-β2m molecules; the remaining core structure maintained its native-like conformation due to the intact disulfide bond between Cys25-C80 (**see Fig 5A**). As a result of domain swapping, the FG-loops of two ΔN6-β2m chains corresponding to residues 83-89 (NHVTLSQ), formed two new anti-parallel β-strands (**see Fig 5A**); the isolated heptapeptide (NHVTLSQ) was shown have intrinsic properties to self-aggregate and form amyloidogenic β-sheet interactions (*78*).

A further attempt to characterize intermediate species of β2m came from Eisenberg and colleagues; they isolated and solved the crystal structure of a covalently linked domain-swapped dimer from on-pathway oligomeric species of β2m amyloidosis in the presence of reducing agents (*79*). The swapped domains of E, F and G strands were covalently linked to the host domain by a disulfide bond created by Cys25 and Cys80 of different molecules (**see Fig. 5B**). The hinge loop connecting the two domains (LSFSKD) was shown to have internal amyoidogenic segments, and the crystal structure of the isolated hexapeptide (LSFSKD) revealed a class 5 steric zipper similar to other amyloid backbone structures (*79*) (**see Fig. 5D**).

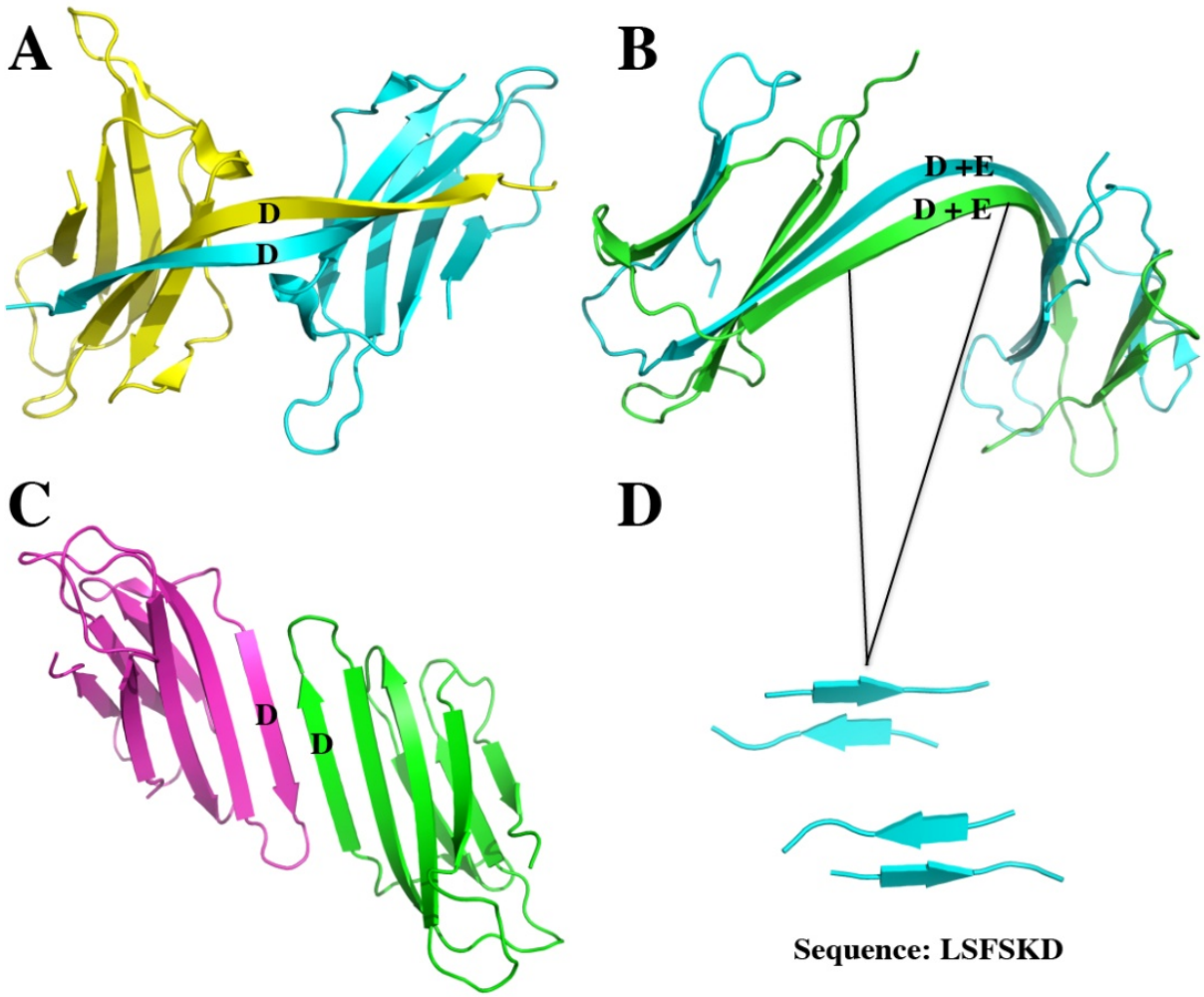

Figure 5. 3D cartoon representations of β2m oligomeric variants: (A) two chains of the ΔN6-β2m domain-swapped dimer are shown in Yellow and Cyan, (pdb code: 2X89); **(B)** two chains of the full length β2m domain-swapped dimer are shown in Green and Cyan (pdb code: 3LOW); **(C)** two chains of the P32A variant β2m that interact *via* two continuous anti-parallel D-strands are shown in Magenta and Green (pdb code: 2F8O); **(D)** Four chains of the hexapeptide (LSFSKD) forming class 5 steric zipper are shown in Cyan (pdb code: 3LOZ).

Recently, three covalently bonded homodimers of β2m were engineered in an attempt to study the protein-protein interaction sites involved in early oligomerisation steps of amyloidosis (*49*). As a result, three independent Cys mutations were introduced at surface sites of β2m, at residues 20, 50 and 88, and used to prepare disulphide-bonded homodimers of β2m, and named DimC20 (i.e. two β2m molecules linked through a Cys20-Cys20 disulphide bond), DimC50 and DimC88, respectively. Interestingly, DimC50 and DimC20 were crystallized as tetramers; a head-to-head arrangement of dimers were observed, mediated by an anti-parallel DD strands interface (**see Fig. 6B, C**), similar to the previously discussed DD strands interface in the hexameric structure of H13F β2m variant (**Fig. 6A**) (*50*). The DimC50 and DimC20 were amyloidogenic in solution, triggering the formation of long straight fibrils,

whereas, DimC60 was not amyloidogenic, apparently due to the disulfide bond position in DimC60 that interferes with the formation of the DD strands interface. Therefore, it was suggested that the DD interface may be directly involved in the formation of β2m oligomeric species under native and non-native conditions (*49*).

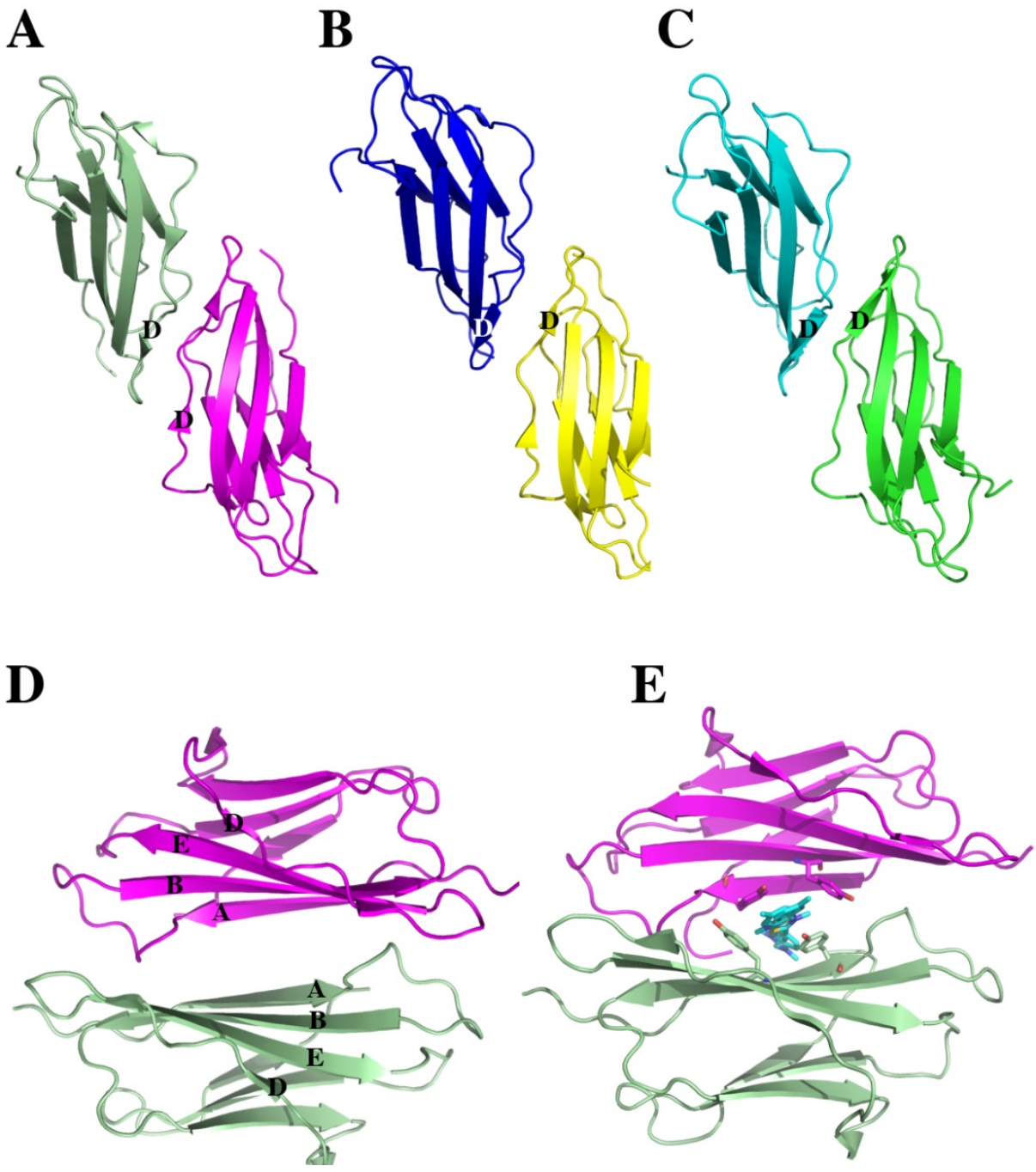

Figure 6. 3D cartoon representations for β2m oligomeric variants: (A) two chains of hexameric H13F β2m variant forming a dimeric DD strands interface are shown in Magenta and Pale-green, (pdb code: 3CIQ); **(B)** two chains of DimC20 interacting through a DD strands interface are shown in Blue and Yellow (pdb code: 3TLR); **(C)** two chains of DimC50 forming a dimeric DD strands interface are shown in Magenta and Green (pdb code: 3TM6). **(D)** two chains of hexameric H13F β2m variant interacting through ABED sheets are shown in Magenta and Pale-green, (pdb code: 3CIQ); **(E)** two molecules of Thioflavin (ThT) in 50% occupancy, is shown as sticks

model in Cyan, bound between two ABDE sheets interface formed in hexameric structure of H13F β2m are shown in Magenta and Pale-green (pdb code: 3MZT).

1.8 Inhibition of amyloidosis

Several strategies have been proposed to inhibit the formation of amyloid fibrils, including the stabilization of protein's native state or blocking the fibril formation by small molecules (*80*), monoclonal antibodies (*78*), small hydrophobic gold nanoparticles (*81*), chaperons (*82*), or by engineering new proteins to bind the amyloidogenic peptide/protein and prevent its aggregation (*83*).

Small molecules such as rifamycin SV (*80*), tetracycline and its analogues (*84*) are known to exhibit potent inhibiting effect on β2m amyloid fibril formation. It has been shown recently, that doxycycline inhibits β2m amyloidosis by stabilizing the native-state of β2m and blocking its oligomerisation process (*84*) with an overall IC_{50} value of ~ 47 μM (*i.e.* reducing the ThT fluorescence binding signal by 50%). The NMR studies revealed that the stabilizing effect of doxycycline results from transient interactions made with β2m specific regions including the end of the A strand, the initial part of strand B and the AB loop (*85*). Molecular dynamics simulation studies also indicated a very similar interaction site of doxycycline with β2m, through stacking interactions of doxycycline with Tyr10 located at the A strand region of β2m (*86*). Clinical analysis conducted on three patients suffering DRA showed positive effects of 100mg doxcycycline daily treatment: articular pain was decreased, passive and active movements were improved, but the amount of amyloid deposits remained unchanged (*87*).

Many amyloid inhibitors are rich in aromatic residues, sharing common structural features with ThT (*88*), a universal amyloid binding dye; therefore, a thorough investigation on the β2m ThT binding site at atomic resolution would be instrumental for driving effective drug-design against β2m amyloidosis (*15*).

1.9 Hereditary systemic amyloidosis due to D76N β2m variant.

In 2012, Valleix and colleagues reported a newly discovered autosomal dominant hereditary systemic amyloidosis caused by a single mutation of Aspartic acid at position 76 to Asparagine in β2m (*89*). The affected members of a French family suffered from a progressive bowel dysfunction, with extensive visceral amyloid deposits; symptoms included chronic diarrhoea, weight loss, *sicca* syndrome, subsequent symmetric sensorimotor axonal polyneuropathy, and severe orthostatic hypotension (*90*). Unlike DRA, the renal function and

plasma concentrations of freely circulating β2m in this case were normal. The amyloid deposits were located in the spleen, liver, heart, salivary glands, and nerves of the patients. Despite the fact that the four affected patients were heterozygous for the D76N β2m mutant encoding gene, amyloid fibrils were solely composed of the full length D76N β2m variant (meaning that wt β2m were also expressed but not integrated into any amyloid).

In contrast to wt β2m, the D76N β2m variant was less stable to unfolding by approximately 2 kcal/mol, as measured through guanidine hydrochloride denaturation. Moreover, the D76N variant showed high tendency to form amyloid fibrils *in vitro* under physiologic extracellular conditions within a few hours of incubation with agitation at 37°C, and without addition of Heparin or pre-formed amyloid seeds; notably, under such conditions wt β2m is completely soluble (*91*). The crystal structure of the D76N β2m variant matched closely those of the wt β2m structure; the main differences included the 1.5 Å shift of Tyr78 towards Asn76, the formation of new hydrogen bonds with the amide N atoms of Thr73 and Asn76 **(Fig. 7A, B),** as well as the change in the theoretical isoelectric point from 6.05 to 6.40 and the formation of more positively charged molecular surface **(Fig. 7C).**

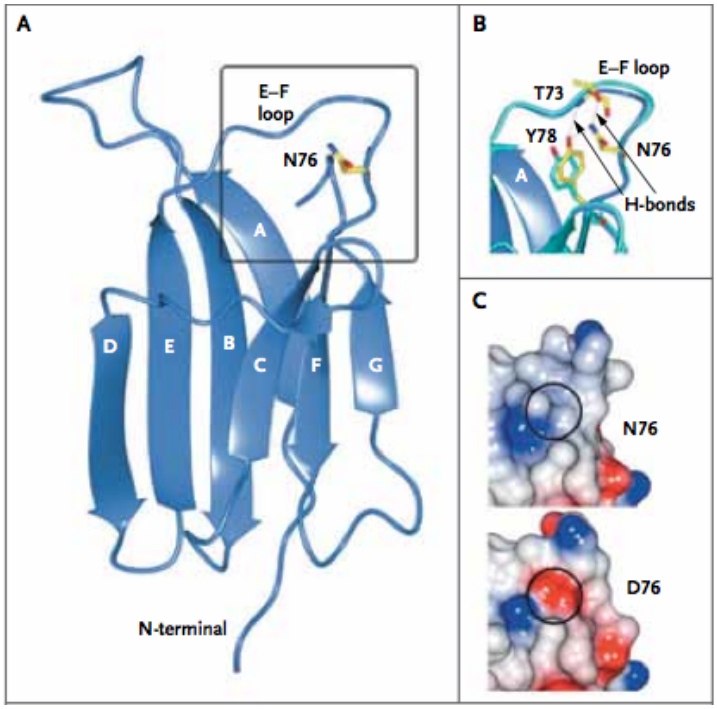

Figure 7. Crystal Structure of D76N β2m variant.
Panel A is a ribbon representation of the D76N variant. **Panel B** is a close-up view of the EF-loop (residues 70 to 80) shown in Panel A, superimposed on the wt β2m structure (blue–green). Residues belonging to the D76N variant are in yellow, and Tyr78 belonging to wt β2m is blue–green; hydrogen (H) bonds are shown as dashed lines. **Panel C** shows the surface electrostatic potential of the EF-loop region in the D76N variant (top) and in wt β2m (bottom); circles indicate the mutated residue. Blue represents positively charged regions, and red negatively charged regions (Figure obtained from Valleix *et al.* NEJM, 2012) (*89*).

2. AIMS OF THE THESIS

Despite the fact that a great variety of precursor proteins and peptides are responsible for different types of amyloid-related diseases, they all end up producing amyloid fibrils with shared structural and biophysical characteristics. β2m is a protein responsible for Dialysis-related amyloidosis and for a recently discovered hereditary systemic amyloidosis due to D76N β2m variant, which makes it an important model to study the underlying mechanisms in full-length protein amyloidosis. Two parallel research projects were carried out during my PhD studies, addressing both types of β2m-related amyloidosis independently, in order to explore the potential effect(s) of the D76N β2m variant on MHCI molecules, and to discover/characterize the oligomeric interfaces involved in β2m oligomerization and amyloid fibril formation in DRA.

2.1 MHCI: the Trojan horse for secretion of amyloidogenic β2m

The newly discovered D76N β2m mutant is so far the only known pathologic mutant of human β_2m, and it is responsible for a hereditary systemic amyloidosis. Although the D76N β2m variant is very unstable and aggregation prone, it is not cleared by the cellular unfolded-protein response (UPR) system, and is found abundantly in extracellular amyloid deposits. Physiologically, β_2m is the light chain of the class I major histocompatibility complex (MHCI) that plays a pivotal role in cellular immune response. Therefore, focusing on the biophysical and structural properties of MHCI bearing the D76N β2m variant as light chain (MHC_{76}) will help us to understand how such aggregation prone variant is protected from degradation, shedding light on the pathogenesis of this newly discovered misfolding disease.

2.2 A covalent homodimer to probe early oligomers along amyloid aggregation

During the early stages of amyloid fibril formation, heterogeneous and transient oligomeric species are accumulated, which represent the building-blocks for initiation and elongation of amyloid fibrils. Moreover, the primary role of oligomeric species in cellular toxicity was highlighted by many literature reports. The self-assembly mechanisms of β2m oligomeric species are still unclear, and, in particular, the atomic resolution description of regions involved in β2m oligomerization is yet to be elucidated. Dimeric intermediate species are shown to populate during the folding process of β2m that are highly amyloidogenic and aggregation-prone; those species display elongated shapes as a result of head to head

interaction of two β2m molecules through an anti-parallel DD strand interface. In several independent crystal structures of β2m variants, we also observed a similar anti-parallel DD strand interface formed between two interacting β2m molecules, suggesting that such interface may be directly involved in β2m dimerization and amyloidosis. In this study, we investigated the role of such DD strand interface in β2m oligomerization and amyloid fibril formation at molecular level, by constraining two β2m molecules to interact via such DD strand interface by mutating Ser33 to Cys, and preparing the corresponding S-S covalent β2m homodimers (DimC33).

3. MAIN RESULTS

3.1 MHCI: the Trojan horse for secretion of amyloidogenic β2m

3.1.1 MHCI reconstitution

The potential effect of D76N β2m variant on the MHCI assembly was studied in comparison with the wild-type counterpart, by generating four different species of MHCI molecules bearing the D76N variant or wt β2m in the presence of short peptides—a 8 to 10 amino-acids long peptide is necessary for a proper MHCI folding, whose stability also depends on the bound peptide. In order to rule out specific effects mediated by the bound peptide, two different peptides were used for production of MHCI, NY-ESO1(Y1V9) and FR20(Y3). The selected epitopes NY-ESO1(Y1V9) and FR20(Y3) are modified peptide variants from the melanoma-associated antigen NY-ESO1 (*92*), and multiple myeloma-associated antigen FR-20 (*93*), respectively. Both epitopes have been modified in order to enhance the overall stability of HLA-A0201 complexes. While peptide positions 1 and 9 were mutated to Tyr and Val (pY1 and pV9, respectively) in NY-ESO1(Y1V9), residue 3 was changed to Tyr(pY3) in FR20.

The prototypic HLA-A0201 (HLA-A2) heavy chain was refolded in the presence of D76N β2m or wt β2m, and of NY-ESO1(Y1V9), or FR20(Y3). As a result, four MHCI species were generated the HLA-A2/wt-β2m/NY-ESO1(Y1V9), HLA-A2/D76N-β2m/NY-ESO1(Y1V9), HLA-A2/wt-β2m/FR20(Y3) and HLA-A2/D76N-β2m/FR20(Y3) complexes, hereafter named WT MHCI pI, MHC_{76} pI, WT MHCI pII and MHC_{76} pII, respectively.

3.1.2 Thermal unfolding stabilities of MHCI species by CD

Thermal unfolding measurements were performed in collaboration with Dr. Alberto Barbiroli (University of Milan) on WT MHCI and MHC_{76}, both in complex with either peptide (pI) or peptide (pII), by monitoring the protein unfolding events with circular dichroism in the far UV region. The thermal unfolding curves of monomeric D76N β2m variant revealed a 9.8 °C decrease in stability compared to the wt β2m, clearly highlighting different thermal stabilities for the two monomeric variants (**see Fig. 8A**); the WT MHCI and MHC_{76}, presenting the same peptide, display very similar thermal stabilities **(Fig. 8B)**. The only observable difference between WT MHCI and MHC_{76}, as expected, was due to the nature of the bound peptide used for preparation of MHCI species; WT MHCI and MHC_{76} associated with peptide (pI) were approx. 6.4 °C more stable than the WT MHCI and MHC_{76}

with peptide (pII). The results suggest that, under these conditions, the D76N mutation does not affect the overall thermal stability of the assembled MHCI (**see Fig. 8 and the included Table for Tm values**).

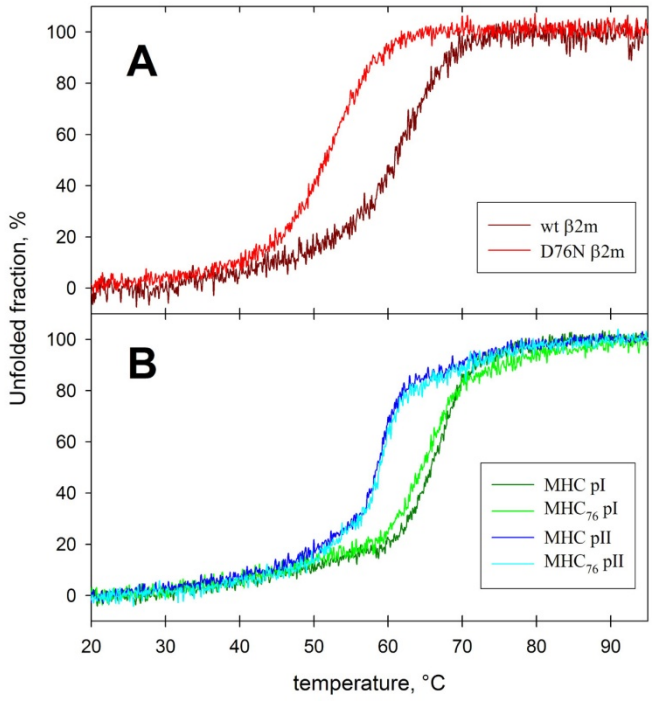

Melting temperatures assessed by means of far-UV

	monomer	MHC pI	MHC pII
wt β2m	62.4 °C*	67.3 °C	58.8 °C
D76N β2m	52.8 °C	65.5 °C	59.1 °C

* as in Santambrogio et al 2010

Figure 8. Overall thermodynamic stability of the different molecular species considered as determined by circular dichroism. Variation of far-UV CD signal as a function of temperature: **(A)** thermal unfolding of monomeric wt and D76N β2m monitored at 202 nm; **(B)** thermal unfolding of WT MHCI and MHC_{76} with either pI or pII monitored at 218 nm. Table: melting temperatures for monomeric proteins and their assemblies as assessed using CD curves.

3.1.3 Comparative analysis of MHC_{76} pI and WT MHCI pI crystal structures

The potential structural effects induced by the Asp76 to Asn mutation on MHCI were assessed by analysis of the crystal structures of MHC_{76} (pI) in comparison with WT MHCI (pI), which were determined at 2.65 Å and 3.1 Å resolutions, respectively. The MHC_{76} and WT MHCI molecules were crystallized in the same orthorhombic space group $P2_12_12_1$. The asymmetric unit contained fourteen MHCI moieties, arranged in two juxtaposed heptameric rings **(Fig. 9A)**, a previously unreported packing for MHC crystal structures, containing 69% solvent content. A cartoon representation of the assembled MHC_{76} 14-meric ring together

with one MHCI complex and the mutated D76N residue region in the protein is shown in **Fig. 9**.

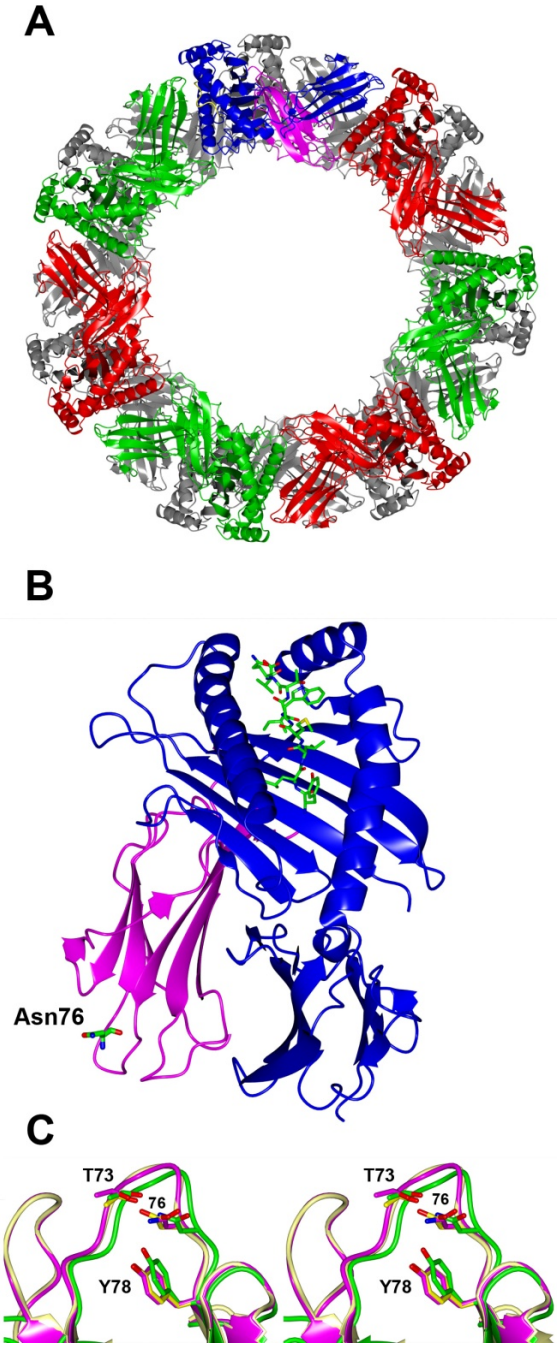

Figure 9. Comparative analysis of MHC_{76} pI and WT MHCI pI crystal structures.
Ribbon representation of the MHC_{76} pI assembly in asymmetric unit. The fourteen MHCI molecules are organised in two juxtaposed heptameric rings: MHCI units from the front ring are differently coloured; those in the back are grey. **(B)**, Ribbon representation of one MHC_{76} unit structure. The D76N mutation site on β2m is presented as a sticks model. The heavy chain, light chain and the bound nonapeptide are in blue, magenta, and green, respectively. **(C)** Stereo representation of the β2m EF-loop from the MHC_{76} structure (magenta), from WT MHCI (yellow) and from the monomeric D76N β2m (green).

In both crystal structures, the electron density is of excellent quality for all the fourteen MHCI units, except for the 87-91 residue stretch in all fourteen heavy chains of MHCI molecules. Data collection and refinement statistics for MHC_{76} and WT MHCI are shown in **Table I**. The fourteen MHC_{76} molecules in the asymmetric unit show negligible structural differences with an average root mean square deviation (r.m.s.d) of 0.29 Å/374 Cα atoms.

Table I. Data collection and refinement statistics for WT MHCI and MHC_{76}.
Values in parenthesis are for the highest resolution shell.

	Structure (PDB entry)	
	WT MHCI (4L29)	MHC_{76} (4L3C)
Data collection		
Beam line	BM-14 (ESRF)	ID14-4 (ESRF)
Space Group	Orthorhombic $P2_12_12_1$	Orthorhombic $P2_12_12_1$
Unit cell constants (Å)	*a* =101.5 *b* =313.3 *c* =314.4	*a* =102.1 *b* =314.5 *c* =316.2
Solvent content (%)	69.0	69.5
Resolution (Å)	53.88 - 3.10 (3.27 - 3.10)	70.63 - 2.65 (2.79 - 2.65)
R_{merge} [a](%)	19.2 (101.5)	16.8 (90.5)
I/sig(I)	9.3 (2.2)	6.8 (1.9)
Completeness (%)	100.0 (100.0)	99.7 (99.7)
Redundancy	5.8 (5.5)	5.3 (5.4)
Unique reflections	182,537 (26405)	293,400 (42513)
Rifinement		
R_{work} [b](%)	17.06	19.91
R_{free} [b](%)	20.05	21.83
Number of atoms	44,629	44,738
Ramachandran plot		
Most favored region	5073 (95.61%)	5059 (95.34%)
Allowed region	233 (4.39%)	247 (4.66%)
Outliers	0 (0.00%)	0 (0%)

[a] R merge = $\sum_{hkl} I_{hkl} - < I_{hkl} > | / \sum_{hkl} I_{hkl}$ where I is the observed intensity and < I > is the average intensity
[b] R work = $\sum_{hkl}$Fo-Fc | / $\sum_{hkl}$Fo for all data except 5% which were used for Rfree calculation.

The MHC_{76} structure matched closely to the WT MHCI structure as well as to previously reported MHCI structure (pdb code: 1S9W) with a r.m.s.d of about 0.5 Å and 0.63 Å, calculated over all the Cα atoms of the assembled complex, respectively. The D76N mutation site is located in the β2m EF-loop that is far from the heavy chain contact site (**Fig. 9B**); accordingly, no major structural effects induced by the D76N mutation are observed at the heavy/light chain interface region. The β2m EF-loop within the MHC_{76} structure superposes well with the corresponding region of WT MHCI structures, as well as with the EF-loop of monomeric wt β2m **(Fig. 9C).** A 1.5 Å shift of Tyr78 towards Asn76, which was previously observed in the crystal structure of the monomeric D76N variant at 1.40 Å resolution (*89*), is not detected in the MHC_{76} structure **(Fig. 9C)**, perhaps as a result of the lower resolution allowed by the MHC_{76} crystals.

Overall, the crystal structure of MHC_{76} does not appear to be affected by the D76N mutation on the light chain β2m; globally and locally it closely matches the 3D structures of WT MHCI. Furthermore, it is worth noting that residue 76 is not involved in any crystal contact with symmetry-related molecules within the crystal packing.

3.1.4 Relative stabilities of MHCI species by Mass Spectrometry

Nano-ESI-MS analyses for all prepared MHCI species (WT MHCI pI, MHC_{76} pI, WT MHCI pII and MHC_{76} pII), under various native and denaturing conditions, were carried out by our collaborators (group of Prof. Rita Grandori) at the University of Milano-Bicocca, to probe any potential effect of the D76N mutation on stoichiometry, conformational states, relative stabilities and dissociation patterns of the complex. These analyses did not highlight any effect mediated by the D76N mutation on MHCI stability or internal hierarchy of the complex; the only observable effect was caused by the two different peptides used in the preparation of four MHCI species, as expected.

3.1.5 Dynamic studies of β2m species by limited proteolysis

The flexibility and dynamics of WT and D76N β2m variants, both in their free-forms and assembled within MHCI molecules were studied by limited proteolysis by our collaborators at University of Pavia (Prof. Vittorio Bellotti's group). The results revealed that the free form of D76N β2m was more prone to proteolytic digestion than the wt β2m; On the contrary, the assembled forms of the two β2m species within MHCI molecules (MHC_{76} and WT MHCI) were fully protected from proteolytic digestion, suggesting that the MHCI heavy chain plays a remarkably protective role on both β2m variants.

3.1.6 In Vivo studies of D76N β2m variant

A transgenic mice expressing the amyloidogenic D76N β2m variant was created by our collaborators at University college London. The D76N variant was localized on the cell surface in assembled form within the MHCI molecules, providing further evidence that the D76N variant escapes cellular quality control mechanisms, and is consistent with the *in vitro* observations that the assembly of β2m within the MHCI masks its intrinsic misfolding propensity.

(The detailed descriptions of the last three experiments can be found in the corresponding paper, in part II of this Thesis: Halabelian *et al.* (2014) J. Biol. Chem. 289, 3318-27).

3.2 A covalent homodimer to probe early oligomers along amyloid aggregation

3.2.1 Recombinant S33C variant β2m homodimers

β2m oligomeric species that generate early along fibril formation in DRA are responsible for cellular cytotoxicity. An anti-parallel DD strand interface was observed in several previous β2m variants, suggesting this as a favorable interaction site in oligomerisation. In order to study the role of the DD interface in β2m oligomers, we mutated Ser33 to Cys, and created the covalently-linked β2m homodimers that would interact via similar DD strand interface previously observed; the two facing Ser33 residues at DD strand interface in previous structures of β2m variants (pdb codes: 3TM6, 3TLR, 3CIQ) were found to fall at suitable distance to be mutated to Cys, yielding a disulphide-bonded β2m homodimer, without disrupting or straining the stereochemical properties of DD interface.

The S33C β2m variant was expressed as inclusion bodies, purified under denaturating conditions, and then refolded according to our standard protocol (*94*). In our previous studies, formation of an intermolecular S-S bridge in other β2m homodimers was achieved through an additional dimerization step at the end of the purification, which required incubating the mutants at high protein concentration (5 mg/mL^{-1}) in the presence of oxidizing agents (H_2O_2) (*94*). Conversely, a S-S bonded dimeric S33C species was abundantly present already during the protein refolding stage, suggesting that the DD strand interface is a favorable interaction site to juxtapose transient dimeric species during the β2m refolding process under these conditions. The covalent dimeric species of S33C β2m variant will be named hereafter DimC33.

3.2.2 Overall Thermodynamic stability of DimC33 by CD

Thermal unfolding stabilities of DimC33 and wt β2m, monitored by circular dichroism at Far-UV, indicates that DimC33 unfolds according to a simple sigmoidal curve, displaying a very similar Tm value compared to the wt protein (Tm_{DimC33} 60.2°C; Tm_{wt} 62.4°C), (**Fig. 10A)**. Then, Far-UV spectra of DimC33 and of wt β2m were measured under three different solvent conditions: under native conditions in phosphate buffer, under denaturing conditions in 10% and 20% 2,2,2,-Trifluoroethanol (TFE). The results showed the maintenance of a native secondary structure content in phosphate buffer, as well as in 10% TFE conditions, for both wt and DimC33 molecules; on the contrary, for the 20% TFE conditions the wt β2m and DimC33 fold appeared severely affected, (**Fig. 10B).** Thus, the

spectroscopic data suggest that the S33C mutation and the generated disulfide-bonded dimer do not alter the β2m thermodynamic stability or its overall fold.

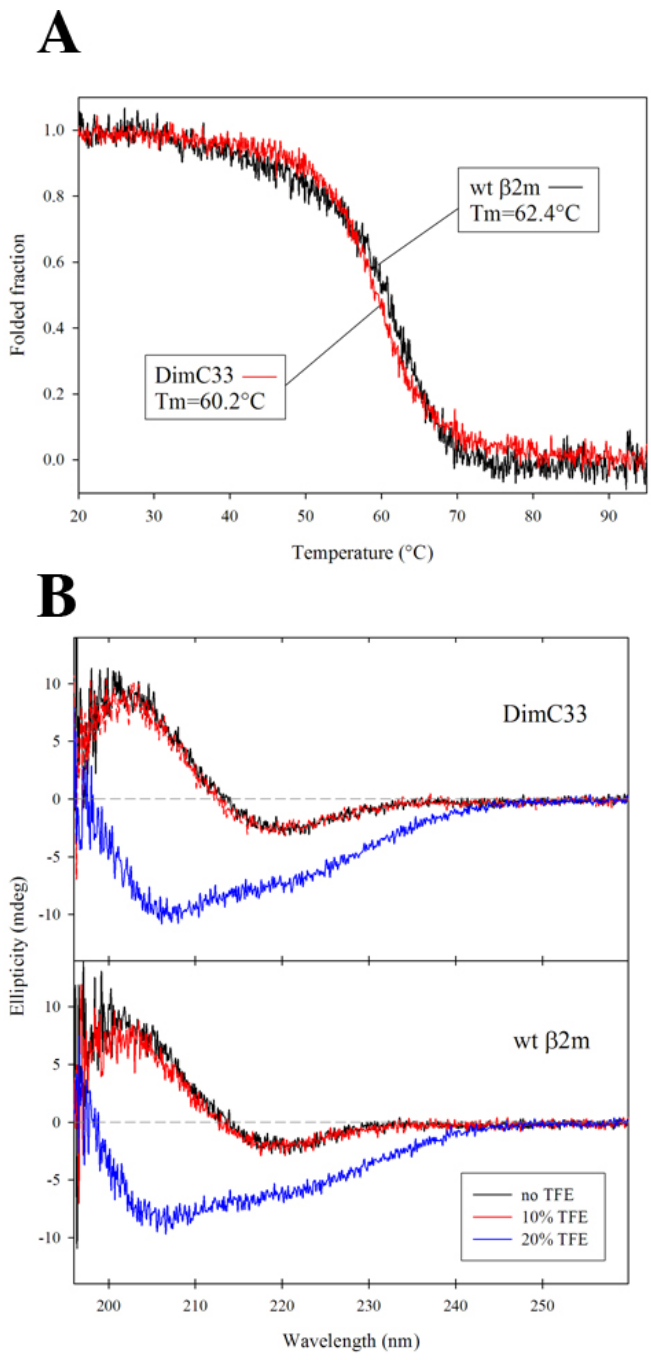

Figure 10. Thermodynamic stability and Far-UV spectra analysis by circular dichroism. (A) Temperature ramps for DimC33 in red and wt β2m in black, monitored at 202 nm, temperature slope 50 °C/h. The melting temperature I values for DimC33 and wt β2m are shown in the graph. **(B)** Far-UV spectra for DimC33 and wt β2m in a buffer containing 100 mM sodium chloride, 50 mM sodium phosphate buffer pH 7.4, recorded at three conditions: No TFE (black curves); in addition of 10% (v/v) TFE (red curves); and 20% (v/v) TFE (blue curves).

3.2.3 Aggregation kinetics of DimC33 and wt β2m in vitro

The kinetics of DimC33 aggregation was assessed *in vitro* under physiological pH conditions (pH 7.4), and in the absence of any pre-fibrillar seeds (which is strictly necessary for wt β2m aggregation under the same conditions). In 20% (v/v) TFE, a 1 mg mL^{-1} DimC33 aggregated aggressively, without an aggregation lag phase, reaching equilibrium within the first 4 hours, and triggering high ThT fluorescence binding signal; under the same conditions wt β2m remained soluble **(Fig. 11A).** Interestingly, in 10% (v/v) TFE—where DimC33 and wt β2m display CD spectra indicative of native secondary structures—a 5 mg mL^{-1} solution of DimC33 also aggregated triggering high ThT binding signal.

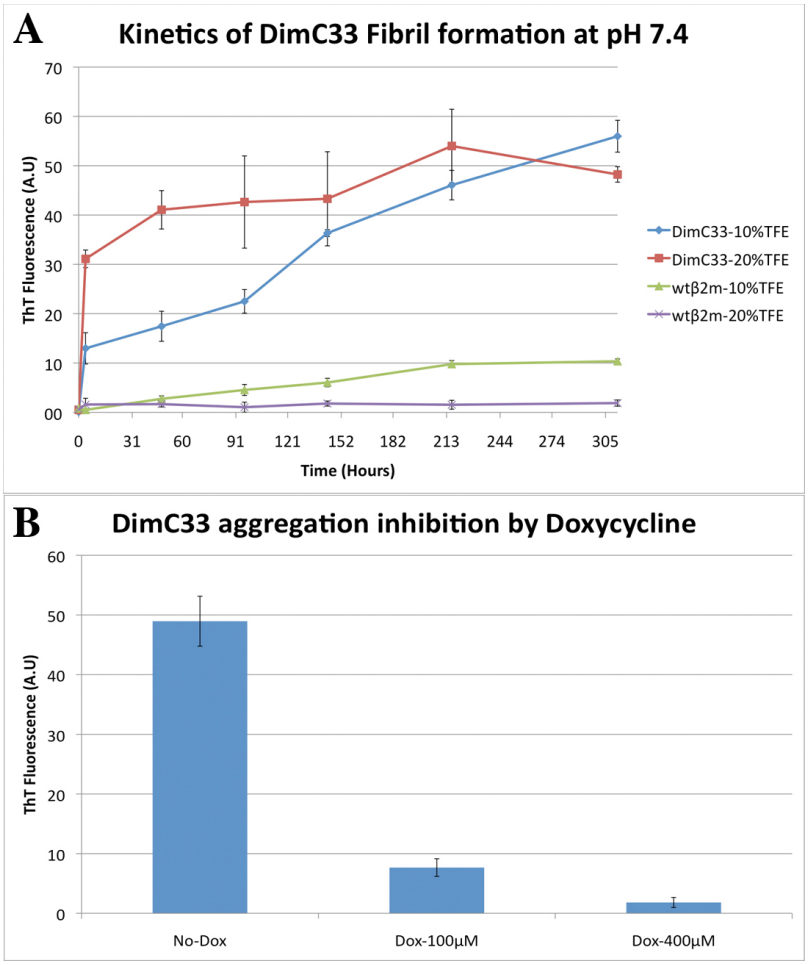

Figure 11. DimC33: fibrillogenesis at pH7.4. (A) Kinetics of DimC33 fibril formation in100mM NaCl, 50 mM Sodium phosphate buffer (pH 7.4) at 37°C incubation for two weeks, monitored by measuring ThT fluorescence signal at time (hours) 0, 4, 48, 96, 144, 216, 312. Four samples were screened: DimC33_20%TFE (5 mg mL^{-1} protein in 20% TFE); DimC33_10%TFE (1 mg mL^{-1} protein in 10% TFE); DimC33/wtβ2m mixture in 1:3 ratio (1 mg mL^{-1} protein mixture in 20% TFE); and wtβ2m_20%TFE as a control model (1 mg mL^{-1} protein in 20% TFE). Values represent the average of three independent experiments and error bars represent SD. **(B)** DimC33 aggregation inhibition analysis monitored by ThT fluorescence signal after one week of incubation at 37°C, using the same aggregation condition as DimC33_20%TFE in three conditions; No Doxycycline (control model), in the presence of 100 µM and 400µM Doxycycline. Values represent the average of three independent experiments and error bars represent SD.

The inhibitory effect of doxycycline on DimC33 aggregation—doxycycline is well-known to inhibit wt β_2m aggregation with an overall IC_{50} value of ~47 μM (*95*)—was assessed under the same DimC33_20%TFE aggregation condition, in the presence of 100 or 400μM doxycycline, and measuring the ThT binding signal after one week of incubation at 37°C. While, 100μM doxycycline was sufficient to inhibit DimC33 aggregation by approx. 85% compared with the control model of DimC33_20%TFE in the absence of any doxycycline; 400 μM doxycycline completely blocked DimC33 aggregation (**see Fig. 11B).**

3.2.4 X-ray crystal structures of DimC33

Two crystal structures of DimC33, displaying different space groups and crystal packings, were determined at 1.4Å and 1.9Å resolution, hereafter named DimC33_high and DimC33_low, respectively; additionally a crystal structure of DimC33 in complex with Thioflavin-T (ThT), was determined at 2.8Å resolution, and named DimC33_ThT. Data collection and refinement statistics for DimC33 crystal structures are shown in **Table II**.

Table II. Data collection and refinement statistics for DimC33.
Values in parenthesis are for the highest resolution shell.

	Structure (PDB entry)		
	DimC33-Low (4R9H)	DimC33-High (4RAH)	DimC33-ThT (4RA3)
Data collection			
Beam line	ID21-3 (ESRF)	ID21-3 (ESRF)	PETRA III, P13 (MX1)
Space Group	$P4_122$	$C222_1$	$P3_221$
Unit cell constants (Å)	a=68.84 b=68.84 c=200.04	a=32.35 b=47.70 c=119.65	a=80.04 b=80.04 c=177.70
Resolution (Å)	65.09 - 1.90 (2.00 - 1.90)	29.91 - 1.40 (1.42 - 1.40)	59.23 - 2.80 (2.95 -2.80)
R_{merge} [a](%)	10.9 (94.0)	6.5 (49.5)	5.9 (113.9)
I/sig(I)	12.4 (2.2)	10.9 (1.9)	21.4 (2.0)
Completeness (%)	99.9 (99.6)	98.7 (86.6)	100.0 (100.0)
Redundancy	8.9 (8.3)	4.5 (3.4)	9.6 (10.0)
Unique reflections	38985 (5533)	18491 (787)	16940 (2432)
Refinement			
R_{work} [b](%)	21.17	16.62	15.08
R_{free} [b](%)	24.73	20.94	18.12
Number of atoms	3480	1021	3407
Average B, all atoms ($Å^2$)	42.0	17.0	111.0
Ramachandran plot			
Most favored region	375 (98.68%)	86 (100%)	367 (94.83%)
Allowed region	4 (1.05%)	0 (0%)	20 (5.17%)
Outliers	1 (0.26%)	0 (0%)	0 (0%)

[a] R merge = $\sum_{hkl}$ I_{hkl} - < I_{hkl} > |/$\sum_{hkl}$ I_{hkl} where I is the observed intensity and < I > is the average intensity.
[b] R work = $\sum_{hkl}$Fo-Fc |/ $\sum_{hkl}$Fo for all data except 5% which were used for Rfree calculation.

The electron density in all three crystal structures is of excellent quality and all molecules are completely traceable. Overall, no major structural effects were observed on the β2m fold as a result of the S33C mutation, neither locally nor globally, in all DimC33 structures (**Fig. 12A, B)**. The monomeric components of DimC33 most closely match the assembled conformation of β2m within MHCI molecule, showing an average r.m.s.d value of 0.90 Å over all the 98 Cα atoms **(Table III).** The only noticeable difference is in the DE-loop

region (residues 57-60) where Trp60 participates in stacking interactions with Phe56 of the same chain and with His51 and Tyr66 of the opposing chain within DD dimer interface; the rotation of Tyr63 side chain of about 90 degrees is also observed as a result of the DE-loop conformational change (**see Fig 12C**).

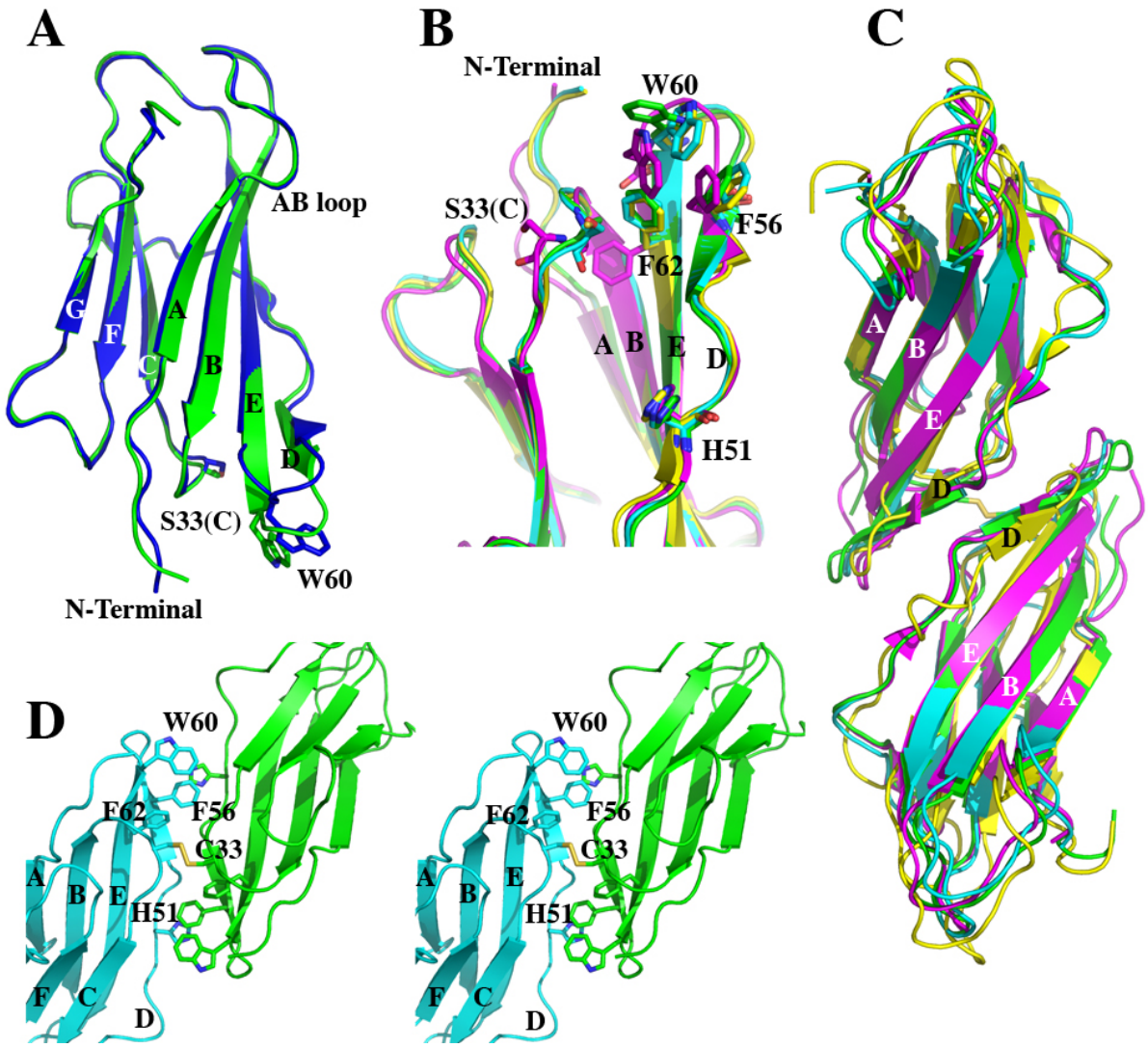

Figure 12. Crystal structure of DimC33 and DD strand interface. (A) Ribbon model of a monomeric of DimC33 (blue) superposed on the structure of wt β2m (green). β-strands are labeled according to standard nomenclature, Cys33 is shown in sticks. **(B)** A zoomed model into DD interface of four superposed crystal structures of DimC33_ThT (in green), hexameric structure of H13F β2m in magenta, DimC50 in cyan and DimC20 in yellow, showing some of the amino acid side chains located near DD interface as sticks model. **(C)** One moleculce of DimC33_ThT (pdb code: 4RA3) in green superposed with three reference models: hexameric structure of H13F β2m in magenta (pdb code:3CIQ), DimC50 structure in cyan (pdb code: 3TM6), and DimC20 structure in yellow (pdb code: 3TLR). **(D)** Stereo view of the DD strand interface formed by the facing molecules as observed in the structure of DimC33_high. The main residues involved in the interface are labeled.

The overall organization of β2m chains within the covalent dimer, in all three DimC33 structures, was well conserved showing averaged r.m.s.d values of 0.57Å/195Cα and 1.17Å/195Cα for DimC33_high superposed on DimC33_ThT, and DimC33_low, respectively. The superposition of DimC33 structures with previously reported β2m variants

(pdb codes: 3TLR, 3TM6, 3CIQ) show similar arrangement of β2m molecules that are associated through formation of the DD strands interface **(Fig. 12C and Table III).**

Table III. The SSM superimposed RMS deviations for DimC33 structures with reference models DimC20, DimC50, hexameric H13F β2m and wt β2m.

	DimC20 (3TLR)	DimC50 (3TM6)	H13F β2m (3CIQ)	wt β2m (1JF1)
DimC33-High(Mono)	0,62/99 Cα	0,59/98 Cα	1,05/97 Cα	0,97/98 Cα
DimC33-High	2,41/182Cα	2,10/192Cα	1,11/192Cα	---

The covalent DD strand interface is structurally well conserved in all three DimC33 structures, where it maintains the same contact surface area of ~ 560 $Å^2$: the main regions involved in the association interface are the BC-loop (residues 31-37), part of D-strand (residues 51-57), the DE-loop (residues 57-60), Phe62 and part of E-strand (residues 64 and 66), which is in agreement with the previous structures of β2m variants (pdb codes: 3TLR, 3TM6, 3CIQ) **(Fig. 12B,D).** The above data indicate that the S33C mutation and the resulting disulfide-linked homodimer maintain native β2m fold, and that the created DD strand interface exhibits very similar intermolecular interactions compared to previous crystal structures of monomeric β2m variants (pdb codes: 3TLR, 3TM6, 3CIQ) (**Fig. 12B, D)**.

3.2.5 The DimC33_ThT complex and the ABDE sheet

The crystal structure of DimC33_ThT was obtained in the presence of 5mM ThT; the asymmetric unit (AU) contained five ThT molecules anchored in two different binding sites formed between two interacting DimC33 molecules **(Fig. 13A).**

In the crystal structure of DimC33_ThT, β2m molecules belonging to different homodimers interact exclusively via two sets of ABDE β-sheet interfaces, creating two distinct ThT binding sites: on one hand, four ThT molecules are wedged between the ABDE β-sheets of two facing β2m molecules (4ThT site) by establishing mutual π-π stacking interactions, and with Tyr10 and Tyr63 of two facing β2m molecules **(Fig. 13C)**; Tyr26 residues from both β2m molecules also help accommodate the ThT hydrophobic rings. On the other, only one ThT molecule is sandwiched between two Tyr10 residues in the ABDE sheets interface of two facing β2m molecules **(Fig. 13B);** Tyr26 and Pro14 from both molecules establish van der Waals contacts with ThT. The binding of ThT does not induce any conformational adjustments in the β2m fold, nor in the DimC33 assembly.

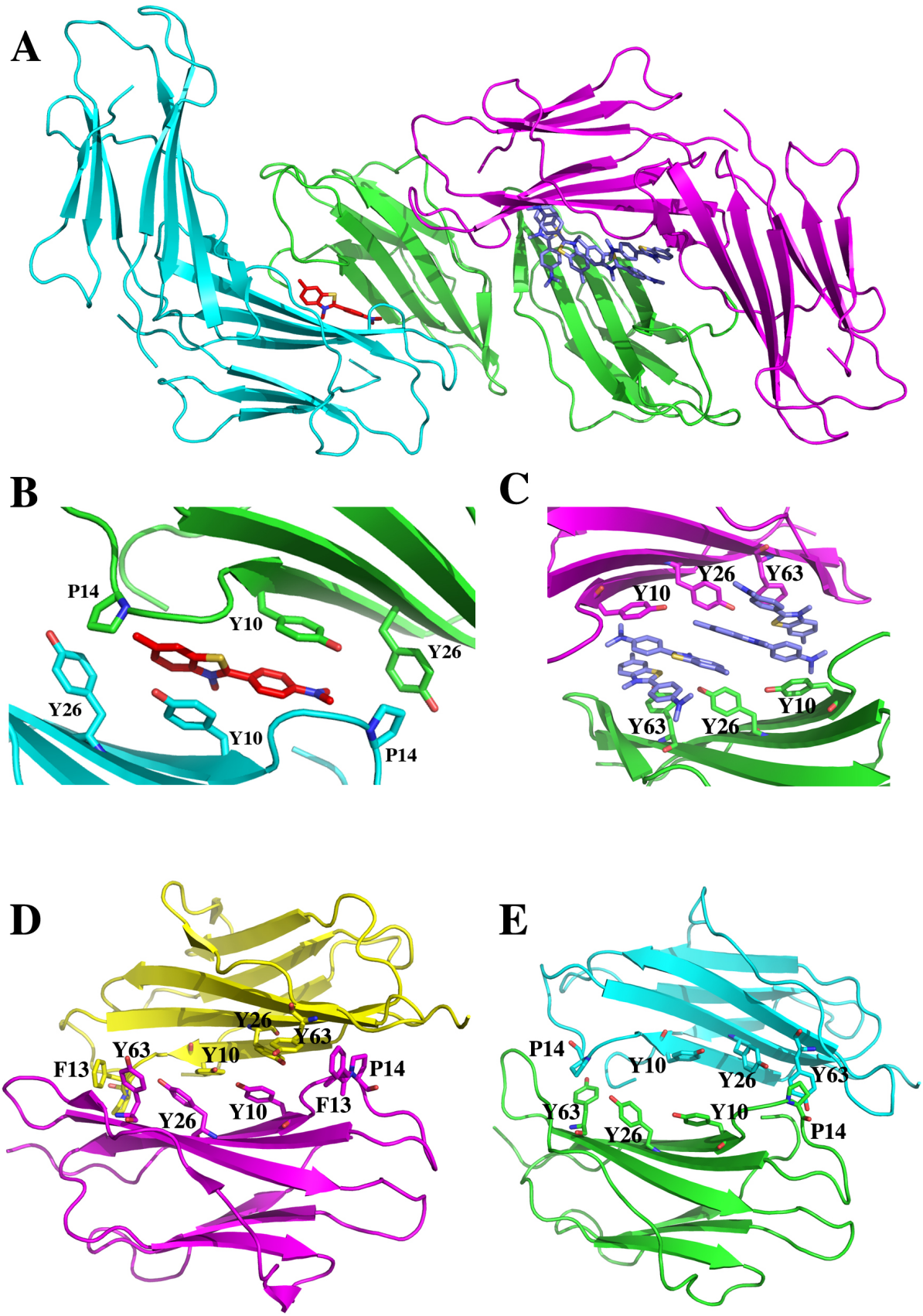

Figure 13. Crystal structures of DimC33_ThT and DimC33_low. (A) Cartoon representation of DimC33 assembly in crystal structure of DimC33_ThT. The three DimC33 colored in cyan, green and magenta. Two ThT binding sites are visible: on the left the four ThT molecules (4ThT site) are colored in slate-blue; while on the right side, one ThT molecule (1ThT site) is colored in red. **(B)** A zoomed representation into 1ThT site showing ThT molecule sandwiched between the ABDE sheets of the two adjacent DimC33. **(C)** A zoomed representation

into 4ThT site where four molecules of ThT in slate-blue are stacked between two facing ABDE sheets. **(D)** Ribbon represenation of ABDE interface as found in the hexameric structure of H13F β2m (pdb code: 3CIQ). **(E)** Ribbon represenation of ABDE interface present in the DimC33_low (pdb code : 4R9H).

The two ThT binding sites share common similarities in the mode of β2m/ThT interaction: in both cases, three aromatic residues (Tyr10, Tyr26 and Tyr63) play a key role in creating the ABDE sheet interface (the ThT binding cavity) built by two facing β2m chains; in particular, Tyr10 establishes direct stacking interactions with ThT molecules at both interaction sites.

A similar ABDE β-sheet interface is also observed in the absence of ThT: in the DimC33_low structure and in the hexameric β2m structure (*50*), highly hydrophobic ABDE interfaces are formed with a surface area of 805 and 970 $Å^2$, respectively. Although the two facing β2m molecules are differently oriented in the two structures, the ABDE interfaces are highly comparable where the aromatic residues of Tyr10, Tyr26 and Tyr63 form the hydrophobic core interface **(see Fig. 13D, E)**. Thus, the four ABDE interfaces found in 1ThT and 4ThT sites of DimC33_ThT, in DimC33_low and in the hexameric structure of H13F β2m (pdb code:3CIQ) strongly point at this sheet as privileged site for interaction during oligomer formation.

All the experiments and results presented under the Section 3.2 are summarized in a manuscript that is under submission at the time of presenting this Thesis work, and can be found in **Part III** of this Thesis: Halabelian *et al.* "A covalent homodimer to probe the first oligomers along amyloid aggregation" (2014).

4. CONCLUSIONS AND FUTURE PERSPECTIVES

4.1 MHCI: the Trojan horse for secretion of amyloidogenic β2m

Unlike DRA, which is caused by elevated serum concentration of free circulating wt β2m in patients with kidney failure, the hereditary systemic amyloidosis is caused by an extremely amylodogenic D76N β2m variant that aggregates in a completely physiological serum concentration and functional kidney conditions (*89*). Although human cells adopt sophisticated and potent systems to control and eliminate partially folded or misfolded proteins (*96*), the D76N β2m variant manages to escape the cellular quality control systems, reaching the extracellular blood circulation where it aggregates by forming huge amyloid deposits (*89*). It is known that once β2m is synthesized in the cell, it is promptly transported by specific transporter proteins into the Golgi apparatus, where it is assembled into a mature MHCI molecule and transported to the cell surface (*24*). In this way, the amyloidogenic D76N β2m variant has only a very brief intracellular existence as an isolated chain.

Our data show that despite the monomeric D76N β2m variant is highly unstable and aggregation prone compared to wt β2m, they both have similar structures, stability and dynamics once assembled within the MHCI molecules. In other words, the MHCI acts as a chaperone to stabilize the D76N β2m variant and protect the cell from D76N β2m aggregation. However, in fulfilling such a role, the MHCI molecules mask and hide the amyloidogenic properties of the D76N variant from the UPR and other cellular quality control systems, leading to the secure transfer to the cellular surface, where during its normal turnover, the MHCI molecules dissociate, releasing β2m and the carried antigen in the extracellular environment. Hence, MHCI molecules act as a Trojan horse for translocation of the D76N β2m variant outside the cell, where the D76N variant aggregates and causes human pathologies.

In this study, we show that the amyloidogenic D76N β2m variant is efficiently stabilized and maintained in its normal structural and physiological properties once assembled within MHCI molecules. Such finding may open new therapeutic approaches for targeting the D76N variant by specific antibodies (77), or small molecules (84), to stabilize and inhibit its aggregation. Finally, the mouse model expressing the D76N variant will serve as a development tool for future studies on systemic amyloidosis, and for testing new therapeutic approaches against D76N β2m dependent systemic amyloidosis.

4.2 A covalent homodimer to probe early oligomers along amyloid aggregation

Oligomeric species generated along the formation of amyloid fibrils are shown to be responsible for cellular cytotoxicity in amyloid-related diseases (*1*). Elucidating the interfaces involved in oligomerization, at molecular level, is of paramount importance for a clear understanding of the aggregation processes that lead to the design/discovery of potential drug targets for therapeutic intervention. In this study, we used β2m as a model to study the interfaces involved in the formation of toxic oligomeric species in DRA. We designed a covalently-linked homodimers of S33C β2m variant to interact via anti-parallel DD strand interface; such interface was previously reported as a favorable interaction site in three independent crystal structures of β2m variants (*50, 94*).

Our results demonstrate that DimC33 is highly amyloidogenic compared to wt β2m, that aggregates in the absence of amyloid seeds in *in vitro* conditions, even though its thermodynamic stability and its structure are virtually identical to those of the wt protein, suggesting that the DD interface could represent the first interaction site favoring oligomerisation and aggregation. Furthermore, DimC33 also aggregates in 10% 2,2,2,-Trifluoroethanol—a condition where β2m fold is still native—indicating that DimC33 can spontaneously form the on-pathway oligomeric species required for fibrillogenesis **(Fig. 10B)**. Similarly to wt β2m (*84*), DimC33 aggregation is inhibited by comparable amounts of doxycycline, suggesting that similar interfaces are involved in both DimC33 and wt β2m oligomerisation and aggregation mechanisms.

Moreover, DimC33 molecules bind Thioflavin-T (ThT)—which is the most widely used fluorescent dye for selective detection of cross-β structures in amyloid fibrils—at an intermolecular interface formed by the ABDE β-sheets of two facing β2m chains belonging to different DimC33 moeties, which provides further evidence on oligomeric interaction sites in β2m aggregation and ThT binding. Only one oligomeric β2m structure that binds ThT has been reported so far (pdb code: 3MZT), which presents severe technical issues (*72*). Therefore, the DimC33_ThT structure reported here, adds substantial information on the molecular mechanisms of ThT binding to amyloidogenic proteins. Given the fact that many small molecule inhibitors of amyloids share common chemical and structural characteristics with the ThT molecule (*88*), then the ThT binding site shown in the crystal structure of DimC33_ThT provides, for the first time, a potential site for targeting drugs against the toxic oligomers.

Finally, an extended ABDE interface of two facing β2m molecules was also observed also in the absence of ThT, in our crystal structure of DimC33_low **(Fig. 13D)** and in the hexameric β2m structure **(Fig. 13E)** reported earlier (*97*), suggesting that the ABDE β-sheet interface could represent a second interface involved in β2m oligomerization. The structural and biophysical analysis of DimC33 reported here give strong clues on how oligomerization may proceed during aggregation: (i) the first dimeric species would be built across the DD strand interface, (ii) the ABDE β-sheets of β2m homodimers will then serve as a second sticky interface leading to the formation of various toxic oligomeric species that would serve as building blocks for amyloid fibril formation.

5. REFERENCES

1. Chiti, F., and Dobson, C. M. (2006) Protein misfolding, functional amyloid, and human disease, *Annu Rev Biochem 75*, 333-366.
2. Eisenberg, D., and Jucker, M. (2012) The amyloid state of proteins in human diseases, *Cell 148*, 1188-1203.
3. Chapman, M. R., Robinson, L. S., Pinkner, J. S., Roth, R., Heuser, J., Hammar, M., Normark, S., and Hultgren, S. J. (2002) Role of Escherichia coli curli operons in directing amyloid fiber formation, *Science 295*, 851-855.
4. Kenney, J. M., Knight, D., Wise, M. J., and Vollrath, F. (2002) Amyloidogenic nature of spider silk, *Eur J Biochem 269*, 4159-4163.
5. Berson, J. F., Theos, A. C., Harper, D. C., Tenza, D., Raposo, G., and Marks, M. S. (2003) Proprotein convertase cleavage liberates a fibrillogenic fragment of a resident glycoprotein to initiate melanosome biogenesis, *J Cell Biol 161*, 521-533.
6. Astbury, W. T., Dickinson, S., and Bailey, K. (1935) The X-ray interpretation of denaturation and the structure of the seed globulins, *Biochem J 29*, 2351-2360 2351.
7. Naiki H, Higuchi K, Matsushima K, Shimada A, Chen WH, Hosokawa M, and T, T. (1990) Fluorometric examination of tissue amyloid fibrils in murine senile amyloidosis: use of the fluorescent indicator, thioflavine T, *Lab Invest 62*, 768-774.
8. Naiki H, Higuchi K, Hosokawa M, and Takeda T. (1989) Fluorometric determination of amyloid fibrils in vitro using the fluorescent dye, thioflavin T1, *Analitical Biochemistry 177*.
9. Assenat H, Calemard E, Charra B, Laurent G, Terrat JC, and Vanel T. (1980) Hemodialyse: Syndrome du canal carpien et substance amyIoide. , *Nouv Presse Méd 24*, 1715.
10. Gejyo, F., Yamada, T., Odani, S., Nakagawa, Y., Arakawa, M., Kunitomo, T., Kataoka, H., Suzuki, M., Hirasawa, Y., Shirahama, T., and et al. (1985) A new form of amyloid protein associated with chronic hemodialysis was identified as beta 2-microglobulin, *Biochem Biophys Res Commun 129*, 701-706.
11. Gejyo, F., Odani, S., Yamada, T., Honma, N., Saito, H., Suzuki, Y., Nakagawa, Y., Kobayashi, H., Maruyama, Y., Hirasawa, Y., and et al. (1986) Beta 2-microglobulin: a new form of amyloid protein associated with chronic hemodialysis, *Kidney Int 30*, 385-390.
12. Gorevic PD, Munoz PC, Casey TT, DiRaimondo CR, Stone WJ, Prelli FC, Rodrigues MM, Poulik MD, and Frangione B. (1986) Polymerization of intact beta 2-microglobulin in tissue causes amyloidosis in patients on chronic hemodialysis., *Proc Natl Acad Sci U S A. 83*, 7908-7912.
13. Vincent C, and Revillard JP. (1990) Serum levels and urinary excretion of B2m in patients under hemodialysis or after renal transplantation *Acta Clin Belg 25*, 31-39.
14. Miyata T, Jadoul M, Kurokawa K, and DeStrihou CVY. (1998) B-2 Microglobulin in Renal Disease, *J Am Soc Nephrol 9*, 1723-1735.
15. Biancalana M, and Koide S. (2010) Molecular Mechanism of Thioflavin-T Binding to Amyloid Fibrils, *Biochem Biophys Acta. 1804*, 1405-1412.
16. Stroud, J. C., Liu, C., Teng, P. K., and Eisenberg, D. (2012) Toxic fibrillar oligomers of amyloid-beta have cross-beta structure, *Proc Natl Acad Sci U S A 109*, 7717-7722.

17. Hodkinson JP, Ashcroft AE, and Radford SE. (2012) Protein Misfolding and Toxicity in Dialysis-Related Amyloidosis, in *Non-fibrillar Amyloidogenic Protein Assemblies - Common Cytotoxins Underlying Degenerative Diseases* (Farid Rahimi, G. B., Ed.), pp 377-405, Springer Netherlands.
18. Myers SL, Jones S, Jahn TR, Morten IJ, Tennent GA, Hewitt EW, and Radford SE. (2006) A Systematic Study of the Effect of Physiological Factors on B2-Microglobulin
Amyloid Formation at Neutral pH, *Biochemistry 45*, 2311-2321.
19. Esposito G, Michelutti R, Verdone G, Viglino P, Hernandez H, Robinson CV, Amoresano A, Dal Piaz F, Monti M, Pucci P, Mangione P, Stoppini M, Merlini G, Ferri G, and Bellotti V. (2000) Removal of the N-terminal hexapeptide from human beta2-microglobulin facilitates protein aggrega- tion and fibril formation., *Protein Sciences 9*, 831-845.
20. Eakin CM, Knight JD, Morgan CJ, Gelfand MA, and Miranker AD. (2002) Formation of a copper specific binding site in non-native states of beta-2-microglobulin., *Biochemistry 41*, 10646-10656.
21. Yamamoto S, Yamaguchi I, Hasegawa K, Tsutsumi S, Goto Y, Gejyo F, and Naiki H. (2004) Glycosaminoglycans enhance the trifluoroethanol-induced extension of beta 2-microglobulin-related amyloid fibrils at a neutral pH., *J. Am. Soc. Nephrol. 15*, 126-133.
22. Relini A, De Stefano S, Torrassa S, Cavalleri O, Rolandi R, Gliozzi A, Giorgetti S, Raimondi S, Marchese L, Verga L, Rossi A, Stoppini M, and Bellotti V. (2008) Heparin strongly enhances the formation of beta2-microglobulin amyloid fibrils in the presence of type I collagen., *J Biol Chem. 283*, 4912-4920.
23. Giorgetti, S., Rossi, A., Mangione, P., Raimondi, S., Marini, S., Stoppini, M., Corazza, A., Viglino, P., Esposito, G., Cetta, G., Merlini, G., and Bellotti, V. (2005) Beta2-microglobulin isoforms display an heterogeneous affinity for type I collagen, *Protein Sci 14*, 696-702.
24. York, I. A., and Rock, K. L. (1996) Antigen processing and presentation by the class I major histocompatibility complex, *Annu Rev Immunol 14*, 369-396.
25. Bennett, M. J., Lebron, J. A., and Bjorkman, P. J. (2000) Crystal structure of the hereditary haemochromatosis protein HFE complexed with transferrin receptor, *Nature 403*, 46-53.
26. Pamer, E., and Cresswell, P. (1998) Mechanisms of MHC class I--restricted antigen processing, *Annu Rev Immunol 16*, 323-358.
27. Floege, J., Bartsch, A., Schulze, M., Shaldon, S., Koch, K. M., and Smeby, L. C. (1991) Clearance and synthesis rates of beta 2-microglobulin in patients undergoing hemodialysis and in normal subjects, *J Lab Clin Med 118*, 153-165.
28. Bernier GM, and Conrad ME. (1969) Catabolism of B2-microgIobulin by the rat kidney., *Am J Physiol 217*, 1350-1362.
29. Iwata K, Matsuura T, Sakurai K, Nakagawa A, and Goto Y. (2007) High-resolution crystal structure of beta2-microglobulin formed at pH 7.0., *J Biochem 142*, 413-419.
30. Bellotti V, Stoppini M, Mangione P, Sunde M, Robinson C, Asti L, Brancaccio D, and Ferri G. (1998) Beta2-microglobulin can be refolded into a native state from ex vivo amyloid fibrils., *Eur J Biochem. 258*, 61-67.
31. Hong DP, Gozu M, Hasegawa K, Naiki H, and Goto Y. (2002) Conformation of beta 2-microglobulin amyloid fibrils analyzed by reduction of the disulfide bond., *J Biol Chem 277*, 21554-21560.

32. Smith DP, and Radford SE. (2001) Role of the single disulphide bond of ’ 2-microglobulin in amyloidosis in vitro, *Protein Sciences 10*, 1775-1784.
33. Verdone, G., Corazza, A., Viglino, P., Pettirossi, F., Giorgetti, S., Mangione, P., Andreola, A., Stoppini, M., Bellotti, V., and Esposito, G. (2002) The solution structure of human beta2-microglobulin reveals the prodromes of its amyloid transition, *Protein Sci 11*, 487-499.
34. Becker JW, and Reeke GNJr. (1985) Three-dimensional structure of beta2-microglobulin., *Proc Natl Acad Sci USA 82*.
35. Sliz P, Michielin O, Cerottini JC, Luescher I, Romero P, Karplus M, and DC., W. (2001) Crystal structures of two closely related but antigenically distinct HLA-A2/melanocyte-melanoma tumor-antigen peptide complexes., *J Immunol 167*, 3276-3284.
36. Hodkinson JP, Radford SE, and Ashcroft AE. (2012) The role of conformational flexibility in β2-microglobulin amyloid fibril formation at neutral pH., *Rapid Commun Mass Spectrom. 26*, 1783-1792.
37. Hee CS, Beerbaum M, Loll B, Ballaschk M, Schmieder P, Uchanska-Ziegler B, and Ziegler A. (2013) Dynamics of free versus complexed β2-microglobulin and the evolution of interfaces in MHC class I molecules., *Immunogenetics 65*, 157-172.
38. Santambrogio C, Ricagno S, Colombo M, Barbiroli A, Bonomi F, Bellotti V, Bolognesi M, and Grandori R. (2010) DE-loop mutations affect B2 microglobulin stability, oligomerization, and the low-pH unfolded form. , *Protein Sciences 19*, 1386-1394.
39. Ricagno S, Colombo M, DeRosa M, Sangiovanni E, Giorgetti S, Raimondi S, Bellotti V, and Bolognesi M. (2008) DE loop mutations affect beta2-microglobulin stability and amyloid aggregation., *Biochem Biophys Res Commun. 377*, 146-150.
40. Eichner T, Kalverda AP, Thompson GS, Homans SW, and SE., R. (2011) Conformational conversion during amyloid formation at atomic resolution., *Molecular Cell 41*, 161-172.
41. Kihara M, Chatani E, Iwata K, Yamamoto K, Matsuura T, Nakagawa A, Naiki H, and Goto Y. (2006) Conformation of amyloid fibrils of beta2-microglobulin probed by tryptophan mutagenesis., *J Biol Chem. 281*, 31061-31069.
42. Esposito, G., Ricagno, S., Corazza, A., Rennella, E., Gumral, D., Mimmi, M. C., Betto, E., Pucillo, C. E., Fogolari, F., Viglino, P., Raimondi, S., Giorgetti, S., Bolognesi, B., Merlini, G., Stoppini, M., Bolognesi, M., and Bellotti, V. (2008) The controlling roles of Trp60 and Trp95 in beta2-microglobulin function, folding and amyloid aggregation properties, *J Mol Biol 378*, 887-897.
43. Chiti F, Mangione, P., Andreola, A., Giorgetti, S., Stefani, M., Dobson, C. M., Bellotti, V., and Taddei, N. (2001) Detection of two partially structured species in the folding process of the amyloidogenic protein beta 2-microglobulin., *J Mol Biol. 307*, 379-391.
44. Chiti F, D. L. E., Grossi S, Mangione P, Giorgetti S, Caccialanza G, Dobson CM, Merlini G, Ramponi G, Bellotti V. (2001) A partially structured species of beta 2-microglobulin is significantly populated under physiological conditions and involved in fibrillogenesis., *J Biol Chem. 276*, 46714-46721.
45. Jahn TR, P. M., Homans SW, Radford SE. (2006) Amyloid formation under physiological conditions proceeds via a native-like folding intermediate., *Nat Struct Mol Biol. 13*, 195-201.
46. Kameda A, H. M., Higurashi T, Takahashi S, Naiki H, Goto Y. (2005) Nuclear magnetic resonance characterization of the refolding intermediate of beta2-microglobulin trapped by non-native prolyl peptide bond., *J Mol Biol. 348*, 383-397.

47. Torbeev VY, H. D. (2013) Both the cis-trans equilibrium and isomerization dynamics of a single proline amide modulate β2-microglobulin amyloid assembly., *Proc Natl Acad Sci U S A. 110*, 20051-20056.
48. Rennella, E., Cutuil, T., Schanda P., Ayala, I., Gabel, F., Forge, V., Corazza, A., Esposito, G., and Brutscher, B. (2013) Oligomeric States along the Folding Pathways of β2-Microglobulin: Kinetics, Thermodynamics, and Structure, *J. Mol. Biol. 425*, 2722-2736.
49. Colombo M, D. M., Bellotti V, Ricagno S, Bolognesi M. . (2012) A recurrent D-strand association interface is observed in b-2 microglobulin oligomers, *FEBS Journal 279*, 1131-1143.
50. Calabrese MF, Eakin CM, Wang JM, and Miranker AD. (2008) A regulatable switch mediates self-association in an immunoglobulin fold, *Nat Struct Mol Biol. 15*, 965-971.
51. Fogolari F, C. A., Viglino P, Zuccato P, Pieri L, Faccioli P, Bellotti V, Esposito G. (2007) Molecular dynamics simulation suggests possible interaction patterns at early steps of beta2-microglobulin aggregation., *Biophys J. 92*, 1673-1681.
52. Miura Y, I. T., Inomata A, Takeda T, Senma S, Okuyama K, Suzuki Y. (1992) Radiolucent bone cysts and the type of dialysis membrane used in patients undergoing long-term hemodialysis., *Nephron. 60*, 268-273.
53. van Ypersele de Strihou C, J. M., Malghem J, Maldague B, Jamart J. (1991) Effect of dialysis membrane and patient's age on signs of dialysis-related amyloidosis. The Working Party on Dialysis Amyloidosis., *Kidney Int. 39*, 1012-1019.
54. Morgan CJ, G. M., Atreya C, Miranker AD. (2001) Kidney dialysis-associated amyloidosis: a molecular role for copper in fiber formation., *J Mol Biol. 309*, 339-345.
55. Eakin CM, A. F., Morgan CJ, Miranker AD. (2004) Oligomeric assembly of native-like precursors precedes amyloid formation by beta-2 microglobulin., *Biochemistry 43*, 7808-7815.
56. Eakin CM, M. A. (2005) From chance to frequent encounters: origins of beta2-microglobulin fibrillogenesis., *Biochim Biophys Acta. 1753*, 92-99.
57. Antwi K, Mahar M, Srikanth R, Olbris MR, Tyson JF, and Vachet RW. (2008) Cu(II) organizes beta-2-microglobulin oligomers but is released upon amyloid formation., *Protein Sciences 17*, 748-759.
58. Giorgetti S, R. A., Mangione P, Raimondi S, Marini S, Stoppini M, Corazza A, Viglino P, Esposito G, Cetta G, Merlini G, Bellotti V. (2005) Beta2-microglobulin isoforms display an heterogeneous affinity for type I collagen., *Protein Sciences 14*, 696-702.
59. Eichner T, and SE., R. (2009) A generic mechanism of beta2-microglobulin amyloid assembly at neutral pH involving a specific proline switch., *J Mol Biol. 386*, 1312-1326.
60. Karamanos TK, K. A., Thompson GS, Radford SE. (2014) Visualization of transient protein-protein interactions that promote or inhibit amyloid assembly., *Mol Cell. 55*, 214-226.
61. Smith DP, J. S., Serpell LC, Sunde M, Radford SE. (2003) A systematic investigation into the effect of protein destabilisation on beta 2-microglobulin amyloid formation., *J Mol Biol. 330*, 943-954.
62. McParland VJ, K. N., Kalverda AP, Brown A, Kirwin-Jones P, Hunter MG, Sunde M, Radford SE. (2000) Partially unfolded states of beta(2)-microglobulin and amyloid formation in vitro., *Biochemistry 39*, 8735-8746.

63. Naiki H, H. N., Suzuki S, Kimura H, Nakakuki K, and Gejyo F. (1997) Establishment of a kinetic model of dialysis-related amyloid fibril exten- sion in vitro. , *Amyloid: Int. J. Expt. Clin. Invest. 4*, 223-232.
64. Smith AM, J. T., Ashcroft AE, Radford SE. (2006) Direct observation of oligomeric species formed in the early stages of amyloid fibril formation using electrospray ionisation mass spectrometry., *J Mol Biol. 364*, 9-19.
65. Santambrogio, C., Ricagno, S., Sobott, F., Colombo, M., Bolognesi, M., and Grandori, R. (2011) Characterization of beta2-microglobulin conformational intermediates associated to different fibrillation conditions, *J Mass Spectrom 46*, 734-741.
66. Relini A, C. C., De Stefano S, Rolandi R, Giorgetti S, Stoppini M, Rossi A, Fogolari F, Corazza A, Esposito G, Gliozzi A, Bellotti V. (2006) Collagen plays an active role in the aggregation of beta2-microglobulin under physiopathological conditions of dialysis-related amyloidosis., *J biol Chem. 281*, 16521-16529.
67. Kirkitadze MD, B. G. a. T. D. (2002) Paradigm Shifts in Alzheimer's Disease and Other Neurodegenerative Disorders: The Emerging Role of Oligomeric Assemblies, *Journal of Neuroscience Research 69*, 567-577.
68. Morris, A. M. (2009) Protein aggregation kinetics, mechanism, and curve-fitting: A review of the literature, *Biochimica et Biophysica Acta*.
69. White HE, H. J., Jahn TR, Cohen-Krausz S, Gosal WS, Müller S, Orlova EV, Radford SE, Saibil HR. (2009) Globular tetramers of beta(2)-microglobulin assemble into elaborate amyloid fibrils., *J Mol Biol. 389*, 48-57.
70. Smith DP, Woods LA, Radford SE, and Ashcroft AE. (2011) Structure and dynamics of oligomeric intermediates in β2-microglobulin self-assembly., *Biophys J. 101*, 1238-1247.
71. Eakin CM, B. A., Miranker AD. (2006) A native to amyloidogenic transition regulated by a backbone trigger., *Nat Struct Mol Biol. 13*, 202-208.
72. Wolfe, L. S., Calabrese, M. F., Nath, A., Blaho, D. V., Miranker, A. D., and Xiong, Y. (2010) Protein-induced photophysical changes to the amyloid indicator dye thioflavin T, *PNAS 107*, 16863-16868.
73. Eichner T, and SE., R. (2011) Understanding the complex mechanisms of β2-microglobulin amyloid assembly, *FEBS J. 278*, 3868-3883.
74. Mendoza VL, V. R. (2009) Probing protein structure by amino acid-specific covalent labeling and mass spectrometry., *Mass Spectrom Rev. 28*, 785-815.
75. Mendoza VL, A. K., Barón-Rodríguez MA, Blanco C, Vachet RW. (2010) Structure of the preamyloid dimer of beta-2-microglobulin from covalent labeling and mass spectrometry., *Biochemistry 49*, 1522-1532.
76. Mendoza VL, B.-R. M., Blanco C, Vachet RW. (2011) Structural insights into the pre-amyloid tetramer of β-2-microglobulin from covalent labeling and mass spectrometry., *Biochemistry 50*, 6711-6722.
77. Domanska, K., Vanderhaegen, S., Srinivasan, V., Pardon, E., Dupeux, F., Marquez, J. A., Giorgetti, S., Stoppini, M., Wyns, L., Bellotti, V., and Steyaert, J. (2011) Atomic structure of a nanobody-trapped domain-swapped dimer of an amyloidogenic beta2-microglobulin variant, *Proc Natl Acad Sci U S A 108*, 1314-1319.
78. Domanska K, V. S., Srinivasan V, Pardon E, Dupeux F, Marquez JA, Giorgetti S, Stoppini M, Wyns L, Bellotti V, Steyaert J. (2010) Atomic structure of a nanobody-trapped domain-swapped dimer of an amyloidogenic β2-microglobulin variant, *PNAS 108*, 1314-1319.

79. Liu C, S. M., Eisenberg D. (2011) β_2-microglobulin forms three-dimensional domain-swapped amyloid fibrils with disulfide linkages., *Nat Struct Mol Biol. 18*, 49-55.
80. Woods, L. A., Platt, G. W., Hellewell, A. L., Hewitt, E. W., Homans, S. W., Ashcroft, A. E., and Radford, S. E. (2011) Ligand binding to distinct states diverts aggregation of an amyloid-forming protein, *Nat Chem Biol 7*, 730-739.
81. Brancolini G, Toroz D, and Corni S. (2014) Can small hydrophobic gold nanoparticles inhibit β_2-microglobulin fibrillation?, *Nanoscale 6*, 7903-7911.
82. Sultan, A., Raman, B., Rao Ch, M., and Tangirala, R. (2013) The extracellular chaperone haptoglobin prevents serum fatty acid-promoted amyloid fibril formation of beta2-microglobulin, resistance to lysosomal degradation, and cytotoxicity, *J Biol Chem 288*, 32326-32342.
83. Härd T, L. C. (2012) Inhibition of amyloid formation., *J Mol Biol. 421*, 441-465.
84. Giorgetti, S., Raimondi, S., Pagano, K., Relini, A., Bucciantini, M., Corazza, A., Fogolari, F., Codutti, L., Salmona, M., Mangione, P., Colombo, L., De Luigi, A., Porcari, R., Gliozzi, A., Stefani, M., Esposito, G., Bellotti, V., and Stoppini, M. (2011) Effect of tetracyclines on the dynamics of formation and destructuration of beta2-microglobulin amyloid fibrils, *J Biol Chem 286*, 2121-2131.
85. Giorgetti S, R. S., Pagano K, Relini A, Bucciantini M, Corazza A, Fogolari F, Codutti L, Salmona M, Mangione P, Colombo L, De Luigi A, Porcari R, Gliozzi A, Stefani M, Esposito G, Bellotti V, Stoppini M. (2011) Effect of tetracyclines on the dynamics of formation and destructuration of beta2-microglobulin amyloid fibrils., *J Biol Chem. 286*, 2121-2131.
86. Fogolari F, C. A., Varini N, Rotter M, Gumral D, Codutti L, Rennella E, Viglino P, Bellotti V, Esposito G. (2010) Molecular dynamics simulation of β_2-microglobulin in denaturing and stabilizing conditions., *Proteins 79*, 986-1001.
87. Montagna G, C. B., Obici L, Uggetti C, Giorgetti S, Porcari R, Ruggiero R, Mangione PP, Brambilla M, Lucchetti J, Guiso G, Gobbi M, Merlini G, Salmona M, Stoppini M, Villa G, Bellotti V. (2013) Benefit of doxycycline treatment on articular disability caused by dialysis related amyloidosis., *Amyloid 20*, 173-178.
88. Chen, J., Armstrong, A. H., Koehler, A. N., and Hecht, M. H. (2010) Small molecule microarrays enable the discovery of compounds that bind the Alzheimer's Abeta peptide and reduce its cytotoxicity, *J Am Chem Soc 132*, 17015-17022.
89. Valleix, S., Gillmore, J. D., Bridoux, F., Mangione, P. P., Dogan, A., Nedelec, B., Boimard, M., Touchard, G., Goujon, J. M., Lacombe, C., Lozeron, P., Adams, D., Lacroix, C., Maisonobe, T., Plante-Bordeneuve, V., Vrana, J. A., Theis, J. D., Giorgetti, S., Porcari, R., Ricagno, S., Bolognesi, M., Stoppini, M., Delpech, M., Pepys, M. B., Hawkins, P. N., and Bellotti, V. (2012) Hereditary systemic amyloidosis due to Asp76Asn variant beta2-microglobulin, *N Engl J Med 366*, 2276-2283.
90. Valleix, S., Gillmore, J.D., Bridoux, F., Mangione, P.P., Dogan, A., Nedelec, B., Boimard, M., Touchard, G., Goujon, J.-M., Lacombe, C., Lozeron, P., Adams, D., Lacroix, C., Maisonobe, T., Plante´-Bordeneuve, V., Vrana, J. A., Theis, J. D., Giorgetti, S., Porcari, R., Ricagno, S., Bolognesi, M., Stoppini, M., Delpech, M., Pepys, M. B., Hawkins, P. N., and Bellotti, V. (2012) Hereditary Systemic Amyloidosis Due to Asp76Asn Variant β2-Microglobulin, *The new england journal of medicine 366*, 2276-2283.
91. Mangione, P. P., Esposito, G., Relini, A., Raimondi, S., Porcari, R., Giorgetti, S., Corazza, A., Fogolari, F., Penco, A., Goto, Y., Lee, Y., Yagi, H., Cecconi, C., Naqvi, M. M., Gillmore, J. D., Hawkins, P. N., Chiti, F., Rolandi, R., Taylor, G. W.,

Pepys, M. B., Stoppini, M., and Bellotti, V. (2013) Structure, Folding Dynamics, and Amyloidogenesis of D76N β2-Microglobulin, *THE JOURNAL OF BIOLOGICAL CHEMISTRY 288*, 30917-30930.
92. Chen JL, Stewart-Jones G, Bossi G, Lissin NM, Wooldridge L, Choi EM, Held G, Dunbar PR, Esnouf RM, Sami M, Boulter JM, Rizkallah P, Renner C, Sewell A, van der Merwe PA, Jakobsen BK, Griffiths G, Jones EY, and Cerundolo V. (2005) Structural and kinetic basis for heightened immunogenicity of T cell vaccines., *J Exp Med. 201*, 1243-1255.
93. Trojan A, S. J., Witzens M, Vonderheide RH, Ladetto M, Donovan JW, Gribben JG. (2000) Immunoglobulin framework-derived peptides function as cytotoxic T-cell epitopes commonly expressed in B-cell malignancies., *Nat Med. 6*, 667-672.
94. Colombo, M., DeRosa, M., Bellotti, V., Ricagno, S., and Bolognesi, M. (2012) A recurrent D-strand association interface is observed in b-2 microglobulin oligomers, *FEBS Journal 279*, 1131-1143.
95. Barbet-Massin E, Ricagno S, Lewandowski JR, Giorgetti S, Bellotti V, Bolognesi M, Emsley L, and Pintacuda G. (2010) Fibrillar vs crystalline full-length beta-2-microglobulin studied by high-resolution solid-state NMR spectroscopy., *J Am Chem Soc. 132*, 5556-5557.
96. Ron, D., and Walter, P. (2007) Signal integration in the endoplasmic reticulum unfolded protein response, *Nat Rev Mol Cell Biol 8*, 519-529.
97. Calabrese, M. F., Eakin, C. M., Wang, J. M., and Miranker, A. D. (2008) A regulatable switch mediates self-association in an immunoglobulin fold, *Nat Struct Mol Biol. 15*, 965-971.

6. ACKNOWLEDGEMENTS

Given the opportunity, I would like to express my special appreciation and thanks to my supervisor Dr. Stefano Ricagno for his aspiring guidance, invaluably constructive criticism and support throughout my PhD studies; his enthusiasm, encouragement and faith in me have been very helpful and productive. Special thanks to my group leader Professor Martino Bolognesi for always being respectful and willing to provide his professional assistance in all aspects of my research.

I thank the University of Milan for their financial support granted through doctoral scholarship. I am also grateful to Professor Vittorio Bellotti for continuous collaboration, Dr. Alberto Barbiroli for his kind help in CD experiments, and to all my colleagues and group members for being friendly, helpful and joyful.

I would like to acknowledge with gratitude, the endless support and love of my parents. Words cannot express how grateful I am to my mother Silva and to my father George for all the sacrifices they've made on my behalf. Finally, special thanks to my beloved wife Nanor who was always my support throughout my studies.

PART II

Published Paper I:

Halabelian L., Ricagno S., Giorgetti S., Santambrogio C., Barbiroli A., Pellegrino S., Achour A., Grandori R., Marchese L., Raimondi S., Mangione PP., Esposito G., Al-Shawi R., Simons JP., Speck I., Stoppini M., Bolognesi M., and Bellotti V. (2014). "Class I major histocompatibility complex, the trojan horse for secretion of amyloidogenic beta2-microglobulin". *J Biol Chem. 289*, 3318-3327.

The paper can be found by following the link:

http://www.jbc.org/content/289/6/3318

PART III

Manuscript in preparation I:

Halabelian L., Barbiroli A., Relini A., Bolognesi M., Ricagno S. (2014). "A covalent homodimer to probe early oligomers along amyloid aggregation".

Side researches not included in the main frame of the Thesis:

Natalello A., Relini A., Penco A., **Halabelian L.,** Bolognesi M., Doglia SM., and Ricagno S. (2014). "Wild type Beta-2 microglobulin and DE loop mutants display a common fibrillar architecture". Under review in PloS One.

A covalent homodimer to probe early oligomers along amyloid aggregation

Levon Halabelian[1], Alberto Barbiroli[2], Annalisa Relini[3], Martino Bolognesi[1], and Stefano Ricagno[1]

[1]Dipartimento di Bioscienze, Università di Milano,Via Celoria 26, 20133 Milano, Italy. [2]Department of Food, Environmental, and Nutrition Sciences, University of Milano, Italy. [3]Dipartimento di Fisica, Università di Genova, via Dodecaneso 33, 16146 Genova, Italy.

Keywords: β2-Microglobulin, Amyloid Fibrils, Oligomerization, intermolecular interface, Thioflavine T, Dialysis-related Amyloidosis.

Abstract

Human Beta2-microglobulin (β2m) is a 99-residue protein responsible for Dialysis-Related Amyloidosis in patients undergoing long-term dialysis linked to kidney failure. The mechanism underlying β2m aggregation into amyloid is only broadly understood; in particular, which protein regions are involved in β2m oligomerization is still matter of debate. Previous evidences suggest that β2m D strand plays a role in initial aggregation. An anti-parallel intermolecular interaction between D strands of facing β2m molecules was observed in several crystal structures, suggesting that that such interface may be relevant for β2m dimerization. In this study, by mutating Ser33 to Cys, and assembling the disulphide-stabilised β2m homodimeric species (DimC33), we constrained two β2m molecules to interact constitutively through such DD strand interface. Although the isolated DimC33 displays stability and behavior similar to wt β2m under native conditions, it shows enhanced amyloid aggregation propensity relative to wt β2m, both under denaturating and native-like conditions. To explore the molecular bases of such enhanced aggregation property, three distinct crystal structures of DimC33 were determined. Based on crystal packing considerations, we suggest that dimerization through the DD interface is instrumental for enhancing DimC33 aggregation propensity. This observation bears implications for wt β2m oligomerization. Furthermore, the crystal structure of DimC33 in its complex with Thioflavine-T (ThT), a well-known amyloid-specific dye, pinpoints a second interface, which likely participates in the first steps of β2m aggregation.

Introduction

Amyloidogenesis is a complex and non-homogeneous process whereby, during the nucleation phase, monomeric protein molecules start to associate, firstly yielding oligomeric species that eventually lead to mature amyloid fibrils {Morris, 2009 #8}. A growing set of evidences indicates that in amyloid-dependent degenerative diseases the early oligomers are the most cytotoxic species {Chiti, 2006 #210}. It is therefore particularly relevant to shed light on the molecular bases of oligomer assembly to design strategies not only against amyloid deposits, but also specifically to inhibit the formation of the cytotoxic species. Nevertheless, since the oligomers are transient species in equilibrium with higher/lower molecular weight aggregates, only in a few cases they have been successfully isolated {Campioni, 2010 #209}. Even when isolated *in vitro,* typically the oligomers are too heterogeneous and unstable for high-resolution structural investigations. Accordingly, a description of oligomers at the molecular level is generally lacking, most evidences on oligomer structure being obtained though spectroscopic techniques or microscopy investigations {Bemporad, 2012 #216}.

In order to elucidate the structural bases of oligomer formation we focused on the amyloidogenic protein beta-2 microglobulin (β2m), whose native fold is structurally well characterized and amyloid formation *in vitro* has been thoroughly described {Platt, 2009 #110}. β2m is a 99-residue globular protein with a typical immunoglobulin-like fold, composed of seven β-strands arranged in two β-sheets, named ABDE and CFG, respectively, according to standard nomenclature of the composing β-strands (Fig. 1a); the two sheets are internally linked by a disulphide bond {Bjorkman, 1987 #11}. β2m is an aggregation-prone protein responsible for two types of amyloid-related diseases: the wild type (wt) protein is responsible for Dialysis-Related Amyloidosis (DRA) {Floege, 1996 #87}, while a severe hereditary systemic amyloidosis is linked to the pathological β2m D76N mutant {Valleix, 2012 #43}. Physiologically, β2m is degraded in the kidneys; DRA patients typically suffer from kidney dysfunction that results in β2m accumulation in the serum following dialysis. Over the years, β2m aggregates in the skeletal joints, bones and muscles, resulting in bone fragility and movement impairment {Gejyo, 1985 #13}.

Wt β2m aggregation propensity has been extensively studied in the last

decades, although one important limitation for the study of β2m aggregation is that the wt protein *in vitro* is stable for months under native conditions. Accordingly, all wt β2m aggregation protocols are based on conditions under which the protein is completely or partially unfolded (low pH, denaturants such 2,2,2-trifluoroethanol (TFE), or sodium dodecylsulphate). Moreover, in order to trigger aggregation, the addition of amyloid-fibril seeds to the reaction mixture is necessary {Jahn, 2008 #211}. Thus, such aggregation protocols may not match the natural β2m oligomerisation occurring in patients. In fact, given the intrinsic β2m stability, the protein is unlikely to be largely unfolded before amyloid deposition takes place *in vivo*; moreover, the addition of seeds allows to study fibril growth, but the seeds fully abolish the key early process of oligomer formation.

Several independent reports suggest that the first oligomeric species formed during β2m aggregation is an elongated dimer: extended oligomers have been observed by mass-spectrometry, and an elongated dimer was proposed to be the starting species in β2m oligomerization {Karamanos, 2014 #208;Rennella, 2013 #213;Smith, 2010 #212;White, 2009 #117}. Several studies aimed at uncovering the structure of β2m oligomers during aggregation have been reported. In particular, Eisenberg and coworkers proposed a domain-swapped covalent dimer {Liu, 2011 #214}: this species is amyloidogenic, however in *ex vivo* samples there is no evidence of comparable covalent oligomers. Miranker and coworkers reported the crystal structure of a hexameric form of the H13F β2m mutant {Calabrese M. F., 2008 #46}, formed under aggregating conditions. Such hexameric assembly is however not amyloidogenic, therefore, at least to some extent, it may represents an off-pathway oligomer {Calabrese, 2008 #75}.

We recently tested a different approach to the study of β2m oligomer formation. Three single Cys mutations were inserted in different β2m surface regions, and disulphide-linked covalent homodimers were prepared. The rationale was that a covalent bond between two β2m molecules acts as a constraint for the architecture of the dimer, which can be aggregation permissive or non-permissive. The three homodimers were structurally and biophysically characterized {Colombo, 2012 #207}. The crystal structures of DimC50 and DimC20 (*i.e.* β2m homodimeric species hosting intermolecular disulphide bridges between pairs of C50 and C20 engineered residues, respectively) showed that a common antiparallel interface between covalent

dimers (named the DD strand interface) was constantly present in their crystal packings. The DimC50 and DimC20 species proved to be amyloidogenic, could be crystallized, and assembled as (non-covalent) dimer of (covalent) dimers in solution. Notably the S-S bond location in the third engineered homodimer (DimC60) hampers the formation of the DD strand interface for steric reasons; thus, DimC60 was not amyloidogenic, purely dimeric in solution and not crystallizable. Based on such observations, the DD strand interface was proposed as a key association interface involved in the early stages of β2m association under native and non-native conditions {Colombo, 2012 #207}.

The DD strand interface involves the apical region of two facing β2m molecules, in such a way that they give rise to a dimer associated through head to head interactions. The D-strands belonging to the facing molecules are antiparallel and the two β2m molecules involved display the same conformation and are well superposable. Within each β2m monomer the DD strand interface involves the D-strand, the DE and BC loops, namely regions that have been reported as major players in β2m amyloid aggregation {Colombo, 2012 #207} (Fig. 1). Such intermolecular association interface had also been noted in the hexameric structure of the H13F β2m mutant {Calabrese, 2008 #75}.

Following our previous approach, in the present study we engineered a β2m homodimer where the DD strand interface is specifically locked by a disulphide bond (linking the engineered C33 residues of two facing β2m molecules – DimC33). We speculated that analysis of such a covalently stabilized dimer should allow us to assess more directly the role played by association through the DD strand interface in β2m oligomerisation and amyloid formation. DimC33 has been characterized in solution and under aggregation conditions; moreover, we determined three different crystal structures of the covalent dimer, one of which hosts the DimC33 complex with Thioflavin (ThT), the hallmark fluorescence dye for amyloid aggregates. The data here reported show that a covalently stabilized DD strand interface facilitates β2m aggregation under denaturating but also under native-like conditions, highlighting DimC33 as the first model system to study β2m aggregation *in vitro* under native-like conditions. Our results recapitulate previous data indicating the DD strand interface as the first and favorite intermolecular contact region between β2m molecules under native or aggregating conditions. Furthermore, analysis of the crystal structure of

DimC33 in complex with ThT strongly points to a second β2m association interface that may be involved in amyloid aggregation.

Results

Recombinant S33C variant β2m homodimers

In order to engineer a β2m covalent dimer displaying a locked DD strand interface, a detailed analysis of the crystal structures displaying such intermolecular association interface (pdb codes: 3TM6, 3TLR, 3CIQ) was performed, and the mutation of Ser33 to Cys was chosen based on the following rationale. Firstly, two Ser33 residues belonging to two facing β2m molecules (in the examined crystal structures) fall at a suitable distance to be mutated to Cys and yield a disulphide bridge without disrupting or altering the DD interface. Secondly, among the residues, which could satisfy the above conditions, a Ser residue was chosen because it is essentially isosteric with Cys.

The S33C β2m variant was expressed and purified under denaturating conditions and then refolded, according to our standard protocols {Esposito, 2008 #61}. In our previous study on covalent β2m homodimers, in order to promote the formation of covalent disulphide linked homodimers, an oxidation reaction proved necessary. To this purpose, after refolding, the monomeric β2m variants were incubated at high protein concentrations in the presence of H_2O_2 {Colombo M, 2012 #47}. Conversely, in the case of the S33C β2m variant, a covalent dimeric species was abundantly present at the end of the purification, in the absence of further oxidation reactions. This finding implies that in solution under native conditions the DD interface is spontaneously formed by monomeric β2m molecules, resulting in the formation of the disulphide-stabilized dimeric species (DimC33).

The stability of DimC33 in solution was assessed by circular dichroism. Thermal unfolding monitored by Far-UV indicates that, as for wt β2m, DimC33 unfolds according to a simple sigmoidal curve and displays a Tm value close to that of the wt protein (Tm_{DimC33} 60.2 ±0.3°C; Tm_{wt} 62.4±0.3°C) (Fig 2a). Then, Far-UV spectra of DimC33 and of wt β2m in phosphate buffer, in 10% and 20% TFE were collected, showing that native spectra are well superposable and that both proteins display a native secondary structure content in 10% TFE; conversely the β2m fold is

perturbed in 20% TFE (Fig. 2b). Thus, the spectroscopic data suggest that the engineered mutation and the achievement of a covalent dimeric state do not alter β2m thermodynamic stability or its overall fold in DimC33.

Aggregation kinetics of DimC33 and wt ß2m in vitro

We studied DimC33 aggregation propensity *in vitro* at physiological pH conditions (pH 7.4) in the absence of any pre-fibrillar seeds. In 20% (v/v) TFE, DimC33 at a final concentration of 1 mg mL^{-1} aggregates promptly without a lag phase, reaching equilibrium within the first 4 hours, and yielding a high ThT binding signal (Fig. 3a); under the same conditions wt β2m remains soluble and does not aggregate. Interestingly, in 10% (v/v) TFE—where DimC33 and wt β2m display CD spectra indicative of native-like conformations—a 5 mg mL^{-1} solution of DimC33 also aggregated.

Doxycycline is a known inhibitor of wt β_2m aggregation {Giorgetti, 2010 #137}. In order to assess doxycycline inhibitory effect on DimC33 aggregation, a DimC33 solution was tested for aggregation in the presence of 100μM and 400μM Doxycycline, in 20% TFE. A 100μM final concentration of Doxycycline was sufficient to block DimC33 aggregation by approximately 85%, compared with a DimC33_20%ThT control solution, whereas 400 μM Doxycycline completely inhibited DimC33 aggregation (Fig 3b). Such results are in keeping with previous data on wt protein reporting an IC50 of 47 μM for doxycycline as aggregation inhibitor {Giorgetti, 2010 #137}.

X-ray crystal structures of DimC33

In order to assess fine details of the molecular structure of DimC33, two crystal structures of DimC33 were determined at 1.9Å and 1.4Å resolution, hereafter named DimC33_low and DimC33_high, respectively; additionally a crystal structure of DimC33 in complex with ThT was determined at 2.8Å resolution, and named DimC33_ThT. Data collection and refinement statistics for the crystal structures are shown in Table I.

The three crystal structures display three different space groups and crystal packings. The electron density is of excellent quality and all β2m molecules are completely traceable in all three structures. Overall, no major structural effects on the β2m fold are induced by the S33C mutation, either locally or globally, in all DimC33

structures, (Fig. 1b-c). The monomeric components of DimC33 most closely match the conformation of wt β2m as observed in its physiologic class I major histocompatibility complex (Table 2). The only noticeable difference occurs in the DE loop (residues 57-60) that displays a slightly modified conformation so that Trp60 participates in stacking interactions with Phe56, of the same chain, and with His51 and Tyr66 of the second chain within DimC33; the rotation of Tyr63 side chain of about 90 degrees is also observed (see Fig. 1b).

The covalent DD strand interface is structurally well conserved in all three DimC33 structures, where it maintains the same contact surface of 560 $Å^2$. The overall dimer organization is conserved (r.m.s.d. 0.57 Å/195 Cα, 1.17 Å/195 Cα, DimC33_high *versus* DimC33_ThT and *versus* DimC33_low, respectively); the main regions involved in the association interface are the BC loop (residues 31-37), the D strand (residues 51-57), the DE loop (residues 57-6), Phe62, the E strand (residues 64 and 66), as observed in previous structures (Fig. 1b-d). The superposition of DimC33 with previously reported β2m dimers, non-covalently associated through the DD strand interface, shows a very similar overall monomer-monomer orientation (Fig. 1c and Table 2) and conserved conformations for the residues involved (Fig. 1b-d and Table 2). All such data indicate that the S33C mutation minimally affects the β2m fold, and that the C33 – 33C disulphide covalently locks the DD strand interface with negligible structural effects compared to the previous crystal structures Fig. 1b-d.

The DimC33 ThT complex and the ABDE sheet

DimC33 was also crystallized in the presence of 5mM ThT. Intriguingly, the crystallographic analysis showed that five ThT molecules are hosted in the crystal asymmetric unit (AU), which contains one DimC33 moiety and two halves of a second one (*i.e.* two additional and independent β2m chains). As a result of crystal packing, β2m molecules belonging to independent DimC33 units interact via their ABDE β-sheets (Fig. 4a); however, two distinct ABDE interfaces can be distinguished. In one of these, four ThT molecules are wedged between the ABDE sheets of two facing β2m molecules (4ThT site); in the other, only one ThT molecule is sandwiched between two facing ABDE sheets (1ThT site) (Fig. 4a). In either case, binding of the ThT molecules does not induce any conformational adjustments in the β2m fold, or in the DimC33 assembly. At the 1ThT site, the ThT molecule is

sandwiched between Tyr10 residues from two facing β2m molecules; moreover, Tyr26 and Pro14 from both molecules establish van der Waals contacts with ThT (Fig. 4b). At the 4ThT site, the four ThT molecules are stacked on each other, and in stacking contacts with Tyr10 and Tyr65 of the β2m molecules defining the binding site. Tyr26 from both β2m molecules also help accommodate the ThT hydrophobic rings (Fig. 4c).

In order to house one or four ThT molecules, the β2m chains, which belong to two distinct DimC33 units, are differently juxtaposed. In particular, the two β2m molecules defining the 4ThT site move about 20Å apart compared to the 1ThT site, to make room for the four ThT molecules. Thus, very limited direct interactions connect the two β2m molecules at the 4ThT site, whereas more direct protein-protein contacts take place at the 1ThT site. Despite such translational adjustments, the two ThT sites maintain very similar structural arrangements. The relative orientation of the two β2m chains defining the ThT sites is comparable, and the protein regions involved in ThT binding are conserved. More specifically, Tyr10, Tyr26 and Tyr63, the three central residues in the ABDE interface, cross diagonally the sheet and confer substantial surface hydrophobicity (Fig. 4). In particular, at both ThT sites Tyr10 establishes direct stacking interactions with ThT molecules, even though the ThT molecules do not share the same orientation in the two sites.

It must be noted that wide intermolecular packing contacts through the ABDE sheet are established also in the absence of ThT. In the structure of DimC33_low (present work) and in the hexameric H13F mutant {Calabrese, 2008 #75}, highly hydrophobic association interfaces are built via facing ABDE sheets (surface areas of 805 and 970 $Å^2$, respectively). Although such two ABDE assemblies are not superposable, the two interfaces are structurally similar and residues Tyr10, Tyr26 and Tyr63 are clustered in their hydrophobic cores (see Fig. 4D,E).

In summary, in the four ABDE packing interfaces examined (the 1ThT and 4ThT sites, and the ABDE interfaces in DimC33_low and in hexameric β2m) the orientations of each β2m monomeric chain may vary, the distances between protein chains are somewhat different, and the packing interactions between the ABDE sheets can be direct or mediated through ThT molecules. However, the overall conservation of protein-protein interaction surface, the binding of ThT, the size of the surfaces, the

structural data and the marked hydrophobicity of the residues involved, all point at this sheet as a favored site for β2m association during oligomer formation.

Discussion

Elucidating the structure and the underlying interactions of on-pathway oligomers that lead to amyloid aggregation is a crucial and challenging task, since it is well established that oligomers are the most cytotoxic species in amyloid-related diseases {Chiti, 2006 #210}. A structural characterization of the first steps of oligomer formation would be key for a deeper understanding of the aggregation process, and potentially for the design of inhibitors hampering the oligomerisation process, hence in principle abolishing cytotoxicity.

We selected β2m as a model of amyloid aggregation, since the protein has been extensively characterized, and several structural determinants of β2m amyloidogenicity have been uncovered {Platt, 2009 #110}. In order to shed light on the intermolecular interactions that drive the first steps of aggregation, a disulphide-linked β2m homodimer was designed according to a previously proposed strategy {Colombo, 2012 #207}. The engineered S-S bond was positioned on the protein surface in order to juxtapose two β2m monomers along the DD strand interface, which was observed as an intermolecular association region in three previous independent β2m crystal structures {Calabrese, 2008 #75;Colombo, 2012 #207}. The mutation Ser33 to Cys is structurally conservative, and designed to bring together two β2m molecules based on structural information from the previously observed intermolecular recognition through the DD strand interface, without altering its structure. From the *in vitro* biophysical data, and from the crystallographic analysis here reported, all evidences suggest that the mutation and the engineered disulphide do not affect β2m properties to a significant extent: thermodynamic stability, secondary structure content in aqueous buffer and in TFE, and the comparison of DimC33 crystal structures with previous wt β2m structures, all support such conclusions.

Under native conditions, we and others have shown that a minor population of wt β2m is oligomeric, mainly dimeric {Rennella, 2013 #213;Santambrogio, 2010 #125}. The observation that the disulphide bridge stabilizing DimC33 forms spontaneously in solution (in the absence of an added oxidizing agent) is indicative of

the spontaneous juxtaposition of two facing C33 residues; it thus strongly suggests that the DD interface is the prevalent association interface underlying β2m dimerisation under such conditions.

The aggregation data show that DimC33 is much more amyloidogenic than wt β2m, even though its thermodynamic stability and its 3D structure are virtually identical to those of the wt protein. Using a standard β2m aggregation protocol in 20% TFE, we have shown that DimC33 aggregates abundantly, but, opposite to wt β2m, does not require fibril seeds for aggregation to start, an indication that DimC33 can spontaneously form the oligomers required for onset of fibrillogenesis. Analogously to wt β2m amyloid formation {Giorgetti, 2010 #137}, doxycyclin proved to be an inhibitor of DimC33 aggregation. Taken together, all the above data suggest that DimC33 and wt β2m aggregate following very similar processes and end products. However, DimC33 was shown to aggregate also in 10% TFE, a condition under which the β2m fold is still native (Fig. 1b). The data available to date indicate that the amyloidogenic intermediates display a native-like structure {Chiti, 2001 #25;Karamanos, 2014 #208;Rennella, 2013 #213}; on these bases, a β2m variant, such as DimC33, which aggregates under native-like conditions may prove to be an proper system to study wt β2m amyloid formation. To the best of our knowledge DimC33 is the first model to study β2m aggregation under native-like conditions *in vitro*.

Recent reports indicate that the first β2m oligomer formed on the pathway to fibril association should be a head-to-head elongated dimer {Karamanos, 2014 #208;Rennella, 2013 #213;Smith, 2010 #128}. In particular, Rennella *et al.* also provided evidence that the dimer association interface should involve the BC loop region {Rennella, 2013 #213}, a finding that is in keeping with our previous data and with a recently published report {Colombo, 2012 #207;Karamanos, 2014 #208}. In this context, we previously showed that hampering the formation of the DD strand interface through proper selection of the engineered disulphide bridge results in non-aggregating β2m covalent dimers {Colombo, 2012 #207}. Thus, the data here reported for DimC33, together with previous results, point to the DD strand interface as the firstly established protein-protein association interface during β2m aggregation. The increased aggregation propensity of DimC33 compared to wt β2m, would then be

the result of the immediate availability of the first on-pathway oligomer, that is DimC33.

Interestingly, the crystal structure DimC33 in complex with ThT provides further information on the β2m aggregation path. ThT fluorescence is the most widely accepted spectroscopic method to discern cross-β fibrils from amorphous aggregate. The ThT molecules are held to intercalate the cross-β structure in the fibrils, resulting into a gain of fluorescence. Only two structures of ThT in complex with amyloidogenic proteins have been so far reported, and both concern β2m {Wolfe, 2010 #215}. In one of these structures (pdb code: 3MYZ) the authors suggest that ThT molecules are simply trapped between β2m molecules packed in the crystal lattice, while the second structure reported (pdb code: 3MZT) presents severe technical issues that prevent a thorough discussion of ThT-β2m interactions (See Supplementary Materials). In this context, the DimC33_ThT structure here reported adds substantially new information on ThT binding mode to an amyloidogenic protein. In the DimC33_ThT complex structure, the ThT molecules are nestled between the ABDE sheets of two facing β2m molecules, in a highly hydrophobic environment. Notably, an extended ABDE interface between facing β2m molecules can also be observed in the absence of ThT in DimC33_low (this work), and in the hexameric β2m structure reported earlier {Calabrese, 2008 #75}. The reciprocal orientation of the two facing ABDE β-sheets displays a high level of variability: in different crystal structures the facing ABDE β-sheets display varying orientations and residue-residue interactions, but in all cases they face each other and the same three aromatic residues (Tyr10, Tyr26 and Tyr63) build the hydrophobic core of the β2m association interface. Such variability can be accounted for by the presence of several Tyr residues and by the capability of hydrophobic interactions to form under different orientations of the contributing residues. The above observations point at the ABDE β-sheet as a second key interface involved in β2m oligomer formation, in keeping with a previous report supports the role of surface aromatic residues in determining β2m amyloid propensity {Platt, 2008 #68}. The structural adaptability of the ABDE surfaces may also explain the formation of several different dimeric/tetrameric building blocks recently proposed by the EM reconstruction of mature β2m fibrils {White, 2009 #117}.

In summary, our study presents an engineered β2m covalent dimer, DimC33, displaying the same biophysical properties of wt β2m in solution. Nevertheless, unlike wt β2m, DimC33 does not require the addition of seeds to start fibrillogenesis, and aggregates under native-like conditions. Given that *in vivo* wt β2m likely aggregates from a native-like folded species, DimC33 could then be considered a proper model to study β2m oligomerization and fibrillogenesis *in vitro,* and to test new aggregation inhibitors. Finally, the properties and the structures of DimC33 recapitulate previous evidences and indicate how oligomerisation may proceed during aggregation. The first dimeric oligomer would be built across the DD strand interface; at a later stage, the aromatic residues located on the ABDE sheet will contribute to the formation of a hydrophobic core for further association, leading to trimers and tetramers through an structurally adjustable ABDE interface.

Materials and methods

Mutagenesis, expression and purification

The synthetic gene of the Ser33 to Cys β2m variant was purchased from Eurofins genomics. The gene of interest was inserted into pET21B expression vector and transformed into BL21 (DE3) *Escherichia coli* strain. The S33C variant β_2m was expressed and purified as previously reported {Esposito, 2000 #38}. At the end, an additional step of purification was introduced to separate the spontaneously formed dimeric species of S33C β2m variant by size-exclusion chromatography column (Superdex75 16/60 GE healthcare) and eluted with 20mM Sodium Phosphate buffer pH 7.4.

Circular dichroism

Circular dichroism (CD) studies were carried out on a Jasco J810 spectropolarimeter equipped with a Peltier system for temperature control and analyzed by means of Jasco software. All measurements were recorded at 0.1 mg/mL protein concentration in 100 mM sodium chloride, 50 mM sodium phosphate buffer pH 7.4 by using a 0.1 cm path length cuvette. Spectra were recorded in plain buffer or in buffer added with 10% or 20% TFE at 37 °C. Temperature ramp measurements

were recorded at 202 nm from 20 to 95 °C (temperature slope 50 °C/h). Tm values were calculated from the first derivative of the recorded traces.

Aggregation kinetics

DimC33 aggregation experiments were performed as unseeded reaction by incubating samples of 100µL at 37°C for two weeks, without agitation.

The following aggregation conditions were tested: DimC33_20%TFE (1 mg mL^{-1} DimC33 in 20% TFE, 100mM Sodium chloride, 50mM Sodium phosphate buffer pH 7.4) according to a standard protocol {Yamamoto, 2004 #41}; DimC33_10%TFE (5 mg mL^{-1} DimC33 in 10% TFE, 100mM Sodium chloride, 50mM Sodium phosphate buffer pH 7.4); DimC33/wtβ_2m (a mixture of DimC33 and wt β_2m in 1:3 ratio with a final protein concentration of 1 mg mL^{-1} in 20% (v/v) TFE, 100mM Sodium chloride, 50mM Sodium phosphate buffer pH 7.4). In each experiment aggregation tests on wt β2m were also performed as a control. Aggregation kinetics measurements were monitored by VARIAN Cary Eclipse spectrofluorimeter by measuring ThT fluorescence signal with excitation and emission wavelength of 445 and 480 nm, respectively {LeVine, 1993 #40}.

The inhibitory effect of Doxycycline hyclate on DimC33 aggregation was studied in the same aggregation condition as of DimC33_20%TFE, by monitoring ThT fluorescence binding signal after one week of incubation at 37°C without agitation. Two Doxycycline concentrations were screened: DimC33_Doxy100 containing 100µM Doxycycline; and DimC33_Doxy400 containing 400µM Doxycycline. A DimC33_20%TFE aggregation was used as control model.

The measurements are the average of three independent experiments. Doxycycline hyclate, TFE and ThT were purchased from SIGMA-Aldrich.

Crystallization and structure determination

DimC33 was crystallized in three different conditions by mixing equal amounts of 8 mg mL^{-1} protein and reservoir solutions containing: (25% v/v PEG 4K, 0,2M Imidazole-Malate pH7,0) for DimC33_low, (28% v/v PEG 400, 0,2M Calcium chloride dihydrate, and 0,1M Hepes sodium pH7,5) for DimC33_high, and (25% v/v PEG 4K, 0,1M Sodium chloride, 5mM ThT, and 0,1M Hepes sodium pH8.0-8.2) for DimC33_ThT crystals, respectively. All DimC33 crystals were grown at 20°C incubators, using sitting drop vapor diffusion crystallization method.

DimC33_low and DimC33_ThT crystals were cryo-protected in 20-33% glycerol solution containing the corresponding crystallization condition, and cryo-cooled in liquid nitrogen. DimC33_low and DimC33_high X-ray diffraction data were collected at ID23-1 beam-line (ESRF Grenoble), and DimC33_ThT X-ray diffraction data were collected at P13 beamline (PETRA Hamburg). DimC33_low X-ray data were processed using MOSFLM {Leslie A.G.W., 2007 #30} and SCALA from CCP4 software suite {Collaborative Computational Project, 1994 #31} and XDS {Kabsch W., 2010 #32} for DimC33_high and DimC33_ThT. The 3D structures of DimC33 were determined by molecular replacement using Balbes software suite {Long F., 2008 #33}. All structures were refined using Phenix.refine {Afonine P.V., 2010 #37} and REFMAC5 {Murdushov G.N., 1997 #35}. An amplitude based twin refinement protocol was applied during DimC33_ThT refinement process in REFMAC5. Model building and structural analysis for all DimC33 structures were carried out with COOT {Emsley P., 2010 #34} and figures were prepared with Pymol {The PyMOL Molecular Graphics System, #36}. Structure factors and coordinates are deposited in the Protein Data Bank under accession codes: 4R9H for DimC33_low, 4RAH for DimC33_high and 4RA3 for DimC33_ThT.

Table 1. Data collection and refinement statistics for DimC33.
Values in parenthesis are for the highest resolution shell.

	Structure (PDB entry)		
	DimC33-Low (4R9H)	DimC33-High (4RAH)	DimC33-ThT (4RA3)
Data collection			
Beam line	ID21-3 (ESRF)	ID21-3 (ESRF)	PETRA III, P13 (MX1)
Space Group	$P4_122$	$C222_1$	$P3_221$
Unit cell constants (Å)	a=68.84 b=68.84 c=200.04	a=32.35 b=47.70 c=119.65	a=80.04 b=80.04 c=177.70
Resolution (Å)	65.09 - 1.90 (2.00 - 1.90)	29.91 - 1.40 (1.42 - 1.40)	59.23 - 2.80 (2.95 -2.80)
R_{merge} [a](%)	10.9 (94.0)	6.5 (49.5)	5.9 (113.9)
I/sig(I)	12.4 (2.2)	10.9 (1.9)	21.4 (2.0)
Completeness (%)	99.9 (99.6)	98.7 (86.6)	100.0 (100.0)
Redundancy	8.9 (8.3)	4.5 (3.4)	9.6 (10.0)
Unique reflections	38985 (5533)	18491 (787)	16940 (2432)
Refinement			
R_{work} [b](%)	21.17	16.62	15.08
R_{free} [b](%)	24.73	20.94	18.12
Number of atoms	3480	1021	3407
Average B, all atoms (Å^2)	42.0	17.0	111.0
Ramachandran plot			
Most favored region	375 (98.68%)	86 (100%)	367 (94.83%)
Allowed region	4 (1.05%)	0 (0%)	20 (5.17%)
Outliers	1 (0.26%)	0 (0%)	0 (0%)

[a] R merge = $\sum_{hkl}$ I_{hkl} - < I_{hkl} > |/$\sum_{hkl}$ I_{hkl} where I is the observed intensity and < I > is the average intensity.
[b] R work = $\sum_{hkl}$Fo-Fc |/ $\sum_{hkl}$Fo for all data except 5% which were used for Rfree calculation.

Table 2. The SSM superimposed RMS deviations for DimC33 structures with reference models DimC20, DimC50, hexameric H13F β2m and wt β2m.

	DimC20 (3TLR)	DimC50 (3TM6)	H13F β2m (3CIQ)	wt β2m (1JF1)
DimC33-High(Mono)	0,62/99 Cα	0,59/98 Cα	1,05/97 Cα	0,97/98 Cα
DimC33-High	2,41/182Cα	2,10/192Cα	1,11/192Cα	-

Legends:

Figure 1. Crystal structure of DimC33 and DD strand interface. (a) Ribbon model of a monomeric of DimC33 (blue) superposed on the structure of wt β2m (green). β-strands are labeled according to standard nomenclature, Cys33 is shown in sticks. (b) A zoomed model into DD interface of four superposed crystal structures of DimC33_ThT (green), hexameric structure of H13F β2m (magenta), DimC50 (cyan) and DimC20 (yellow), showing the main residues involved in the DD interface as sticks model. (c) Superposition of four dimers built through the DD strand interface: DimC33_ThT (pdb code: 4RA3) in green, hexameric structure of H13F β2m in magenta (pdb code: 3CIQ), DimC50 structure in cyan (pdb code: 3TM6), and DimC20 structure in yellow (pdb code: 3TLR). (d) Stereo view of the DD strand interface formed by the facing molecules as observed in the structure of DimC33_high. The main residues involved in the interface are shown in sticks.

Figure 2. Thermal stability and Far-UV spectra analysis by circular dichroism. (1a) Temperature ramps for DimC33 in red and wt β2m in black monitored at 202 nm, temperature slope 50 °C/h. Signals were reported as fractional variation of the total change. The melting temperature (Tm) values for DimC33 and wt β2m are shown in the graph. (1b) Far-UV spectra for DimC33 and wt β2m in a buffer containing 100 mM sodium chloride, 50 mM sodium phosphate buffer pH 7.4, recorded at three conditions: No TFE (black curves); in presence of 10% (v/v) TFE (red curves); and of 20% (v/v) TFE (blue curves).

Figure 3. DimC33: fibrillogenesis at pH7.4. (a) Kinetics of DimC33 fibril formation in100mM NaCl, 50 mM Na phosphate buffer (pH 7.4) at 37°C incubation for two weeks, monitored by measuring ThT fluorescence signal at time (hours) 0, 4, 48, 96, 144, 216, 312. Four samples were screened: DimC33_20%TFE (5 mg mL^{-1} protein in 20% TFE); DimC33_10%TFE (1 mg mL^{-1} protein in 10% TFE); DimC33/wtβ2m mixture in 1:3 ratio (1 mg mL^{-1} protein mixture in 20% TFE); and wtβ2m_20%TFE as a control model (1 mg mL^{-1} protein in 20% TFE). Values represent the average of three independent experiments and error bars represent SD. (b) DimC33 aggregation inhibition analysis monitored by ThT fluorescence signal after one week of incubation

at 37°C, using the same aggregation condition as DimC33_20%TFE in three conditions; No Doxycycline (control model), in the presence of 100 μM and 400μM Doxycycline. Values represent the average of three independent experiments and error bars represent SD.

Figure 4. Crystal structures of DimC33_ThT and DimC33_low. (a) Cartoon representation of DimC33 assembly in crystal structure of DimC33_ThT. The three DimC33 units colored in cyan, green and magenta. Two ThT binding sites are visible: on the right the 4ThT site (four ThT molecules are colored in blue); while on the left side, the 1ThT site where the ThT molecule is colored in red. (b-c) A zoomed representation into 1ThT site (b) and into 4ThT site (c) showing ThT molecules sandwiched between the ABDE sheets of the two adjacent DimC33. (d) Ribbon represenation of ABDE interface observed in the DimC33_low (pdb code : 4R9H). (e) Ribbon represenation of ABDE interface as found in the hexameric structure of H13F β2m (pdb code: 3CIQ).

Fig. 1

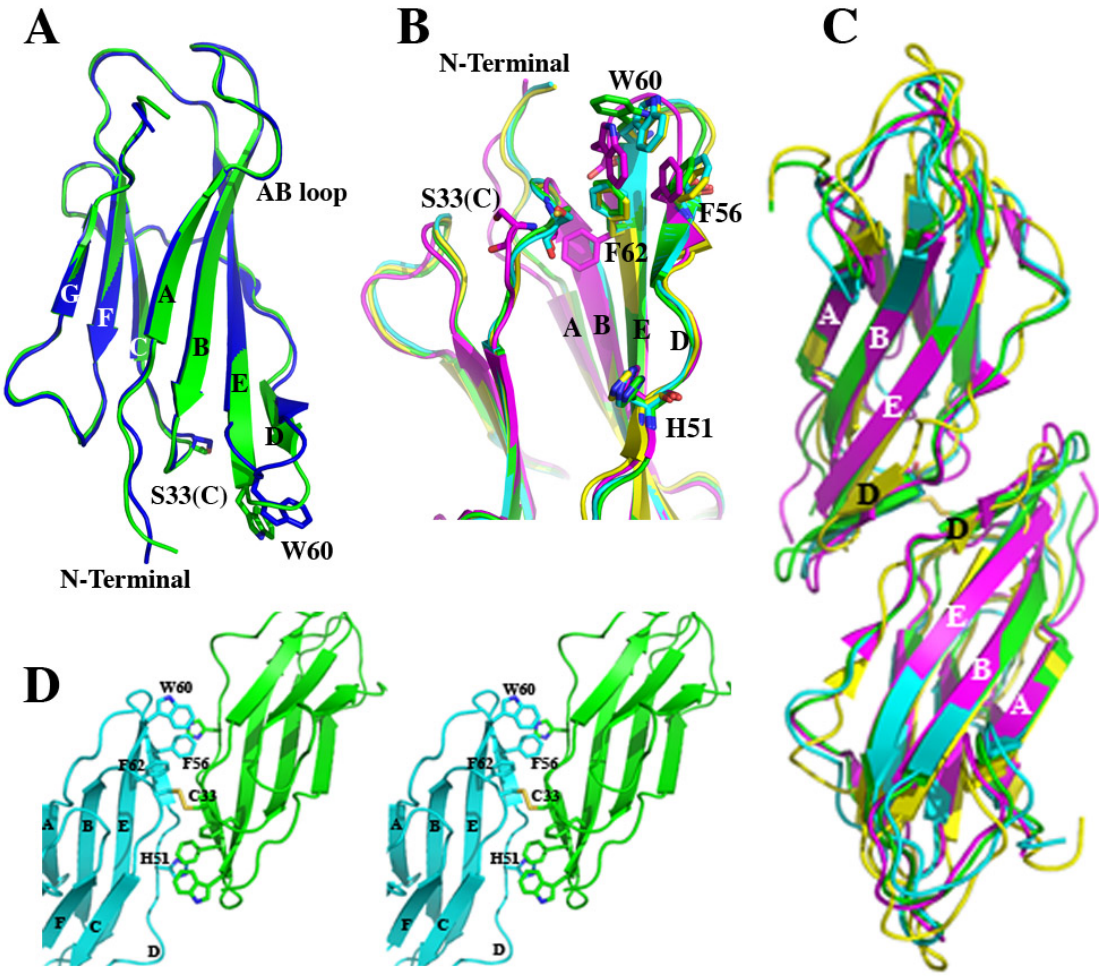
A
AB loop
G
F
C
A
B
E
D
S33(C)
W60
N-Terminal
B
N-Terminal
W60
S33(C)
F56
F62
A B E D
H51
C
A
B
E
D
D
E
B
A
D
W60
F62
F56
C33
A
B
E
H51
F
C
D
W60
F62
F56
C33
A
B
E
H51
F
C
D

Fig 2A

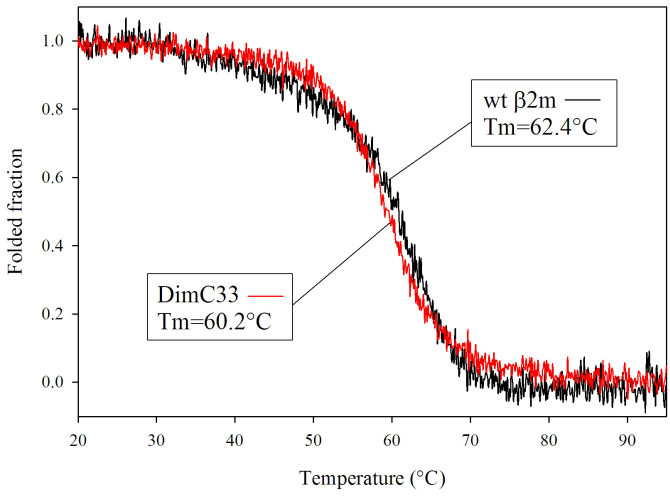
Folded fraction
1.0
0.8
0.6
0.4
0.2
0.0
20
30
40
50
60
70
80
90
Temperature (°C)
wt β2m
Tm=62.4°C
DimC33
Tm=60.2°C

PART III:A covalent homodimer to probe early oligomers along amyloid aggregation.

Fig 2B

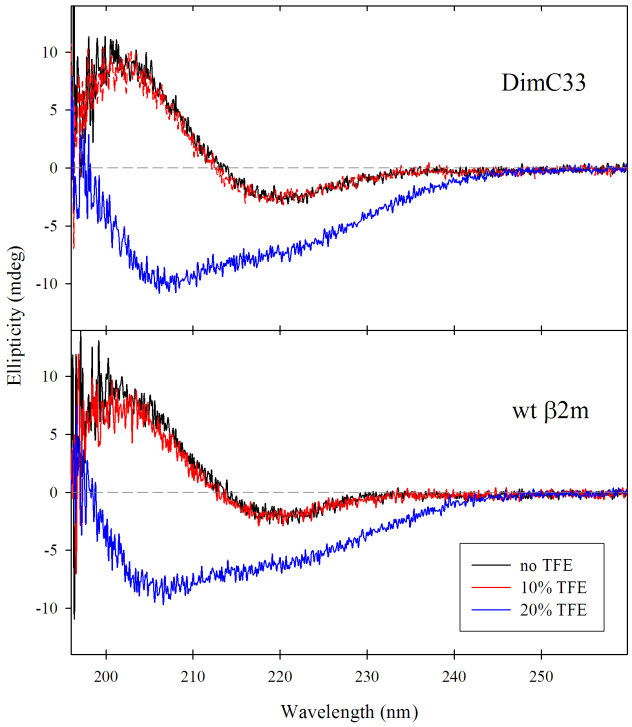

Fig 3A

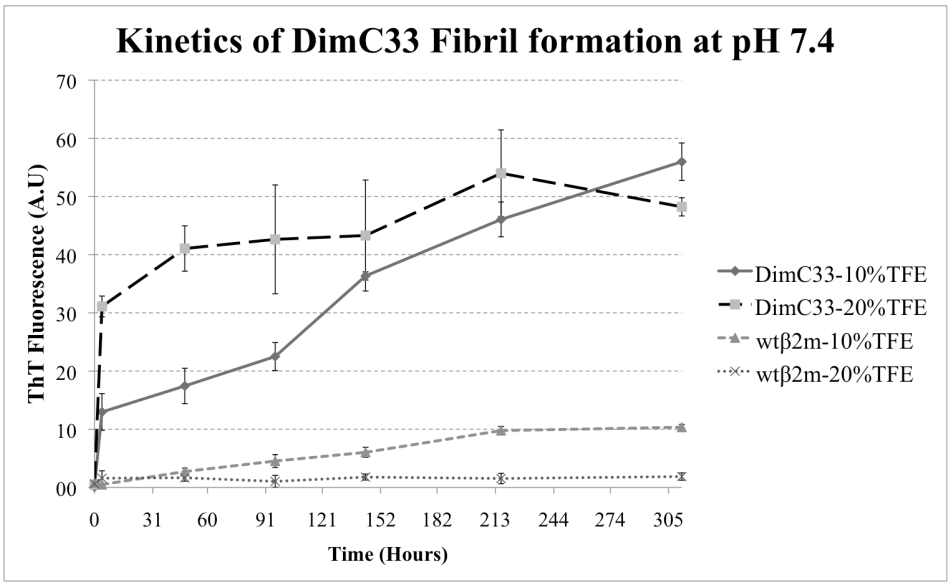

Fig 3B

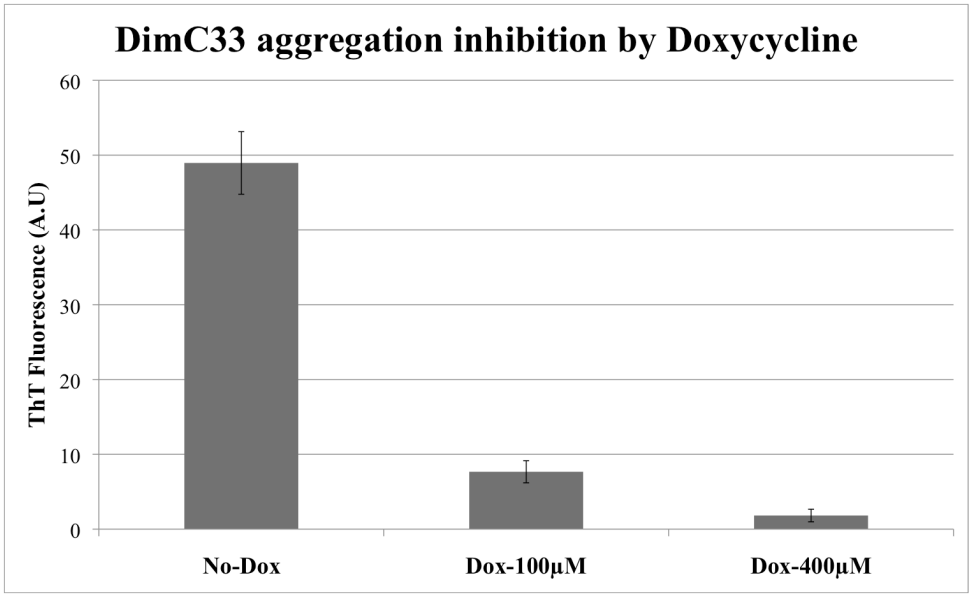
DimC33 aggregation inhibition by Doxycycline
ThT Fluorescence (A.U)
60
50
40
30
20
10
0
No-Dox
Dox-100µM
Dox-400µM

Fig 4

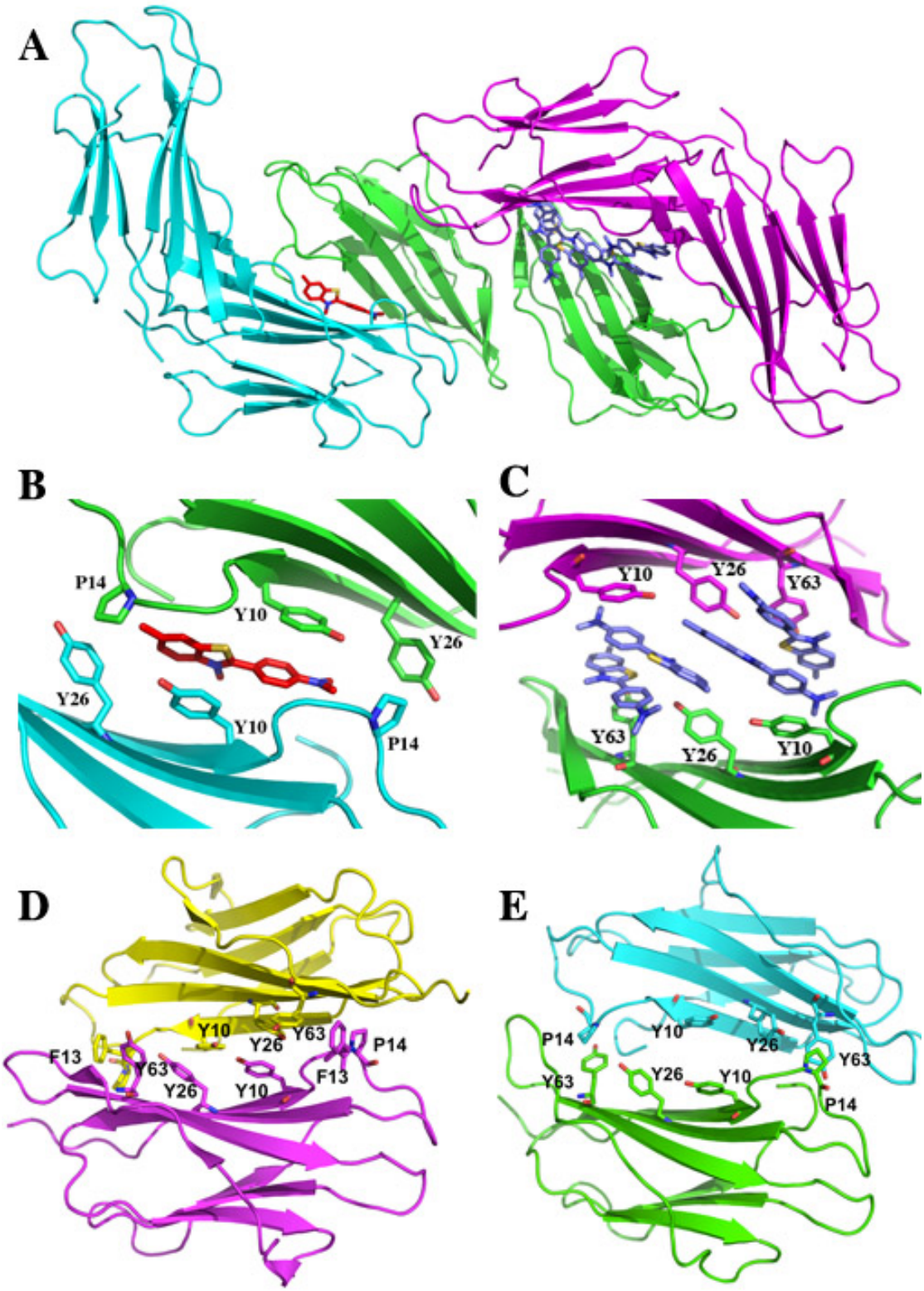
A
B
P14
Y10
Y26
Y26
Y10
P14
C
Y10
Y26
Y63
Y63
Y26
Y10
D
Y10
Y26
Y63
P14
F13
Y63
Y26
Y10
F13
E
P14
Y10
Y26
Y63
Y63
Y26
Y10
P14

Supplementary

Analysis of 3MZT Structure

The structure with the PDB code 3MZT was reported as a complex of hexameric H13F β2m mutant together with Thioflavin (ThT). The structure was determined to 2.70Å resolution. Three ThT molecules have been modeled sandwiched at the three of the intermolecular interfaces present in the hexameric assembly. All three ThT molecules have been modeled in two alternative but almost superposable conformations (0.5 occupancy each). Temperature factors for ThT atoms range between 80 and 120 $Å^2$ for each of the two conformations.

Furthermore, once the structure was refined in absence of the ThT molecules the residual electron density for ThT is reduced to a little blob of the size of a water molecule.

Wild type Beta-2 microglobulin and DE loop mutants display a common fibrillar architecture

Antonino Natalello[1]#, Annalisa Relini[2]#, Amanda Penco[2], Levon Halabelian[3], Martino Bolognesi[3], Silvia Maria Doglia[1], Stefano Ricagno[3]*

[1] Dipartimento di Fisica G. Occhialini and Dipartimento di Biotecnologie e Bioscienze, Università di Milano-Bicocca, P.zza della Scienza 2, 20126 Milano (Italy)

[2] Dipartimento di Fisica, Università di Genova, via Dodecaneso 33, 16146 Genova, Italy

[3] Dipartimento di Bioscienze, Università di Milano, Via Celoria 26, 20133 Milano, Italy

# AN and AR equally contributed to this work

* to whom correspondence should be addressed:
Dipartimento di Bioscienze,
Università di Milano
Via Celoria, 26
I-20133 Milano - Italy
phone: +39 02 50314914
fax: +39 02 50314895
e-mail: stefano.ricagno@unimi.it

Manuscript: Words 6479, Characters 41565

Keywords: Beta-2 microglobulin, amyloid fibrils, DE loop, Atomic force microscopy, Infrared spectroscopy.

ABSTRACT

Beta-2 microglobulin (β2m) is the protein responsible for a pathologic condition known as dialysis related amyloidosis. In recent years an important role has been assigned to the peptide loop linking strands D and E (DE loop) in determining β2m stability and amyloid propensity. Several mutants of the DE loop have been studied, showing a good correlation between DE loop geometrical strain, protein stability and aggregation propensity. However, it remains unclear whether the aggregates formed by wild type (wt) β2m and by the DE loop variants are of the same kind, or whether the mutations open new aggregation pathways. In order to address this question, fibrillar samples of wt and mutated β2m variants have been analysed by means of atomic force microscopy and infrared spectroscopy. The data here reported indicate that the DE loop mutants form aggregates with morphology, structural organisation and dynamics very similar to the wt protein. Therefore, the main effect of β2m DE loop mutations is proposed to stem from the different stabilities of the native fold. Considerations on the structural role of the DE loop in the free monomeric β2m and as part of the Major Histocompatibility Complex are also presented.

INTRODUCTION

Amyloidosis is characterized by the conversion of a protein from its native state into insoluble highly organized fibrillar aggregates, being at the roots of several protein misfolding diseases in man, such as Alzheimer, Parkinson and Huntington diseases [1]. β2-microglobulin (β2m) is the light chain of class I major histocompatibility complex (MHC-I) [2]. It is a 99-residue protein displaying a classic immunoglobulin fold, based on two facing β-sheets that are linked by a disulphide bond. Under physiological conditions, β2m turnover takes place in kidneys, where it is degraded. In case of renal failure, the degradation of β2m does not occur, and the protein accumulates in the blood increasing its concentration up to 50-fold in hemodialysed patients [3]. When such high β2m blood level is retained over the years, the protein self-associates into amyloid fibrils [4], which accumulate around the skeletal joints, bones and muscles. Such condition, known as dialysis related amyloidosis, is characterized by typical symptoms such as movement impairment, bone fragility, and carpal syndrome [4].

Somehow contradictory is the observation that *in vitro* β2m is a very stable protein, reaching mM concentrations without precipitating or aggregating, and yet *in vivo* at much lower concentration β2m turns into amyloid deposits [5]. Although several factors, such as type I collagen and glycosaminoglycans (GAGs) [6-8] have been reported to facilitate β2m aggregation, very little light has been shed on the β2m regions that trigger or mediate the fibril formation.

Many studies have shown the relevance of different β2m stretches in determining the protein aggregation propensity. Among others, the *cis* to *trans* isomerisation of Pro32, in the BC-loop, has been shown to be one of the fundamental steps of the conversion from the native fold to the amyloidogenic intermediate [9]; in keeping with this observation, no *cis*-Pro residues have been observed in the mature β2m fibrils [10]. Moreover, the N-terminal six residues are known to stabilise the β2m fold; accordingly, the natural variant ΔN6 (*i.e.* β2m

devoid of the first six residues) is highly amyloidogenic [11]. Notably, the natural β2m mutant (D76N), recently discovered, highlights the role of the EF loop in determining β2m stability and aggregation propensity [12].

Over the years Trp60 and in general the β2m DE-loop (residues 57-60) have been shown to be crucial in determining many of the wild type (wt) β2m biochemical and biophysical properties (Fig. 1A) [13-15]. Trp60 is a highly conserved residue in vertebrate β2m, being primarily involved in the association interface linking β2m to the heavy chain within the MHC-I complex [16]. We recently showed that the interactions within the MHC-I complex greatly stabilise the β2m fold (Fig. 1B) [17]; however, while the DE-loop is designed to play a role in formation of the MHC-I complex, it appears as an element of instability for monomeric β2m in solution. Many data collected over the past few years support such view. First of all, the DE-loop displays a non-ideal backbone geometry [16,18]. In order to test whether the DE-loop geometry might be relevant for β2m biochemical and aggregation properties, Trp60 was mutated to Gly, to obtain a less strained DE-loop (W60G mutant) [16], and to Val, to verify the effect of the Trp side chain alone (W60V mutant) [18]. Asp59 was mutated to Pro (D59P mutant), to evaluate the effects of an even more rigid DE-loop on the overall β2m molecule [19]. β2m thermodynamic stability, measured by temperature and chemical unfolding, correlates well with the DE-loop geometry [15]. Aggregation kinetics indicate that the lower is the thermodynamic stability, the faster and more abundant is the aggregation [13]. However, other data are indicating some direct role of Trp60 in β2m aggregation: first of all electrospray-mass spectrometry under native conditions showed that while wt β2m in solution presents a non-negligible population of small oligomers, the mutant W60G and W60V showed markedly reduced tendency to native aggregation [15]. Under standard conditions the W60V mutant is aggregating less abundantly than wt β2m [18].

Overall, the above evidence clearly indicates that the DE-loop is a major determinant of β2m fold thermodynamic stability and aggregation propensity. However, one main

question about the effect(s) of the DE-loop mutations on β2m amyloid aggregation remains open. The mutations in the DE-loop may result in thermodynamic (de)stabilization of the native protein, which in turn can alter the kinetic barrier(s) along the aggregation process, while the aggregation pathway remains unaltered. An alternative possibility is that such mutations may affect β2m aggregation propensity by opening new aggregation pathways and leading to different and unrelated kind(s) of β2m aggregates. To address this question, we performed a comparative biophysical characterisation of amyloid aggregates formed by wt β2m and DE loop mutants. In particular, the morphology and structural organization of early aggregates and mature fibrils have been analysed by Atomic Force Microscopy (AFM); then, the dynamics and the overall secondary structure content for the fibrils of the four β2m variants have been monitored by Fourier transform infrared (FTIR) spectroscopy. Previous data showed that the DE loop mutations exert a major effect on the stability of the β2m native fold and affect the aggregation kinetics [13, 15] while the experiments here presented indicate that the fibrils of the DE loop variants and of wt β2m have comparable architecture and dynamics, suggesting that mutations at the DE loop effects are limited to the β2m aggregation process, and do not alter the end stage of the aggregation pathway.

METHODS

Sample preparation

Wt β2m and the three mutated variants (W60G, D59P, W60V) were expressed and purified as previously described [16].

The aggregated samples were prepared as follows: 100 μM β2m was incubated at 37 °C under shaking (600 rpm) in 50 mM Na phosphate buffer, 100 mM NaCl, pH 7.4, in the presence of 20% (v/v) TFE [20]; 20 μg/ml of β2m fibril seeds were added to the samples. Wt β2m and its variants were incubated for 24 h or for one week under the aggregation

conditions. The formation of fibrillar aggregate has been monitored by measuring Thioflavin T (ThT) fluorescence according to LeVine [21].

Atomic force microscopy

For AFM inspection, samples were diluted 500-fold and a 10 μl aliquot was deposited on a freshly cleaved mica substrate, and dried under mild vacuum. Alternatively, to recover fibrillar material, samples were centrifuged at 4000 rpm for 10 min using an Eppendorf 5417R centrifuge, the pellet was suspended in an equal volume of water, and a 10 μl aliquot was deposited on mica and dried under mild vacuum.

AFM images were acquired in tapping mode in air using a Dimension 3100 Scanning Probe Microscope equipped with a 'G' scanning head (maximum scan size 100 μm) and driven by a Nanoscope IIIa controller, and a Multimode Scanning Probe Microscope equipped with ''E'' scanning head (maximum scan size 10 μm), driven by a Nanoscope IV controller (Digital Instruments – Bruker). Single beam uncoated silicon cantilevers (type OMCL-AC160TS, Olympus) were used. The drive frequency varied between 270 and 330 kHz, the scan rate was between 0.5 and 0.8 Hz. Aggregate size was measured from the height in cross section of topographic AFM images.

Fourier transform infrared spectroscopy

The infrared absorption spectra were collected in the attenuated total reflection (ATR) mode on a single reflection diamond element (Golden Gate, Specac, USA). The fibrils of the β2m variants, obtained by centrifugation at 17000 x g for 15 min at 4°C and resuspended in the fibrillogenesis buffer for a second centrifugation, were transferred to the ATR plate and dried at room temperature in order to obtain a protein hydrated film [22-24]. In order to study the hydrogen/deuterium (H/D) exchange of the sample, the FTIR spectra were collected on the protein films before and after the addition of 3μL of D_2O [22]. FTIR measurements were performed using the Varian 670-IR spectrometer (Varian Australia Pty

Ltd, Mulgrave VIC, Australia) under the following conditions: 2 cm^{-1} resolution, a scan speed of 25 kHz, triangular apodization, and a nitrogen-cooled Mercury Cadmium Telluride detector. In order to follow the H/D exchange kinetics, the number of scan coadditions was adjusted from 15 (immediately after D_2O addition) to 2000 (starting from about 6 hours after D_2O addition). The measured spectra were smoothed by the Savitsky-Golay method before the second derivative analysis, both performed by the Resolutions-Pro software (Varian Australia Pty Ltd, Mulgrave VIC, Australia). As controls, the same FTIR characterisations have been performed on the native wt β2m (at 5 mg/mL concentration in Na phosphate buffer 50mM, pH 7.4) and on the supernatant of W60G mutant. In this last case, after one week incubation under fibrillogenesis conditions, the W60G sample was centrifuged at 17000 x g for 15 min at 4°C and the supernatant was concentrated three times by a centrifugal filter device (Microcon, Millipore Corporation, Bedford, MA, USA) at 4°C. The protein film, obtained from a supernatant volume of 3μL, was subjected to the FTIR characterisations as described above for the β2m fibrils.

RESULTS

Amyloid fibril preparation

Purified samples of wt β2m and of the three DE loop variants have been placed under standard aggregation conditions (see methods). Aggregated samples after 24 hours and after one week incubation have been tested for thioflavin fluorescence (Table I) and have been analysed by means of AFM and FTIR.

Characterisation of the amyloid aggregates by AFM

Tapping mode AFM allowed us to inspect the morphologies of the β2m aggregates formed by the different variants. Representative images of the samples aggregated for 24 h,

and deposited on the mica substrate after dilution, are reported in Figure 2. Wt β2m mainly displayed isolated oligomers with a height of 5-10 nm, or oligomer chains (Fig. 2A), while the D59P variant extensively formed planar sheets of fibrils, about 4 nm high (Fig. 2B). The height of these fibrils is significantly lower than that measured for mature fibrils, suggesting that the thinner fibrils are either intermediate structures or structures resulting from an epitaxial growth induced by the mica substrate. In any case, they reflect a strong tendency to fast aggregation, which is distinctive for this variant. Large oligomer clusters were observed for the W60V variant (Fig. 2C). For the W60G variant, oligomers with a height of 8 - 15 nm, and very short protofibrils formed by few oligomeric units, were found (Fig. 2D). Mature fibrils were not observed for any of the variants, probably due to the relatively low fraction of fibrillar material. Therefore, samples were centrifuged and the pellet was analysed to check for the presence of mature fibrils. In all cases except for W60G β2m, mature fibrils were abundant in the pellet and were intertwined in clusters (Fig. 2E-G). A different behaviour was found for the W60G variant, which exhibited only very short, almost isolated, fibrillar structures (Fig. 2H).

To increase the fraction of fibrillar material and ensure that all the variants yielded mature fibrils, aggregated samples incubated for one week were prepared. Topographic images of the mature fibrils obtained for the wt and the different mutants after prolonged incubation are shown in Fig. 3A-D. Both wt β2m and the variants formed fibril clusters, but for the W60G mutant the cluster size was smaller than for the other variants. In many cases fibrils exhibit a twist with a periodicity varying between 40 and 60 nm. The fibril height distributions are reported in Fig. 3E-H. All the height distributions share a main peak at about 7 nm, indicating the presence of a common fibrillar structure as a main component. However, for W60V β2m the measured height values span a much broader range than in other cases, indicating the formation of more complex assemblies, which can still be recognized as isolated fibrils. W60G β2m fibrils are shorter than those formed by the other variants. The fibril mean lengths were (28±5)·10 nm, (70±1)·10 nm and (40±6)·10 nm for W60G β2m,

W60V β2m and D59P β2m, respectively. For wt β2m, most fibrils were so closely intertwined that single fibrils could not be distinguished, preventing an estimate of the fibril length.

Collectively, the results of the AFM analysis suggest that a common mechanism of fibril formation takes place for wt β2m and the variants, although the details of the aggregation process can be different. The differences observed between the variants may be ascribed to their different aggregation propensities.

Structure and dynamics of amyloid fibrils monitored by FTIR

The structural properties of the wt and DE loop β2m variants were examined by FTIR spectroscopy. In particular, we studied the fibril secondary structures and the hydrogen/deuterium (H/D) exchange kinetics of their core intermolecular β-sheet structures. As control experiments, the FTIR absorption spectra of the native wt β2m were also measured before and after D_2O addition (Fig. 4A-C). To disclose the protein secondary structures the second derivatives of the absorption spectra were obtained (Fig. 4B) [25,26]. The Amide I band (1700-1600 cm^{-1}) of native wt β2m is characterised by the two components at ~1637 cm^{-1} and at ~1691 cm^{-1} that can be assigned to the intramolecular antiparallel β-sheet structures of the protein, in agreement with previous FTIR characterisations [13,27,28]. Other minor components (Fig. 4B) around 1678 cm^{-1} and 1668 cm^{-1} (assigned to turns) and around 1614 cm^{-1} (likely due to β-sheets or amino acid side-chains) were observed [13,27-29]. Upon the addition of D_2O, a fast reduction of the band at 1535-1537 cm^{-1} (Amide II band mainly due to the amide groups NH bending vibrations) takes place with a simultaneous increase of the band at 1443-1447 cm^{-1} (called Amide II'), evidence of the H/D exchange (Fig. 4A), where the amide protons in accessible protein regions are replaced by deuterium [22]. The exchange of the different protein secondary structures can be monitored by the downshift of their peak positions in the second derivative spectra, as reported in Figure 4C. In particular, the main intramolecular β-sheet component of native wt protein downshifted from ~1637 cm^{-1}

to ~1633 cm^{-1} (Fig. 4B and 4C), whereas the high-wavenumber β-sheet component downshifted from ~1691 cm^{-1} to ~1682 cm^{-1}. The final peak positions of the native β-sheet components obtained in the D_2O-hydrated film are in agreement with those found for the deuterated β2m in previous FTIR studies performed in transmission mode [13,27,30].

The FTIR absorption spectra of fibrillar wt β2m and their second derivatives are reported in Figures 4D and 4E, respectively. The main Amide I component occurs around 1621 cm^{-1} that, with the 1693 cm^{-1} weaker component, can be unambiguously assigned to the intermolecular β-sheet structures of the undeuterated fibrils. The assignment of the additional components in the 1675-1634 cm^{-1} spectral region is not unequivocal. Indeed, as discussed in the literature [25,27,30-32], they can be assigned to turns (typically in the 1686-1660 cm^{-1} range), to loops (typically in the 1650-1640 cm^{-1} range), to native-like structures (around 1634 cm^{-1}) or to a peculiar arrangement of the β-strands in the protein supramolecular assemblies [30]. We should note that the relative intensities of these components displayed a slight heterogeneity in independent fibril preparations; therefore, in Figure 4E two representative second derivative spectra of wt (undeuterated) fibril films are reported.

To study the dynamics of the fibril core β-sheet structure, H/D exchange experiments were performed, as reported in Fig. 4D-F. In particular, during incubation in D_2O, the main intermolecular β-sheet peak downshifted from ~1621 cm^{-1} in the undeuterated fibrils to ~1618 cm^{-1} after 23 hours of incubation in D_2O (Fig. 4E and 4F). The same characterisations have been performed on the fibrils of the DE-loop mutants (Fig. 5).

The undeuterated fibrils of D59P and of W60V variants share with aggregates of wt β2m the same two main Amide I components around 1693 cm^{-1} and 1621cm^{-1} that can be assigned to the intermolecular β-sheet structures (Fig. 5B and 5D). This result is in agreement with previous FTIR characterizations [13] on the same b2m variants studied here. Indeed, in these earlier experiments, the aggregation of unseeded wt and DE loop mutants took place inside the infrared cell, leading to final aggregates characterized by the same intermolecular β-sheet Amide I' components.

Concerning the H/D exchange experiments presented in this work, as observed for wt fibrils, the main intermolecular β-sheet peak of D59P and of W60V fibrils was found to downshift from ~1621 cm^{-1} to around 1618 cm^{-1} after 23 hours of incubation in D_2O (Fig. 5A-D). The time dependence of this peak position is reported in Figure 5E for the wt, D59P, and W60V variants. A similar H/D exchange kinetics was observed for these three variants as can be seen from the partially overlapped standard deviations of independent fibril preparations (Figure 5E). Indeed, the fibril second derivative spectra of the variants displayed similar Amide I components, with the main intermolecular β-sheet band peaked at the same wavenumber and characterized by a comparable H/D exchange (Fig. 4-5). These results suggest that the fibrils of the three variants are characterized by comparable intermolecular β-sheet structures and dynamics. However, the relative intensity of the other weaker Amide I components (at ~1647-1644 cm^{-1} and ~1634 cm^{-1}) was found to vary in the final fibrils of the variants, indicating that minor structural rearrangements occurred in the presence of the mutations.

In agreements with the low aggregation propensity of the W60G mutant [13,16], a low amount of fibrils was obtained by centrifugation of this sample after 1 week incubation under fibrillogenic conditions. The absorption spectrum of the W60G fibrils displayed the same Amide I maximum as observed for the other variants (Fig. 5F). Unfortunately, the low amount of the collected W60G fibrils did not allow to obtain high quality ATR/FTIR spectra suitable for second derivative analysis and H/D exchange experiments and a significant amount of the W60G protein was instead found in the supernatant. In particular, the spectrum of the supernatant (Fig. 5F and 5G) displayed two main components at ~1691 cm^{-1} and at ~1636 cm^{-1}, assigned to native-like intramolecular β-sheet structures, which after 23 hours incubation in D_2O downshifted, respectively, to ~1688 cm^{-1} and ~1634 cm^{-1}.

All this considering, the FTIR results indicate that the wt β2m and the three DE loop variants investigated here (D59P, W60V, W60G) formed, under the same aggregation conditions, amyloid fibrils characterized by a common intermolecular β-sheet structure, with comparable H/D exchanges, and by limited structural differences among the different

mutants. The previously reported low aggregation propensity of the W60G mutant was also confirmed here [13,16].

DISCUSSION

Amyloid aggregation is a life threatening process, which is at the basis of many severe pathologic conditions. Protein aggregation is a complex process, and the heterogeneity of such process adds serious challenges to its structural and biophysical characterisation. The lack of detailed structural data on amyloid formation undermines our understanding of the pathologic process and hampers the design of pharmacological therapies. Over the last 10-20 years one of the most successful strategies to gather biochemical and biophysical evidence on protein aggregation has been to mutate the polypeptide sequence, testing the aggregation properties of the mutated variants, thus inferring the role played by selected residues during amyloid aggregation. However, mutations may introduce several independent effects; mutations can subtly affect the structure of the protein, its dynamics, its thermodynamic stability, the energetic barriers between different states *etc*. Therefore, not only is it crucial to observe that a modified aggregation propensity stems from a specific mutation, but it is also necessary to understand which effect(s) the mutation exerts on aggregation end point. In particular, many cases are known where mutations lead to off-pathway states or trigger a different kind of aggregation. The elegant crystal structure of hexameric β2m reveals many interesting intermolecular interactions, however such hexameric form does not aggregate under standard conditions [33], leaving open the question on which are the interactions that set the hexamer off-pathway. Specific mutations may structurally protect the protein from the aggregation pathway undertaken by the wt protein, but in parallel open new paths to amyloid formation, as recently exemplified by protective mutations on Acylphosphatase from *Sulfolobus solfataricus* [34,35].

To date, using different techniques, we have shown that many marked effects stemmed from mutations in the DE loop: thermodynamic stability and aggregation propensity vary according to the DE loop geometry [15,18]. However, in order to draw conclusions on the role of the DE loop on β2m amyloid aggregation it is crucial to establish whether the final step of aggregation (*i.e*. the amyloid fibrils) is maintained. Should the starting and the end points of the aggregation process be conserved in wt β2m and in the mutants, we could propose a conservation of the aggregation process for the four explored variants. In such a scenario the effects previously observed upon mutations in the DE loop could be discussed in the context of the wt protein aggregation process. Conversely, formation of aggregates by the DE loop mutants not sharing structural features with those displayed by the wt protein would imply the onset of distinct aggregation pathway(s), ultimately preventing us from assigning any role to the DE loop in the aggregation of wt β2m. Based on such considerations, we deemed relevant to investigate the nature of the amyloid aggregates produced by the DE loop mutants, compared to those formed by wt β2m, to clarify the role played by the loop on β2m amyloid propensity.

First, quantitative information about aggregate size and shape has been obtained by AFM. The images acquired from samples incubated for 24 hours confirm, as previously reported [13], that wt β2m and the three DE loop variants display different aggregation kinetics. In particular, D59P β2m exhibited a fast aggregation, giving rise to sheets of thin fibrils, which were not observed either in wt β2m or in the other variants. W60G β2m showed the slowest aggregation, as after 24 hours fibrils were rare and short even in the pellet, differently from the other samples. In the pellets of samples incubated for a week, mature fibrils were found for wt β2m and the three variants. The analysis of fibrils cross-sections indicates that in all cases the fibril populations share a peak at about 7 nm in the height distributions. The fibril heights observed for the samples analysed in the present study are consistent with those reported by Ohhashi *et al.* for wt β2m fibrils formed at neutral pH by ultrasonication in the presence of SDS [36]. Although these aggregation conditions are not the

same as in our study, they can be considered as somewhat equivalent; in fact, it has been observed that both TFE and SDS act as hydrophobic co-solvents favouring fibrillation [37].

The AFM analysis indicates that despite differences in the aggregation kinetics, the wt β2m and three mutants give rise to fibrils with comparable heights that suggest a common fibrillar architecture. Moreover, the secondary structure content detected by ATR/FTIR in mature aggregates, shows that all four kind of fibrils are characterised by the same Amide I components due to the intermolecular β-sheet structures of the final protein assemblies. Finally, H/D exchange was employed to evaluate structural dynamics, compactness, and stability, providing information on fibril molecular packing. In keeping with the biophysical characterizations reported above, H/D exchange kinetics observed for wt β2m and the DE loop mutants aggregates are well comparable, further suggesting that the overall fibril assembly is shared among the four protein variants.

CONCLUSIONS

In summary, the data presented here suggest that the mutations in the DE loop do not alter significantly the overall structural properties of the β2m amyloid aggregates. Given that β2m native fold and the mature fibrillar aggregates appear unaltered ([18] and this work), we propose that the aggregation process is conserved for the β2m mutants examined here, and that the DE loop is a crucial region determining the wt β2m aggregation propensity, affecting the aggregation kinetics. In particular, it has been found that the DE loop has a strong thermodynamic influence on the β2m native state. This loop is a source of instability that likely determines the energies associated with the different folded states and the energetic barriers between them, resulting in the aggregation propensity observed for monomeric wt β2m. By simple modifications of residues and of the geometry in this loop it is possible to tune the stability of the β2m fold and to practically abolish (or to increase) β2m amyloid formation. Such observations can be reconciled with the evolution of β2m as structural part of

the MHC-I complex. Notably the DE loop of human β2m has the main role of properly orienting Phe56 (just upstream the loop) and Trp60 for the interaction with the heavy chain in the MHC-I (Fig. 1B). The presence and the positioning of the bulky Trp60 side chain is ideal for the interaction with an amphipathic cleft of the neighbouring heavy chain; therefore in general the loop strained geometry and the overall β2m fold are efficiently stabilised by the tight interactions between β2m and the heavy chain in the MHC-I complex [17]. However, once wt β2m is released in the blood as a monomer, even if it is globally very stable, it presents in the DE loop all the ingredients for misfolding: a conformational strain which makes the D strand and DE loop region flexible and unstable [16], and a patch of solvent-exposed aromatic side chains in the D and E strands and in the DE loop, which will drive an overall entropy gain upon protein aggregation (see also [38]).

Acknowledgments

We are grateful to Prof. Vittorio Bellotti, University College London (UK) and University of Pavia (Italy) for continuous discussion and support. We thank Diletta Ami, University of Milano-Bicocca (Italy), for assistance in the FTIR analysis and for insightful discussion. This work was supported by the Italian Ministry of University and Research Project FIRB RBFR109EOS (to SR), by Cariplo Foundation (Milano, Italy: Project n 2013-0964 to SMD, AR and AN) and by University of Genoa (Fondi di Ateneo, to AR and AP).

REFERENCES:

1. Merlini G, Bellotti V (2003) Molecular mechanisms of amyloidosis. N Engl J Med 349: 583-596.
2. Porcelli SA, Modlin RL (1999) The CD1 system: antigen-presenting molecules for T cell recognition of lipids and glycolipids. Annu Rev Immunol 17: 297-329.
3. Floege J, Ketteler M (2001) beta2-microglobulin-derived amyloidosis: an update. Kidney Int Suppl 78: S164-171.
4. Gejyo F, Yamada T, Odani S, Nakagawa Y, Arakawa M, et al. (1985) A new form of amyloid protein associated with chronic hemodialysis was identified as beta 2-microglobulin. Biochem Biophys Res Commun 129: 701-706.
5. Okon M, Bray P, Vucelic D (1992) 1H NMR assignments and secondary structure of human beta 2-microglobulin in solution. Biochemistry 31: 8906-8915.
6. Myers SL, Jones S, Jahn TR, Morten IJ, Tennent GA, et al. (2006) A systematic study of the effect of physiological factors on beta2-microglobulin amyloid formation at neutral pH. Biochemistry 45: 2311-2321.
7. Relini A, Canale C, De Stefano S, Rolandi R, Giorgetti S, et al. (2006) Collagen plays an active role in the aggregation of beta2-microglobulin under physiopathological conditions of dialysis-related amyloidosis. J Biol Chem 281: 16521-16529.
8. Relini A, De Stefano S, Torrassa S, Cavalleri O, Rolandi R, et al. (2008) Heparin strongly enhances the formation of beta2-microglobulin amyloid fibrils in the presence of type I collagen. J Biol Chem 283: 4912-4920.
9. Eakin CM, Berman AJ, Miranker AD (2006) A native to amyloidogenic transition regulated by a backbone trigger. Nat Struct Mol Biol 13: 202-208.
10. Barbet-Massin E, Ricagno S, Lewandowski JR, Giorgetti S, Bellotti V, et al. (2010) Fibrillar vs crystalline full-length beta-2-microglobulin studied by high-resolution solid-state NMR spectroscopy. J Am Chem Soc 132: 5556-5557.
11. Esposito G, Michelutti R, Verdone G, Viglino P, Hernandez H, et al. (2000) Removal of the N-terminal hexapeptide from human beta2-microglobulin facilitates protein aggregation and fibril formation. Protein Sci 9: 831-845.
12. Valleix S, Gillmore JD, Bridoux F, Mangione PP, Dogan A, et al. (2012) Hereditary systemic amyloidosis due to Asp76Asn variant beta2-microglobulin. N Engl J Med 366: 2276-2283.
13. Ami D, Ricagno S, Bolognesi M, Bellotti V, Doglia SM, et al. (2012) Structure, stability, and aggregation of beta-2 microglobulin mutants: insights from a Fourier transform infrared study in solution and in the crystalline state. Biophys J 102: 1676-1684.
14. Rennella E, Corazza A, Giorgetti S, Fogolari F, Viglino P, et al. (2010) Folding and fibrillogenesis: clues from beta2-microglobulin. J Mol Biol 401: 286-297.
15. Santambrogio C, Ricagno S, Colombo M, Barbiroli A, Bonomi F, et al. (2010) DE-loop mutations affect beta2 microglobulin stability, oligomerization, and the low-pH unfolded form. Protein Sci 19: 1386-1394.
16. Esposito G, Ricagno S, Corazza A, Rennella E, Gumral D, et al. (2008) The controlling roles of Trp60 and Trp95 in beta2-microglobulin function, folding and amyloid aggregation properties. J Mol Biol 378: 885-895.
17. Halabelian L, Ricagno S, Giorgetti S, Santambrogio C, Barbiroli A, et al. (2014) Class I Major Histocompatibility Complex, the Trojan Horse for Secretion of Amyloidogenic beta2-Microglobulin. J Biol Chem 289: 3318-3327.
18. Ricagno S, Raimondi S, Giorgetti S, Bellotti V, Bolognesi M (2009) Human beta-2 microglobulin W60V mutant structure: Implications for stability and amyloid aggregation. Biochem Biophys Res Commun 380: 543-547.

19. Ricagno S, Colombo M, de Rosa M, Sangiovanni E, Giorgetti S, et al. (2008) DE loop mutations affect beta-2 microglobulin stability and amyloid aggregation. Biochem Biophys Res Commun 377: 146-150.
20. Yamamoto S, Yamaguchi I, Hasegawa K, Tsutsumi S, Goto Y, et al. (2004) Glycosaminoglycans enhance the trifluoroethanol-induced extension of beta 2-microglobulin-related amyloid fibrils at a neutral pH. J Am Soc Nephrol 15: 126-133.
21. LeVine H, 3rd (1993) Thioflavine T interaction with synthetic Alzheimer's disease beta-amyloid peptides: detection of amyloid aggregation in solution. Protein Sci 2: 404-410.
22. Goormaghtigh E, Raussens V, Ruysschaert J-M (1999) Attenuated total reflection infrared spectroscopy of proteins and lipids in biological membranes. Biochimica et Biophysica Acta - Reviews on Biomembranes 1422: 105-185.
23. Natalello A, Frana AM, Relini A, Apicella A, Invernizzi G, et al. (2011) A Major Role for Side-Chain Polyglutamine Hydrogen Bonding in Irreversible Ataxin-3 Aggregation. PLoS ONE 6: e18789.
24. Natalello A, Mattoo RUH, Priya S, Sharma SK, Goloubinoff P, et al. (2013) Biophysical Characterization of Two Different Stable Misfolded Monomeric Polypeptides That Are Chaperone-Amenable Substrates. Journal of molecular Biology 425: 1158-1171.
25. Barth A (2007) Infrared spectroscopy of proteins. Biochimica Et Biophysica Acta-Bioenergetics 1767: 1073-1101.
26. Susi H, Byler DM (1986) Resolution-Enhanced Fourier-Transform Infrared-Spectroscopy of Enzymes. Methods in Enzymology 130: 290-311.
27. Fabian H, Naumann D (2012) Millisecond-to-Minute Protein Folding/Misfolding Events Monitored by FTIR Spectroscopy. In: Fabian H, Naumann D, editors. Protein Folding and Misfolding: Springer Berlin Heidelberg. pp. 53-89.
28. Kardos J, Okuno D, Kawai T, Hagihara Y, Yumoto N, et al. (2005) Structural studies reveal that the diverse morphology of beta(2)-microglobulin aggregates is a reflection of different molecular architectures. Biochimica Et Biophysica Acta-Proteins and Proteomics 1753: 108-120.
29. Valdivia AA, Barth A, Batista YR, Kumar S (2013) Characterization of recombinant antibodies for cancer therapy by infrared spectroscopy. Biologicals 41: 104-110.
30. Fabian H, Gast K, Laue M, Jetzschmann KJ, Naumann D, et al. (2013) IR spectroscopic analyses of amyloid fibril formation of beta(2)-microglobulin using a simplified procedure for its in vitro generation at neutral pH. Biophysical Chemistry 179: 35-46.
31. Fabian H, Gast K, Laue M, Misselwitz R, Uchanska-Ziegler B, et al. (2008) Early stages of misfolding and association of beta(2)-microglobulin: Insights from infrared spectroscopy and dynamic light scattering. Biochemistry 47: 6895-6906.
32. Gelain F, Silva D, Caprini A, Taraballi F, Natalello A, et al. (2011) BMHP1-Derived Self-Assembling Peptides: Hierarchically Assembled Structures with Self-Healing Propensity and Potential for Tissue Engineering Applications. Acs Nano 5: 1845-1859.
33. Calabrese MF, Eakin CM, Wang JM, Miranker AD (2008) A regulatable switch mediates self-association in an immunoglobulin fold. Nat Struct Mol Biol.
34. de Rosa M, Bemporad F, Pellegrino S, Chiti F, Bolognesi M, et al. (2014) Edge strand engineering prevents native-like aggregation in Sulfolobus solfataricus acylphosphatase. FEBS J.
35. Soldi G, Bemporad F, Chiti F (2008) The degree of structural protection at the edge beta-strands determines the pathway of amyloid formation in globular proteins. J Am Chem Soc 130: 4295-4302.
36. Ohhashi Y, Kihara M, Naiki H, Goto Y (2005) Ultrasonication-induced amyloid fibril formation of beta2-microglobulin. J Biol Chem 280: 32843-32848.
37. Yamaguchi K, Naiki H, Goto Y (2006) Mechanism by which the amyloid-like fibrils of a beta 2-microglobulin fragment are induced by fluorine-substituted alcohols. J Mol Biol 363: 279-288.

38. Platt GW, Routledge KE, Homans SW, Radford SE (2008) Fibril growth kinetics reveal a region of beta2-microglobulin important for nucleation and elongation of aggregation. J Mol Biol 378: 251-263.

LEGENDS:

Figure 1: DE loop in monomeric β2m and in interaction within the MHC-I

(A) Ribbon representation of monomeric β2m (PDB code 2YXF). The DE loop residues are shown in yellow sticks. (B) Stereo view of the DE loop and Phe56 (yellow sticks) when interacting with the heavy chain in the MHC-I (electrostatic surface and green sticks). Trp60 is establishing a H-bond with Asp122 from the heavy chain (PDB code 4L29).

Figure 2: AFM characterisation of wt β2m and DE loop mutants aggregates incubated for 24 h

Tapping mode AFM images (top, height data; bottom, amplitude data) of wt β2m and DE loop mutants aggregated for 24h. Scan size 1.4 μm; Z range A) 30 nm; B) 35 nm; C) 100 nm; D) 60 nm. E-H) fibrils found in the pellets of samples A-D). Scan size 860 nm.

Figure 3: AFM characterisation of wt β2m and DE loop mutants aggregates incubated for one week

Tapping mode AFM images (height data) of mature fibrils of wt β2m and DE loop mutants obtained after one week incubation. Scan size 1.2 μm; Z range: A, D) 55 nm; B) 70 nm; C) 65 nm. E-H) histograms of fibril height measured from fibril cross-sections in the topographic AFM images.

Figure 4: ATR/FTIR characterisation of wt β2m in the native and the fibrillar state.

A) The absorption spectra of the native β2m in form of a protein film were collected before and after incubation in D_2O for different times. Spectra are reported in the regions of Amide I (AI), Amide II (AII), and Amide II' (AII'). Arrows point at increasing incubation time in D_2O. Absorption spectra are normalized at the Amide I maximum. B) Second derivatives of the absorption spectra of (A) in the Amide I region. The spectra collected after

D_2O addition were normalized at the tyrosine band [31]. The marked peak positions of the two components due to the native antiparallel β-sheet structures refer to the spectrum of the undeuterated sample. C) Time course of the peak position of the main native β-sheet component reported after D_2O addition to the protein film. Error bars represent the standard deviation of three independent samples. The peak positions were taken from the second derivative spectra. D) Absorption spectra of the wt β2m fibrils collected before and after incubation in D_2O, reported as in (A). E) Second derivatives of the absorption spectra of (D) in the Amide I region. Spectra of two undeuterated fibrils obtained from independent preparations are compared to show fibril heterogeneity. The spectra collected after D_2O addition were normalized at the tyrosine band [31]. The peak positions of the main components are indicated. F) Time course of the peak position of the main intermolecular β-sheet component is reported after D_2O addition. Error bars represent the standard deviation of three independent fibril preparations. The peak positions were taken from the second derivative spectra.

Figure 5: ATR/FTIR characterisation of DE loop mutants in the fibrillar state.

A) The absorption spectra of the D59P fibrils were collected before and after incubation in D_2O for different times. Spectra are reported in the regions of Amide I, Amide II, and Amide II' bands. Arrows point to the spectral changes at increased incubation time in D_2O. Absorption spectra are normalized at the Amide I maximum. B) Second derivatives of the absorption spectra of (A) in the Amide I region. The spectra collected after D_2O additions were normalized at the tyrosine band [31]. The peak positions of the main components are indicated. C) The absorption spectra of the W60V fibrils were collected before and after incubation in D_2O for different times and reported as in (A). D) Second derivatives of the absorption spectra of (C) in the Amide I region. E) Time course of the peak positions of the main intermolecular β-sheet component of wt, D59P, and W60V amyloid fibrils are reported after D_2O addition to the protein films. Error bars represent the standard deviation of at least three independent fibril preparations. The peak positions were taken from the second derivative spectra. F) The absorption spectra of W60G, wt, D59P, and W60V fibrils and that

of W60G supernatant are reported in the Amide I region. The intermolecular β-sheet structure absorption band is marked. G) Second derivative spectra of the W60G supernatant collected before and after 23 hours from D_2O addition. The peak positions of the main components are indicated.

Striking image

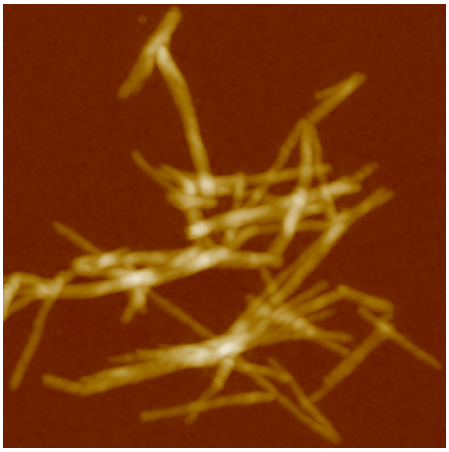

Tapping mode AFM image (height data) of mature fibrils of the W60G variant. Scan size 1.2 μm; Z range 55 nm.

Table I. Amyloid fibril formation of wt β2m, D59P, W60G and W60V β2m variants monitored by ThT fluorescence (given in arbitrary units).

	wt β2m	**D59P β2m**	**W60G β2m**	**W60V β2m**
24 hour incubation	40 (± 2)	46 (± 4)	18 (± 1)	29 (± 1)
1 week incubation	79 (± 21)	62 (± 15)	12 (± 2)	69 (± 22)

Fig. 1a

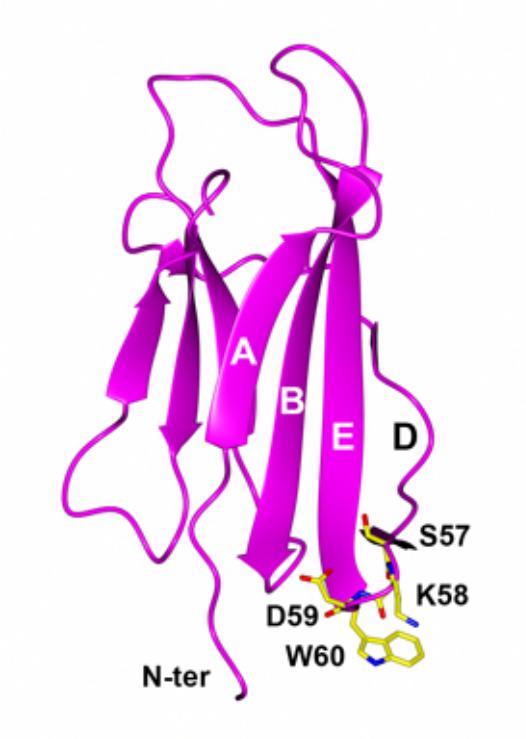

Fig. 1b

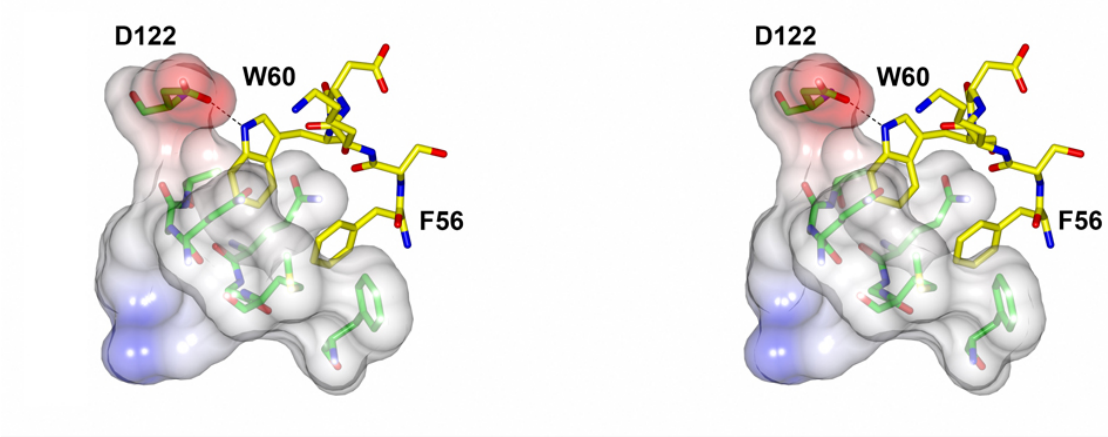

Fig. 2

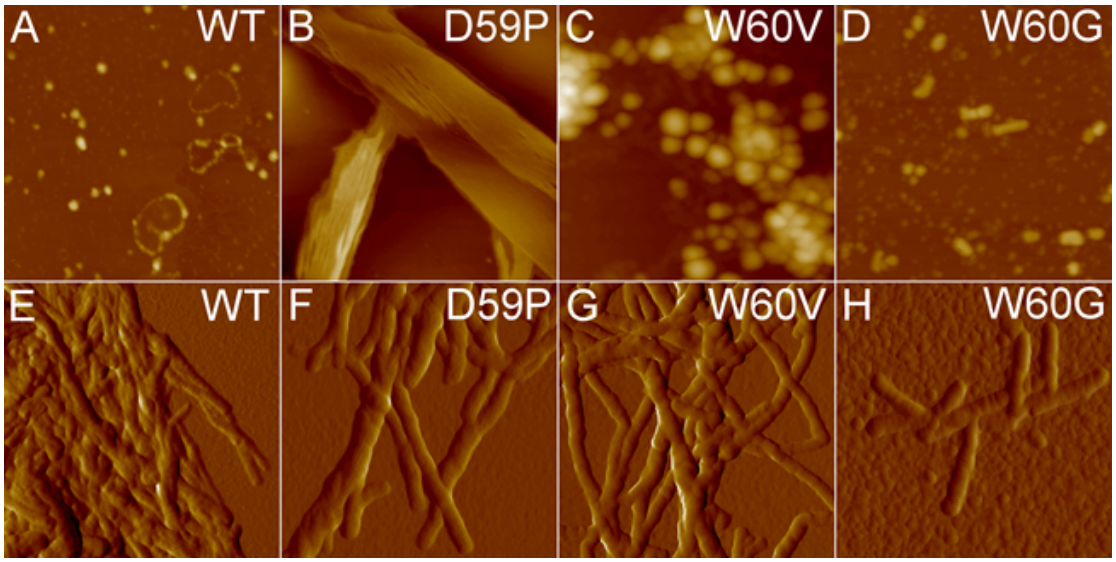
A WT
B D59P
C W60V
D W60G
E WT
F D59P
G W60V
H W60G

Fig. 3

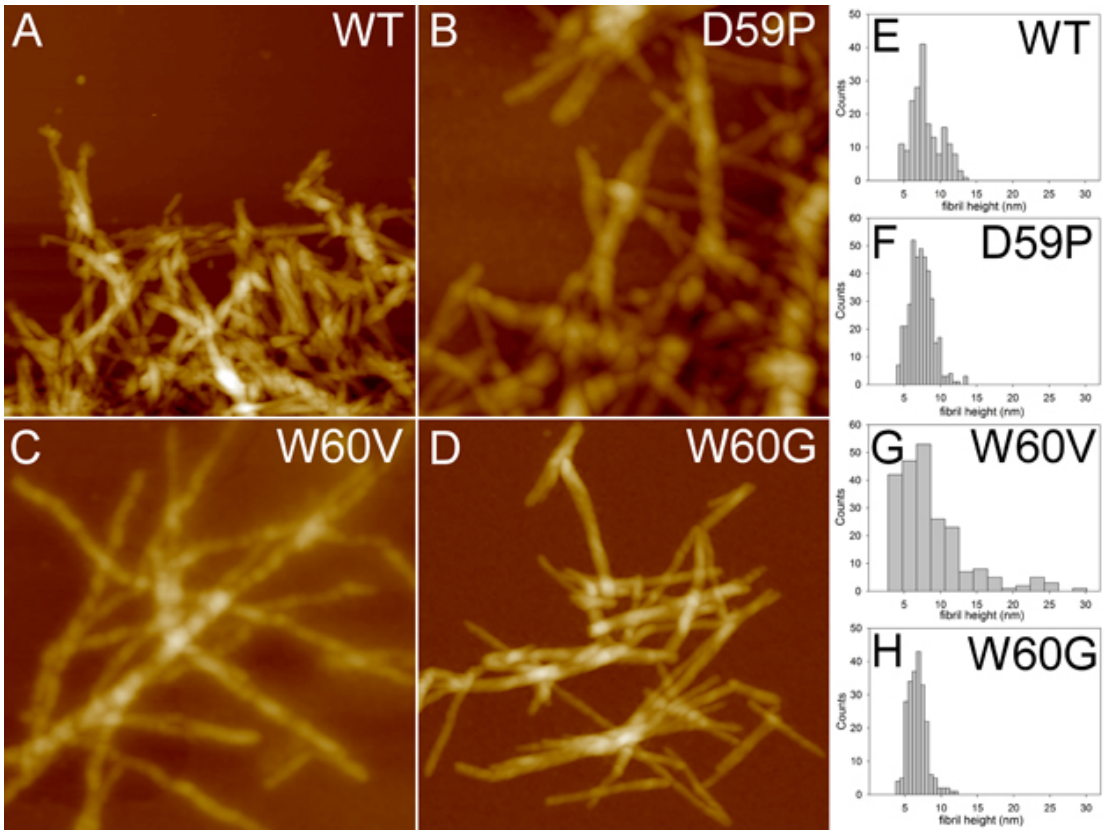
A WT
B D59P
C W60V
D W60G
E WT
F D59P
G W60V
H W60G
Counts
fibril height (nm)

Fig. 4

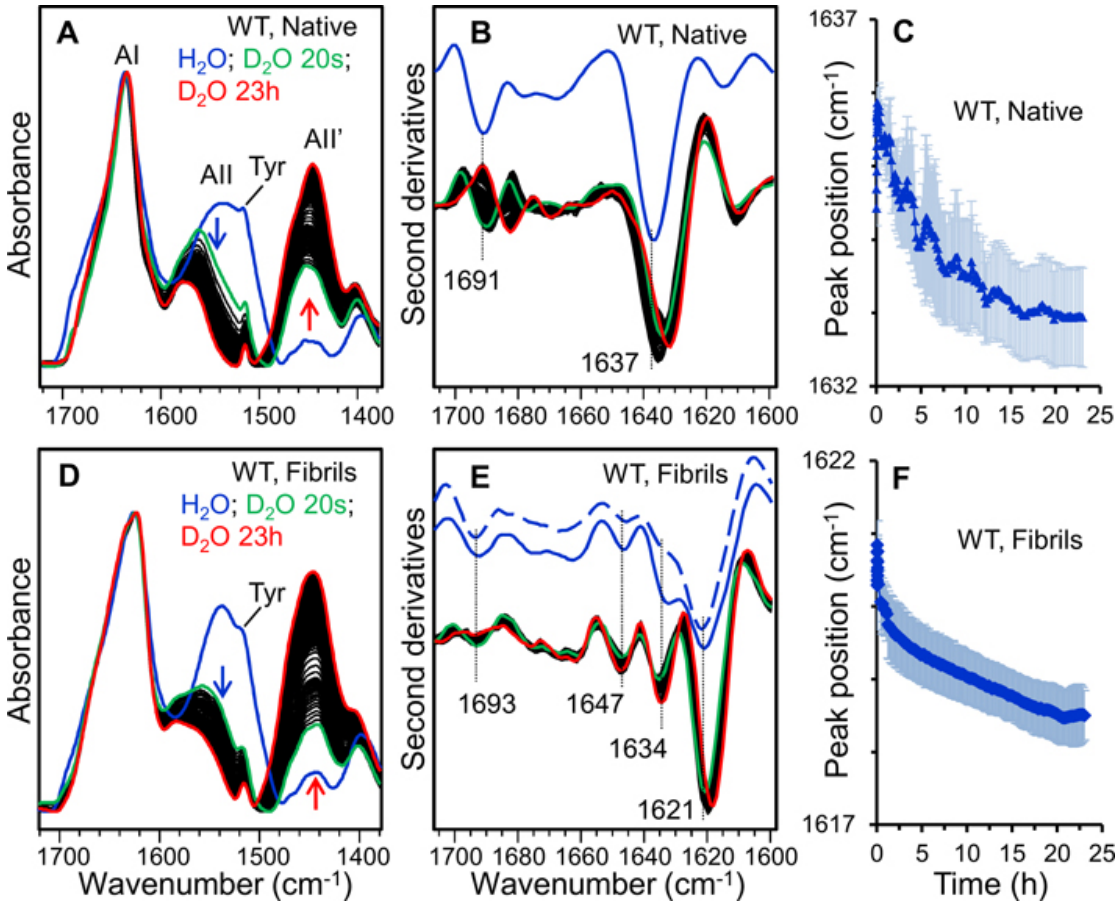
A
WT, Native
H2O; D2O 20s;
D2O 23h
AI
AII
Tyr
AII'
Absorbance
1700 1600 1500 1400
B
WT, Native
Second derivatives
1691
1637
1700 1680 1660 1640 1620 1600
C
WT, Native
Peak position (cm-1)
1637
1632
0 5 10 15 20 25
D
WT, Fibrils
H2O; D2O 20s;
D2O 23h
Tyr
Absorbance
Wavenumber (cm-1)
E
WT, Fibrils
Second derivatives
1693
1647
1634
1621
Wavenumber (cm-1)
F
WT, Fibrils
Peak position (cm-1)
1622
1617
Time (h)

Fig. 5

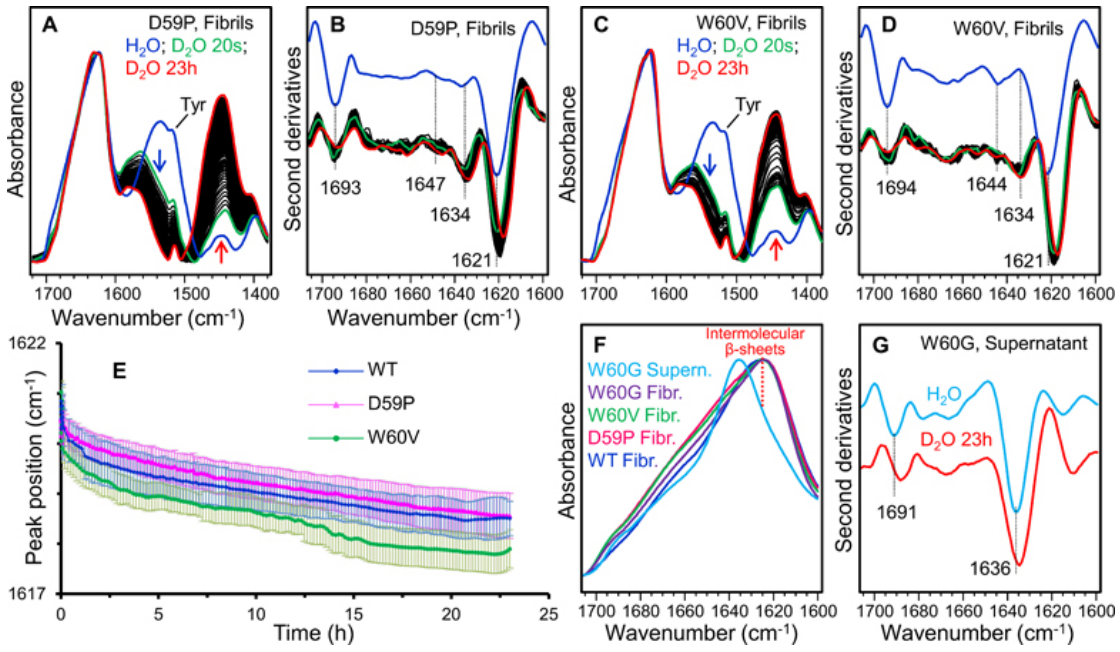
A
D59P, Fibrils
H2O; D2O 20s;
D2O 23h
Tyr
Absorbance
Wavenumber (cm-1)
B
D59P, Fibrils
Second derivatives
1693
1647
1634
1621
C
W60V, Fibrils
H2O; D2O 20s;
D2O 23h
Tyr
D
W60V, Fibrils
1694
1644
1634
1621
E
WT
D59P
W60V
Peak position (cm-1)
Time (h)
F
Intermolecular
β-sheets
W60G Supern.
W60G Fibr.
W60V Fibr.
D59P Fibr.
WT Fibr.
G
W60G, Supernatant
H2O
D2O 23h
1691
1636